

AD-A185 968

NORSAR DETECTION PROCESSING SYSTEM(U) ROYAL NORWEGIAN  
COUNCIL FOR SCIENTIFIC AND INDUSTRIAL RESEARCH KJELLER  
L. B. LOUGHRAN 31 MAY 87 NORSAR-SCIENTIFIC-2-86/87  
F08606-86-C-0004

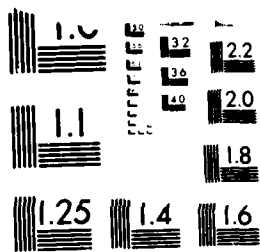
1/2

UNCLASSIFIED

P. G. 17/10

NL

52



MICROCOPY RESOLUTION TEST CHART  
ANSI AND ISO STANDARDS

AD-A185 968

**NORSAR**

NORWEGIAN COUNCIL FOR SCIENTIFIC AND INDUSTRIAL RESEARCH

DTIC FILE COPY

4

NORSAR Scientific Report No. 2-86/87

**SEMIANNUAL TECHNICAL SUMMARY**

1 October 1986 - 31 March 1987

L.B. Loughran (ed.)

DTIC  
ELECTE  
S OCT 16 1987 D  
D  
ce

Kjeller, May 1987



APPROVED FOR PUBLIC RELEASE, DISTRIBUTION UNLIMITED

87 10 6 030

UNCLASSIFIED  
SECURITY CLASSIFICATION OF THIS PAGE

REPORT DOCUMENTATION PAGE				Form Approved OMB No. 0704-0188	
1a. REPORT SECURITY CLASSIFICATION UNCLASSIFIED		1b. RESTRICTIVE MARKINGS NOT APPLICABLE			
2a. SECURITY CLASSIFICATION AUTHORITY NOT APPLICABLE		3. DISTRIBUTION/AVAILABILITY OF REPORT APPROVED FOR PUBLIC RELEASE DISTRIBUTION UNLIMITED			
2b. DECLASSIFICATION/DOWNGRADING SCHEDULE NOT APPLICABLE		4. PERFORMING ORGANIZATION REPORT NUMBER(S) Scientific Report 2-86/87			
4. PERFORMING ORGANIZATION REPORT NUMBER(S) Scientific Report 2-86/87		5. MONITORING ORGANIZATION REPORT NUMBER(S) Scientific Report 2-86/87			
6a. NAME OF PERFORMING ORGANIZATION NTNF/NORSAR		6b. OFFICE SYMBOL (if applicable) GSD		7a. NAME OF MONITORING ORGANIZATION HQ/AFTAC/TCX	
6c. ADDRESS (City, State, and ZIP Code) POST BOX 51 N-2007 KJELLER, NORWAY		7b. ADDRESS (City, State, and ZIP Code) PATRICK AFB, FL 32925-6001			
8a. NAME OF FUNDING/SPONSORING ORGANIZATION DEFENCE ADVANCED RESEARCH PROJECTS AGENCY		8b. OFFICE SYMBOL (if applicable)		9. PROCUREMENT INSTRUMENT IDENTIFICATION NUMBER CONTRACT NO. F08606-86-C-0004	
8c. ADDRESS (City, State, and ZIP Code) 1400 WILSON BLVD. ARLINGTON, VA 22209-2308		10. SOURCE OF FUNDING NUMBERS			
		PROGRAM ELEMENT NO. R&D	PROJECT NO. NORSAR PHASE 3	TASK NO. SOW TASK 5.0	WORK UNIT ACCESSION NO. SEQUENCE NO. 003A
11. TITLE (Include Security Classification) SEMIANNUAL TECHNICAL SUMMARY 1 OCT 1986 - 31 MAR 1987 (UNCLASSIFIED)					
12. PERSONAL AUTHOR(S) L.B. LOUGHRAN (ED.)					
13a. TYPE OF REPORT SCIENTIFIC SUMMARY		13b. TIME COVERED FROM 1 Oct 86 - 31 Mar 87		14. DATE OF REPORT (Year, Month, Day) MAY 1987	
15. PAGE COUNT 124					
16. SUPPLEMENTARY NOTATION NOT APPLICABLE					
17. COSATI CODES			18. SUBJECT TERMS (Continue on reverse if necessary and identify by block number)		
FIELD	GROUP	SUB-GROUP			
8	11		NORSAR, NORWEGIAN SEISMIC ARRAY		
19. ABSTRACT (Continue on reverse if necessary and identify by block number)					
This Semiannual Technical Summary describes the operation, maintenance and research activities at the Norwegian Seismic Array (NORSAR) for the period 1 Oct 86 - 31 Mar 87.					
20. DISTRIBUTION/AVAILABILITY OF ABSTRACT <input type="checkbox"/> UNCLASSIFIED/UNLIMITED <input type="checkbox"/> SAME AS RPT. <input type="checkbox"/> DTIC USERS			21. ABSTRACT SECURITY CLASSIFICATION UNCLASSIFIED		
22a. NAME OF RESPONSIBLE INDIVIDUAL MAJOR JAMES A. ROBB			22b. TELEPHONE (Include Area Code) (305) 494-7665		22c. OFFICE SYMBOL AFTAC/TCX

DD Form 1473, JUN 86

Previous editions are obsolete.

SECURITY CLASSIFICATION OF THIS PAGE

UNCLASSIFIED

UNCLASSIFIED

19. (cont.)

The NORSAR Detection Processing system has been operated through the reporting period with an average uptime of 99.6 per cent. A total of 2028 seismic events have been reported by NORSAR in the period. The performance of the continuous alarm system and the automatic bulletin transfer by telex to AFTAC have been satisfactory. Processing of requests for full NORSAR/NORESS data on magnetic tape has progressed without problems.

Investigations into further potential improvements in the NORSAR array processing system have continued. A new Detection Processor (DP) program has been developed and tested in an off-line mode. This program is flexible enough to conduct both NORSAR and NORESS detection processing as is done today, besides incorporating improved algorithms. The program will be implemented after some further testing and refinements have been made.

Field maintenance activity has included regular preventive maintenance at all subarrays and occasional corrective actions as required. No special problems have been noted in the performance of the field installations. In addition, field maintenance personnel have participated in experiments involving the NORESS array as well as a planned second small aperture array.

A wide-band slowness estimation technique has been investigated by processing data from several events from the same location. Ten quarry blasts at a dam construction site in western Norway, ten explosions from a mining area in western Russia and sixteen Semipalatinsk nuclear explosions were selected. The major conclusion from this study is that employing a wider frequency band clearly tends to increase the stability of the slowness estimates, provided the signal-to-noise ratio is adequate over the band of interest. The stability was found, particularly for Pn, to be remarkably good for the western Norway quarry blasts when using a fixed frequency band for each phase for all ten events. This approach also contributed a full separation between Sn and Lg phases in slowness space, with associated average phase velocities of 4.71 km/s and 3.91 km/s, respectively. This clear separation could not be obtained for the western USSR events, partly due to narrower usable bandwidth. On the other hand, the Semipalatinsk explosions, at teleseismic distances, showed very consistent results when applying the wide-band technique.



approximations. Having in mind the observed frequency dependent wave-number anomalies at NORESS, we plan to apply the method to scattering by surface topography as well. This will enable us in the future to compare the frequency dependent phase perturbations to the usual static corrections due to topography.

A large-scale study has been completed with the aim to determine phase characteristics and detectability of mine explosions and rock bursts in Polish mining areas. We have obtained a data base of more than 500 extremely well-located seismic events (hypocentral uncertainty a few tens of meters) of magnitude range 1.5-3.5 ( $M_L$ ). Conclusions from the study are that RONAPP automatic P-detection is excellent (90 per cent threshold  $M_L$  2.7-2.8 for the Lubin area at 1060 km distance), whereas automatic detection of secondary phases seldom occurs. The main reason is that the Tornquist-Teisseyre tectonic zone in Poland acts as a barrier to  $L_g$  propagation. Using NORESS-recorded P and S phases in conjunction with S azimuths gives reasonable location estimates for those events where both phases can be seen; typically the location error is 50-60 km.

The accuracy of estimated arrival times and azimuths depends strongly on the shape and corner frequency of recorded phases. Characteristic patterns of P-wave records might provide important information into an expert system approach to regional array processing.

AFTAC Project Authorization : T/6141/B/PMP  
ARPA Order No. : 4138  
Program Code No. : OF10  
Name of Contractor : Royal Norwegian Council  
for Scientific and  
Industrial Research  
Effective Date of Contract : 1 October 1985  
Contract Expiration Date : 30 September 1987  
Project Manager : Frode Ringdal (06) 81 71 21  
Title of Work : The Norwegian Seismic Array  
(NORSAR) Phase 3  
Amount of Contract : \$ 818,107.00  
Contract Period Covered by the Report : 1 Oct 1986 - 31 Mar 1987

The views and conclusions contained in this document are those of the authors and should not be interpreted as necessarily representing the official policies, either expressed or implied, of the Defense Advanced Research Projects Agency, the Air Force Technical Applications Center or the U.S. Government.

This research was supported by the Advanced Research Projects Agency of the Department of Defense and was monitored by AFTAC, Patrick AFB, FL 32925, under contract no. F08606-86-C-0004.

TABLE OF CONTENTS

	<u>Page</u>
I. SUMMARY	1
II. OPERATION OF ALL SYSTEMS	3
II.1 Detection Processor operation	3
II.2 Data communication	8
III. ARRAY PERFORMANCE	13
IV. IMPROVEMENTS AND MODIFICATIONS	14
V. MAINTENANCE ACTIVITIES	32
V.1 Activities in the field and at the Maintenance Center	32
V.2 Improvements and modifications	36
V.3 Array status	36
VI. DOCUMENTATION DEVELOPED	37
VII. SUMMARY OF TECHNICAL REPORTS/PAPERS PREPARED	38
VII.1 Wide-band slowness estimation using a small aperture array	38
VII.2 NORESS noise spectral studies. Noise level characteristics	46
VII.3 Initial results from data analysis using the FINESA experimental small aperture array	59
VII.4 Multiple scattering by topographic relief	84
VII.5 NORESS capability for detection and location of mining tremors in the Lubin area in Poland	91

I. SUMMARY

This Semiannual Technical Summary describes the operation, maintenance and research activities at the Norwegian Seismic Array (NORSAR) for the period 1 Oct 1986 - 31 Mar 1987.

The uptime of the NORSAR online detection processor system has averaged 99.6 per cent during the reporting period as compared to 99.3 for the previous period. There have been a number of problems with the communication lines to subarray 04C for most of the period. Otherwise the system has generally shown a reliable performance. A total of 2028 seismic events were reported in the NORSAR monthly seismic bulletins in this period, giving a daily average of 11.1 events.

The new Detection Processor (DP) program has now been tested and found to perform satisfactorily. This DP system is described in some detail and some preliminary results from processing done so far are documented.

Field maintenance activity has included regular preventive maintenance at all subarrays and occasional corrective actions as required. No special problems have been noted in the performance of the field installations. In addition, field maintenance personnel have participated in planning for the installation of the NORESS II array in Finnmark.

The research activity is summarized in section VII. Section VII.1 describes wide-band slowness estimation using a small aperture seismic array. Section VII.2 presents NORESS noise spectral studies, with special emphasis on noise level characteristics. In Section VII.3 initial results from data analysis using the FINESA experimental small aperture array are presented. Section VII.4 describes a method to account for multiple scattering due to topography of internal boundaries or of the free surface. In Section VII.5 NORESS capability for detection and location of mining tremors in the Lubin area in Poland is discussed.

II. OPERATION OF ALL SYSTEMS

II.1 Detection Processor (DP) Operation

There have been 90 breaks in the otherwise continuous operation of the NORSAR online system within the current 6-month reporting interval. The uptime percentage for the period is 99.6 as compared to 99.3 for the previous period.

Fig. II.1.1 and the accompanying Table II.1.1 both show the daily DP downtime for the days between 1 October 1986 and 31 March 1987. The monthly recording times and percentages are given in Table II.1.2.

The breaks can be grouped as follows:

a) Hardware failure	1
b) Stops related to program work or error	0
c) Hardware maintenance stops	3
d) Power jumps and breaks	5
e) TOD error correction	12
f) Communication lines	59

The total downtime for the period was 16 hours and 14 minutes. The mean-time-between-failures (MTBF) was 2.0 days, as compared to 2.5 for the previous period.

J. Torstveit

Month	DP uptime hours	DP uptime %	No. of DP breaks	No. of days with breaks	DP MTBF* (days)
OCT	737.35	99.1	13	12	2.2
NOV	715.78	99.4	19	14	1.6
DEC	743.73	99.9	13	9	2.2
JAN	742.98	99.9	21	7	1.4
FEB	668.26	99.4	7	4	3.5
MAR	743.65	99.9	18	9	1.6
		99.6	90	55	2.1

\* Mean-time-between-failures = total uptime/no. of up intervals.

Table II.1.2 Online system performance, 1 Oct 1986 - 31 Mar 1987.

TOTAL NUMBER OF HOURS DOWN PER DAY

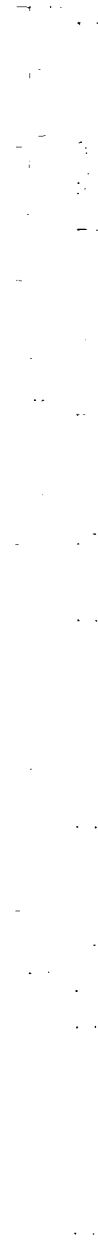


Fig. II.1.1.1 Detection Processor downtime in the period 1 Oct 1986 - 31 Mar 1987.

LIST OF BREAKS IN DP PROCESSING THE LAST HALF-YEAR		STOP COMMENTS.....		DAY		START		STOP		COMMENTS.....	
DAY	START	STOP	COMMENTS.....	DAY	START	STOP	COMMENTS.....	DAY	START	STOP	COMMENTS.....
276	7	0	7	1	TOD RETARD 25MS	346	12	35	12	36	LINE FAILURE
280	7	1	7	2	TOD RETARD 25MS	346	13	13	13	14	LINE FAILURE
283	9	37	9	39	TOD RETARD 12MS	346	13	27	13	30	LINE FAILURE
286	8	13	8	15	TOD RETARD 32MS	348	14	47	14	49	LINE FAILURE
287	10	45	10	46	LINE FAILURE	349	14	14	14	15	LINE FAILURE
290	7	1	7	2	TOD RETARD 34MS	353	9	2	9	3	LINE FAILURE
293	7	2	7	3	TOD RETARD 23MS	353	9	59	10	1	LINE FAILURE
295	7	12	7	14	TOD RETARD 23MS	357	15	11	15	12	LINE FAILURE
297	8	29	10	59	CE SERVICE DISK	363	7	44	7	45	LINE FAILURE
297	11	45	15	40	CE SERVICE DISK	5	8	28	8	29	LINE FAILURE
300	7	32	7	33	LINE FAILURE	6	7	0	7	2	LINE FAILURE
303	0	0	0	1	TOD RETARD 7MS	6	7	8	7	10	LINE FAILURE
304	10	20	10	21	TOD RETARD 10MS	6	7	15	7	16	LINE FAILURE
305	8	2	8	4	LINE FAILURE	7	10	1	10	9	CE MAINTENANCE
307	0	45	9	20	LINE FAILURE	7	13	26	13	27	LINE FAILURE
308	8	50	8	54	TOD RETARD 33MS	7	13	32	13	33	LINE FAILURE
310	7	0	7	2	TOD RETARD 23MS	7	13	43	13	44	LINE FAILURE
314	10	19	10	50	POWER FAILURE	7	13	50	13	51	LINE FAILURE
314	10	50	13	57	MDCOMP FAILURE	8	8	36	8	37	LINE FAILURE
315	7	1	7	2	TOD RETARD 32MS	9	7	8	7	9	LINE FAILURE
318	7	53	7	54	LINE FAILURE	9	12	58	13	0	LINE FAILURE
318	8	12	8	14	TOD RETARD 23MS	19	11	52	11	53	LINE FAILURE
318	8	27	8	28	LINE FAILURE	22	13	4	13	5	LINE FAILURE
320	0	7	0	11	LINE FAILURE	25	10	5	10	9	LINE FAILURE
321	11	3	11	11	POWER BREAK	25	10	17	10	18	LINE FAILURE
322	13	32	13	34	TOD RETARD 33MS	26	13	26	13	53	POWER FAILURE
324	7	1	7	2	TOD RETARD 23MS	28	11	59	12	0	LINE FAILURE
324	7	33	7	34	LINE FAILURE	28	12	34	12	36	LINE FAILURE
328	13	41	13	42	LINE FAILURE	28	12	37	12	38	LINE FAILURE
328	14	4	14	5	TOD RETARD 33MS	28	13	57	13	58	LINE FAILURE
329	0	30	0	42	LINE FAILURE	32	23	47	24	0	LINE FAILURE
331	7	3	7	4	TOD RETARD 30MS	35	20	47	23	49	POWER FAILURE
335	7	21	7	22	TOD RETARD 30MS	37	7	45	8	0	POWER FAILURE
338	12	14	12	15	TOD RETARD 30MS	37	9	3	9	4	LINE FAILURE
342	7	2	7	3	TOD RETARD 30MS	58	7	14	7	15	LINE FAILURE
342	12	7	12	8	LINE FAILURE	58	7	31	7	32	LINE FAILURE

Table II.1.1 Daily DP downtime in the period 1 Oct 1986 - 31 Mar 1987.

LINE	YEAR	REASON	HALF-YEAR
68	7	LINE FAILURE	
69	7	LINE FAILURE	
70	7	LINE FAILURE	
71	7	LINE FAILURE	
72	7	LINE FAILURE	
73	7	LINE FAILURE	
74	7	LINE FAILURE	
75	7	LINE FAILURE	
76	7	LINE FAILURE	
77	7	LINE FAILURE	
78	7	LINE FAILURE	
79	7	LINE FAILURE	
80	7	LINE FAILURE	
81	7	LINE FAILURE	
82	7	LINE FAILURE	
83	7	LINE FAILURE	
84	7	LINE FAILURE	
85	7	LINE FAILURE	
86	7	LINE FAILURE	
87	7	LINE FAILURE	
88	7	LINE FAILURE	
89	7	LINE FAILURE	
90	7	LINE FAILURE	
91	7	LINE FAILURE	
92	7	LINE FAILURE	
93	7	LINE FAILURE	
94	7	LINE FAILURE	
95	7	LINE FAILURE	
96	7	LINE FAILURE	
97	7	LINE FAILURE	
98	7	LINE FAILURE	
99	7	LINE FAILURE	
100	7	LINE FAILURE	
101	7	LINE FAILURE	
102	7	LINE FAILURE	
103	7	LINE FAILURE	
104	7	LINE FAILURE	
105	7	LINE FAILURE	
106	7	LINE FAILURE	
107	7	LINE FAILURE	
108	7	LINE FAILURE	
109	7	LINE FAILURE	
110	7	LINE FAILURE	
111	7	LINE FAILURE	
112	7	LINE FAILURE	
113	7	LINE FAILURE	
114	7	LINE FAILURE	
115	7	LINE FAILURE	
116	7	LINE FAILURE	
117	7	LINE FAILURE	
118	7	LINE FAILURE	
119	7	LINE FAILURE	
120	7	LINE FAILURE	
121	7	LINE FAILURE	
122	7	LINE FAILURE	
123	7	LINE FAILURE	
124	7	LINE FAILURE	
125	7	LINE FAILURE	
126	7	LINE FAILURE	
127	7	LINE FAILURE	
128	7	LINE FAILURE	
129	7	LINE FAILURE	
130	7	LINE FAILURE	
131	7	LINE FAILURE	
132	7	LINE FAILURE	
133	7	LINE FAILURE	
134	7	LINE FAILURE	
135	7	LINE FAILURE	
136	7	LINE FAILURE	
137	7	LINE FAILURE	
138	7	LINE FAILURE	
139	7	LINE FAILURE	
140	7	LINE FAILURE	
141	7	LINE FAILURE	
142	7	LINE FAILURE	
143	7	LINE FAILURE	
144	7	LINE FAILURE	
145	7	LINE FAILURE	
146	7	LINE FAILURE	
147	7	LINE FAILURE	
148	7	LINE FAILURE	
149	7	LINE FAILURE	
150	7	LINE FAILURE	
151	7	LINE FAILURE	
152	7	LINE FAILURE	
153	7	LINE FAILURE	
154	7	LINE FAILURE	
155	7	LINE FAILURE	
156	7	LINE FAILURE	
157	7	LINE FAILURE	
158	7	LINE FAILURE	
159	7	LINE FAILURE	
160	7	LINE FAILURE	
161	7	LINE FAILURE	
162	7	LINE FAILURE	
163	7	LINE FAILURE	
164	7	LINE FAILURE	
165	7	LINE FAILURE	
166	7	LINE FAILURE	
167	7	LINE FAILURE	
168	7	LINE FAILURE	
169	7	LINE FAILURE	
170	7	LINE FAILURE	
171	7	LINE FAILURE	
172	7	LINE FAILURE	
173	7	LINE FAILURE	
174	7	LINE FAILURE	
175	7	LINE FAILURE	
176	7	LINE FAILURE	
177	7	LINE FAILURE	
178	7	LINE FAILURE	
179	7	LINE FAILURE	
180	7	LINE FAILURE	
181	7	LINE FAILURE	
182	7	LINE FAILURE	
183	7	LINE FAILURE	
184	7	LINE FAILURE	
185	7	LINE FAILURE	
186	7	LINE FAILURE	
187	7	LINE FAILURE	
188	7	LINE FAILURE	
189	7	LINE FAILURE	
190	7	LINE FAILURE	
191	7	LINE FAILURE	
192	7	LINE FAILURE	
193	7	LINE FAILURE	
194	7	LINE FAILURE	
195	7	LINE FAILURE	
196	7	LINE FAILURE	
197	7	LINE FAILURE	
198	7	LINE FAILURE	
199	7	LINE FAILURE	
200	7	LINE FAILURE	

Table II.1.1 (cont.)

II.2 Array communications:

Reference is made to Table VII.2.1 in connection with communication system performance in the period.

The most affected systems have been 04C and 06C, 04C due to reduced line performance and 06C due to an assumed intermittent operating equalizer.

Besides, a nonlocated noise source has affected all communications systems, especially during night hours. Although not causing an excessive error rate, the irregularity caused many resynchronizations of the communications lines. It is clear that the noise is created somewhere along the NTA's carrier systems. All our communications systems are located within the same channel group. On 27 April, NTA switched to a different equipment group, and this particular problem then disappeared.

Otherwise, and as the table indicates, most systems have been reliable.

NTA/Lillestrøm and Hamar will take a new initiative medio April regarding 04C. The line will be remeasured and if a certain degree of improvement in the line condition is found, new modems will be hooked up to see if their equalizers can handle the line distortion. The modems will then be kept until the line is repaired.

**Summary**

Oct 86 03C had been unreliable for some time, continued week 40. Apart from an irregularity week 42, the 03C communication system remained stable throughout the period.

02B was affected week 43 (19.7%) caused by an assumed line fault toward the subarray.

The performance of the remaining systems was acceptable.

Average communication system outage/degradation 5 weeks all systems: 1.67% and 0.11% (- 02C).

Nov 86 Apart from 04C, reliable performance all systems. Although having a significant amount of errors (0.93%) subarray 04C was not permanently masked.

Average communication system outage/degradation 4 weeks all systems: 0.15% and 0.02% (- 04C).

Dec 86 04C still out of operation due to changed cable/line characteristics. NTA/Hamar visited the subarray 2 Dec. Level measurements revealed too high input level (-13 dBm), which, unless other irregularities also existed, isolated should not cause problems.

NMC visited the subarray 12 and 18 Dec. Attempts were made to replace modems and loop control logic, but without improvements. Communications lines between Kjeller and the subarray were measured with respect to attenuation distortion for the actual frequencies 300-2400 Hz. Between 300 and 800 Hz the attenuation was 0.6 and 1.0 dB m in the directions Kjeller-CTV and CTV-Kjeller, respectively. Between 800 and 2400 Hz the attenuation CTV-Kjeller was 0.5 dBm, while between Kjeller and the CTV the attenuation was 2.2 dBm, the latter normal.

Late December NTA/Elverum swapped cable pairs between Berg Central and the CTV without improving the quality. Due to very low temperatures and deep snow in the subarray area, no further actions were expected until conditions changed.

06C was affected frequently week 52, causing high outage figures. An intermittent operating equalizer was probably the reason. After 29 December the performance has been reliable. Average communication system outage/degradation 4 weeks all systems: 11.6%, and 0.02% (-04C, 06C).

Jan 87 It has been necessary to mask 01B and 03C a few times due to spikes in data (between 5 and 12 Jan).

04C. No progress with regard to the communication system outage. NTA/Hamar has checked equalizers (Elverum), and cables between Hernes and Berg Central. Cables between Berg Central and the subarray remain to be measured thoroughly.

02C was affected 27 January in connection with planned cable work in Mesnali (NTA/Hamar).

In connection with expansion/improvement of the telecommunication circuits in the Kjeller-Lillestrøm area most institutions were affected, including NORSAR and the neighboring institution RBK.

In our operator/modem office, the data and telecommunication junction box was replaced and cables were cut/spliced. A new cable (20 pairs) was installed between the junction box and RBK telephone central. The above-mentioned activities took place between 28 January and 1 February, and all our data and telecommunication circuits were broken for short periods.

06C. Communication circuit instability continued through 20 December, but reliable performance after 2 January.

Average communication system outage/degradation 5 weeks all systems (- 04C): 0.17%.

Feb 87 04C still out of operation as NTA/Hamar was not able to repair the cable between Berg Central and the CTV.

NMC visited the subarray 27 February and several tests were carried out in cooperation with NDPC. Error rate, especially in the direction towards Kjeller, was high.

Average communication system outage/degradation 4 weeks:  
0.02% (- 04C).

Mar 87 NTA/Hamar and Lillestrøm ready for a new initiative mid-April in connection with 04C. The complete communication path will be remeasured. If positive changes in line quality since last measurements, new modems (with automatic equalization) will be hooked up in the CTV and here at the NDPC. If usable results are obtained with the modems, they will be kept until cables or other parts of the communication system causing the trouble are repaired.

06C. Error figures for March (13.80%) were also very high, mainly due to frequent resynchronization of the communication system.

Since 23 March all NORSAR communication systems were affected by a nonlocated noise source, mainly during night hours. Although moderate error rate, such conditions cause unwanted line resynchronization, and extra load on the communication processor. This problem persisted until 27 April, when NTA switched their channel group equipment for all lines to a spare channel group.

Average communication system outage/degradation 3 weeks (10-12), all systems (- 04C): 0.13%. 4 weeks (10-13), 01A-03C (- 04C, 06C): 0.77%.

O.A. Hansen

Sub-array	OCT 86 (5) (29.9-2.11)	NOV 86 (4) (3-30.11)	DEC 86 (4) (1-28.12)	JAN 87 (5) (29.12-1.2)	FEB 87 (4) (2.2-1.3)	MAR 87 (4) (2-29.3)	Average 1/4 yr
01A	0.10	0.02	0.02	0.19	0.03	3.60	0.06
01B	0.05	0.02	0.02	0.20	0.04	0.07	0.07
02B	*3.98	0.03	0.02	0.02	0.03	0.06	0.69
02C	0.04	0.01	0.02	0.21	0.02	0.07	0.06
03C	*7.22	0.02	0.04	0.02	0.03	0.07	1.23
04C	0.07	*0.93	*63.09	*100.00	*100.00	*100.00	60.68
06C	0.18	0.02	*18.33	0.37	0.47	*13.88	5.54
AVER	1.66	0.15	11.65	14.40	14.37	16.82	9.85
Less	0.28	0.02	0.03	0.17	0.10	2.95	1.37
02B,02C	0.08	0.02	0.03	0.03	0.03	0.46,06C	0.54

\* see item II.2 regarding figures preceded by an asterisk.

Table II.2.1 Communications performance. The numbers represent error rates in per cent based on total transmitted frames/week (1 Oct 1986 - 31 Mar 1987).

III. ARRAY PERFORMANCE

Event Processor Operation

In Table III.1 some monthly statistics of the Event Processor operation are given:

	Teleseismic	Core Phases	Sum	Daily
OCT 86	195	255	450	14.5
NOV 86	224	126	350	11.7
DEC 86	175	145	320	10.3
JAN 87	205	74	279	9.0
FEB 87	188	107	295	10.5
MAR 87	244	90	334	10.8
	1231	797	2028	11.1

Table III.1 Event Processor Statistics, October 1986 - March 1987.

B. Paulsen

#### IV. IMPROVEMENTS AND MODIFICATIONS

In NORSAR Scientific Report No. 1-86/87 we outlined an implementation plan for the upgrade of the NORSAR processing system.

Part 1, to implement new NORSAR offline detection system, has been completed, and tested parallel to the present recording and detection system. This new program system, DP - Detection Processor - has been found to perform most satisfactorily the NORSAR detection task.

In the 'old' system, the detection processing is divided into two steps. A MODCOMP computer system communicates with the NORSAR subarrays and performs filtering and subarray beamforming on the data. Thereafter, the data is transmitted each 0.5 second to the IBM 4341/L01 processor, where array beamforming and STA/LTA detection is done. The new system performs all operations in one program, to be run on the IBM 4341. As opposed to the 'old' system where array beamforming is done using subarray beams, the new system forms beams using individual delays for all the 42 instruments. Incoherent beamforming is, however done using subarray beams.

In this report we will describe some of the details of the DP system and document some preliminary results from the processing done so far.

In Scientific Rep. No 1-86/87, we outlined some general rules for developing processing programs and gave examples of application of two parts of a data analysis program: the data retrieval part and the presentation of the data or the results. The actual analysis part in between these steps consists of applying a variety of processing techniques, and we will classify these into two main categories: "segmented" and "continuous".

We define segmented processing as applying some analysis to a segment of data and present results for that segment. Continuous processing is defined as a repeatable, cyclic process applied to a data stream that in principle is of infinite length.

In a detection system, the processes applied (filtering, STA/LTA operators, beamforming) need at any time point some of the 'old' data. Therefore, we cannot produce detector results by only processing only a few seconds of the data, we need at least some minutes before detector statistics stabilize.

Continuous processing may be implemented as segmented processing of long data intervals which follow in time, and continuity may be secured by reprocessing some part of the data. Memory requirements may be too large for such an approach, but this can be solved by dividing the job into smaller steps, and let each step output intermediate results.

Another approach is to process a smaller segment of data and retain some of the previously processed data for continuity when the next segment is brought into processor memory. We define this as "continuous segmented" processing, and this is the technique implemented in the new DP system. For each segment, the routines operate as if only one single segment of data were to be processed. The idea is that some processes then require only one program routine, such that program parts of different systems may use the same routines.

In practice, the continuous segmented processing is implemented by keeping all data in a memory buffer. At any time instant, a process which uses some 'old' data (e.g. filtering and beamforming) may reference time points backwards. This is made possible by always keeping a defined amount of data as 'old' data. E.g., for NORSAR processing, the amount of 'old' data needed at any time point is derived from the maximum beamforming delays and from the delay used when up-

dating LTA. Currently this parameter is 9 seconds. That is, if 60.0 seconds of data segment length is used, then we always keep 69.0 seconds of data. Each time a new segment is brought in, 9.0 seconds of data is moved. Processing time for this moving of data is only about 0.2 % of the total time spent on processing the NORSAR array data. All the routines then process 60.0 seconds segment of data.

The system may process a defined number of segments (steps), or do processing as long as there are data. The DP system is thus designed to allow for both segmented and continuous segmented techniques.

The program system is divided into several FORTRAN subroutines. We have earlier described the benefits of defining a common internal data buffer structure for use at NORSAR. The new analysis program developed by T. Kværna (SSA - Seismic Signal Analyzer), uses the same data read routines as the detection system, and the same internal data structure. So far we may use all the data recorded by NORSAR systems. (NORSAR, NORLSS, NORESS High frequency system, FINESA, Level 2 data). CSS data format will also be implemented. Using this structure, the processing code is not tied to specific data, and coding done for segmented processing in the SSA system may be adopted by the detection system.

The principal idea behind the internal structure is to use one large buffer for all data. Instrument data are called 'channels', likewise any other vector. The buffer then contains a number of channels, each channel described by its position in buffer, number of points, name, distance between points (sample rate) etc.

The DP system currently consists of the following main routines: an initialization routine, a processor scheduling routine, routine for

filtering, routine for beamforming, routine for STA/LTA detection, routine for incoherent STA/LTA detection, and routines for forming STA, LTA, and STA/LTA time series. There are of course also routines for reducing detector output, and recording of detections.

The detector initialization routine will either read commands from the terminal keyboard, or from a detector recipe coded by the user. The initialization part will build up the data buffer (by initializing channel pointers), and build up processing orders for the scheduler.

Figs. IV.1, IV.2 and IV.3 show extracts from the NORSAR and NORESS detection recipes, which may be used as examples for the commands used by the current DP system. The commands are:

TERMINAL - Switch from disk to terminal input.  
TYPE - Define amount of screen output from routines.  
STEP - The number of segments to process. Start time is given by main controlling program.  
DPTIME - If start time for processing is specified with DPTIME command, then the system will process the number of segments specified, and at end of processing, the data segment in the buffers will contain that time.  
DATA BUFFER LENGTH 60.0 SECONDS  
- Set segment processing length to 60.0 seconds.  
OLD BUFFER LENGTH 9.0 SECONDS  
- Set necessary backup time to 9.0 seconds.  
SET DETECTION STATE TRUE  
- Initially for the first segment, the program will believe that all beams have STA/LTA greater than threshold.  
SET INITIAL LTA 8.0  
- Set initial LTA value of 8.0.  
SET REFERENCE 02B00  
- Set reference station to 02B00.

SET THRESHOLD 3.2

- Set STA/LTA threshold to 3.2.

SET STX LENGTH 0.5 SECONDS.

- Set length of STX to 0.5 second. STX is then the average of 0.5 second of rectified data. STX's will be sampled with a rate equal to its length and are not overlapping.

SET STA LENGTH 1.5 SECONDS.

- Set STA length of 1.5 second. STA will be the average of STX's over 1.5 second. STA must cover an integer number of STX's and is sampled with the same rate as STX.

SET LTA SIGMA 7.0

- LTA at one time instance will be  $STX * 2.0^{**(-SIGMA)}$  plus the former  $LTA * (1.0 - 2.0^{**(-SIGMA)})$ . The STX used is not from 'current' time point, but delayed 9.0 seconds. (See SET LTA DELAY).

SET LTA BETA 6.0

- If STA/LTA is above threshold, the LTA will be updated with BETA during this detection state rather than SIGMA.

SET LTA DELAY 9.0 SECONDS

- See LTA SIGMA comment.

SET REDUCTION 3.0 SECONDS

- Time constant used for detection reduction. For an event, a great number of beams may detect. If detection start time is closer than 3.0 seconds to another detection, then the detections are reported as one detection, using the detector results for the one with largest STA/LTA.

INPUT THE FOLLOWING STATIONS:

- Give a list of station names to get the data.

FILTER FILNAM FILTER FLTYP BANDLW BANDHG IORD

1 FBI BU BP 1.2 3.2 3

- Give a list of filters that may be used.

Filters are later referred to by name (FBI).

FILTER ALL WITH FBI OUTPUT xxxxxFBI or

FILTER xxx WITH FBI OUTPUT yyy

- Filter all stations with filter FBI and give name to the output filtered stations by using the first 5 characters of the input (unfiltered) station concatenated with the filter name. Or filter station with name xxx with filter FBI (example) and give output channel name yyy.

DEFINE NAO-AB AS ALL xxxxxFBI

- Define a configuration. Give the name NAO-AB to that configuration. In this example use all channels with FBI in the name.

USE NAO-AB

- In the following, use configuration NAO-AB for beamforming.

USE BEAM-TABLE NAO-451 TABLE \*

- In the file : NAO-451 TABLE \* , the program will find a list of delays for a number of beams.

USE MAX AMPLITUDE 3.0

- If an input unfiltered instrument has a maximum absolute amplitude that is at least 3.0 times the average of the maximum amplitudes at all channels for a segment, then treat that instrument as inoperative for the whole segment.

USE NUMBER OF ITERATIONS 2 FOR MAXIMUM\_AMPLITUDE MASKING

- Iterate the maximum amplitude spike detector 2 times. Exclude bad instruments from average from each iteration.

STATIONS

- Give list of stations for which delays are given in a beam delay table.

DELAYS FOR BEAM-TABLE NAO-451

- List of beams follow. A beam-table entry has name of the beam, number of stations for which there are delays, and the delays for those stations. For one beam-table, there must be the same number of stations giving delays (as defined in the STATIONS command). When using a

DETECT ON BEAM command, the system will find the stations in the configuration used, and the delays for that configuration (a subset of STATIONS).

DETECT ON ALL

- For each of the beams, which are defined so far by a USE BEAM-TABLE command, form the individual beam, and run STA/LTA detector on that beam.

DETECT ON BEAM xxx

- Form beam xxx and run STA/LTA detector on that beam, which is defined so far by a USE BEAM-TABLE command.

DETECT ON xxx

- Run STA/LTA detector on the channel named xxx. For incoherent detection, use DETECT INCOHERENT ON.

MAKE BEAM xxx OUTPUT yyy (USING ccc) (VEL v) (AZI a)

- Form a beam. If xxx is a name of a beam in a beam-table, form that beam using those delays. Give the beam name yyy. Use configuration ccc if specified. Use given velocity v and azimuth a if specified. If beam name xxx does not exist, give name xxx to a new beam entry.

MAKE STX OF xxx OUTPUT yyy

MAKE STA OF xxx OUTPUT yyy

MAKE LTA OF xxx OUTPUT yyy

MAKE SNR OF xxx OUTPUT yyy

- Make STX, STA, LTA, or STA/LTA time series from the data channel named xxx. Output resulting data channel will be given name yyy.

The commands are used to build up processing orders (tasks to do) for the processing scheduler, and must therefore be given in the correct order of processing sequence. The user must decide whether to beamform first and then filter the beam or filter before beamforming, and do the things in correct order. When initializing the system, the program builds up memory buffers necessary to handle the recipe, and gives error messages if buffers are exceeded. The program also checks

for consistency with regard to sample rate, STX/STA integration lengths, and data buffer lengths.

These commands are sufficient to perform all operations concerning the STA/LTA detector algorithms used at NORSAR. Incoherent beamforming may be done by either using STA or STX time series for beamforming and/or detection. STA rate may be made equal to instrument sample rate by setting STX length to original sample interval time. Beam delays are given in seconds and must be given as relative arrival times. A positive delay thus means arrival time later than the reference instrument. The program system itself corrects all delays, such that the instrument with latest arrival gets zero delay, and all other delays are negative. The program system may easily be adjusted to do weighted beamforming, do power STA/LTA detection, or other processes that fit a continuous processing scheme.

By using these commands we have programmed a recipe for doing NORSAR subarray and/or array beamforming, coherent and incoherent. We are also able to reproduce the RONAPP detector results from NORESS data, and we have been testing a NORESS recipe with 72 coherent and 12 incoherent beams. The results for NORESS with the RONAPP recipe are exactly the same as for RONAPP itself, when using same detector parameters. For NORSAR data, the results are better than the old NORSAR system, as coherent beams normally have 20% higher signal-to-noise ratio without increasing false alarm rate. Most false detections due to spikes in data are eliminated or identified as such. Incoherent detection results for NORSAR are equal to or better than in the old system. These better results are obtained even though new delays within subarrays have not been implemented. In Figure 4 some of the detection results are listed.

So far, the DP system has been implemented for research and testing purposes. The code contains a number of interactive options, and nothing has yet been done to reduce overhead for data administration. However, the beamforming and filtering routines are coded to be as fast as possible with FORTRAN. In addition the optimizer option is used for compilation. Analyzing the time consumed by the different routines, we learn that beamforming is the most time-consuming part for the NORSAR system. Filtering is most time-consuming for the NORESS system. To run the NORSAR recipe for 180 coherent beams and 64 incoherent beams, the system uses 105% of an IBM 4341/L01 or 40 % of an IBM 4381/P02. The relative performance of IBM 4341/L01, 4341/M12 and 4381/P02 for adding vectors only is 1.0, 1.5 and 2.6 respectively. The requirement for doing the same job as RONAPP for detection only, is about 1/3 of the NORSAR processing. An early version of the program has been run on SUN/UNIX system. The current version of the system has been especially designed to avoid possible differences between IBM/CMS and SUN/UNIX systems.

One option in the DP system that we have found very useful, is to stop the system at some selected time point, and look at the current data buffers. An example is given in Fig. IV.5. Any of the data 'channels' may be displayed, and the effect of varying LTA update parameters may be visualized. Likewise different STX integration lengths may be studied to see the capability of STX as a measure to pick arrival times.

To put the new NORSAR detection system into operation requires only minor changes in the current recording system. We need to eliminate subarray beamforming and filtering on the MODCOMP computer, and we need to replace detection processing on the IBM side. However, the current IBM 4341/L01 will not be able to keep up with real time. We may solve this problem in two ways. Either by trying to further speed up the system (some overhead may be reduced by making a copy of the program which is able to process NORSAR data only), or to resample the data to 10 Hz after filtering has been done. The latter resampling

will reduce the load by about 40 %. We will look further into these matters.

The DP system is still in an initial version. The system has proved very flexible in practice, e.g., newly started research on using an expanded beam set for the NORESS array has been easily adopted by the system. However, we feel that there is still room for improvements. One improvement may be to include weighted beamforming. As the program may easily use either tape or NORSAR online disk, we may compare detector results for any period of time. Inclusion of beamforming weights or other detectors can be easily adopted in the program. Better performance for NORSAR by including new delays on the subarray level may be included by no program change, as this is input through the recipe. Maybe the best potential for improved NORSAR detector performance will be the addition of high frequency digital filters. The computer load may, however, give a limitation on this, at least in the near future.

J. Fyen

```
DATA BUFFER LENGTH 40.0 SECONDS
OLD BUFFER LENGTH 9.0 SECONDS
*
INPUT THE FOLLOWING NOTATIONS:
01A01      01A02      01A03      01A04SPZ      01A05      01A00
01B01      01B02      01B03      01B04      01B05      01B00
02B01      02B02      02B03      02B04      02B05      02B00
02C01      02C02      02C03      02C04      02C05      02C00
03C01      03C02      03C03      03C04      03C05      03C00
04C01      04C02      04C03      04C04      04C05      04C00
06C01      06C02      06C03      06C04      06C05SPZ      06C00
END
*
SET DETECTION STATE TRUE
SET REDUCTION      3.000 Seconds
SET INITIAL LTA    3.000
SET THRESHOLD      3.200
SET STX LENGTH     0.500 Seconds
SET STA LENGTH     1.500 Seconds
SET LTA SIGMA      7.000
SET LTA BETA       6.000
SET LTA DELAY      9.000 Seconds
*
FILTER  FILNAM  FILTER FLTYP BANDLW BANDHG IORD
      1  FB1     BU      BP      1.2   3.2   3
      2  FB2     BU      BP      1.6   3.2   3
      3  FB3     BU      BP      4.0   6.0   3
*
FILTER ALL WITH FB1 OUTPUT xxxxxFB1
FILTER ALL WITH FB2 OUTPUT xxxxxFB2
*
DEFINE NAO-AB AS ALL xxxxxFB1
*
USE NAO-AB
*
USE BEAM-TABLE NAO-451 TABLE *
*
DETECT ON ALL
*
DEFINE 01A AS 01A01FB2 01A02FB2 01A03FB2 01A04FB2 01A05FB2 01A00FB2 END
DEFINE 01B AS 01B01FB2 01B02FB2 01B03FB2 01B04FB2 01B05FB2 01B00FB2 END
DEFINE 02B AS 02B01FB2 02B02FB2 02B03FB2 02B04FB2 02B05FB2 02B00FB2 END
DEFINE 02C AS 02C01FB2 02C02FB2 02C03FB2 02C04FB2 02C05FB2 02C00FB2 END
DEFINE 03C AS 03C01FB2 03C02FB2 03C03FB2 03C04FB2 03C05FB2 03C00FB2 END
DEFINE 04C AS 04C01FB2 04C02FB2 04C03FB2 04C04FB2 04C05FB2 04C00FB2 END
DEFINE 06C AS 06C01FB2 06C02FB2 06C03FB2 06C04FB2 06C05FB2 06C00FB2 END
*
* NORSAR Subarray beam # 1 for incoherent beams.
*
MAKE BEAM 01A01 OUTPUT 01A00SAB USING 01A VEL 18.854 AZI 44.236
MAKE BEAM 01B01 OUTPUT 01B00SAB USING 01B VEL 18.854 AZI 44.236
MAKE BEAM 02B01 OUTPUT 02B00SAB USING 02B VEL 18.854 AZI 44.236
MAKE BEAM 02C01 OUTPUT 02C00SAB USING 02C VEL 18.854 AZI 44.236
MAKE BEAM 03C01 OUTPUT 03C00SAB USING 03C VEL 18.854 AZI 44.236
MAKE BEAM 04C01 OUTPUT 04C00SAB USING 04C VEL 18.854 AZI 44.236
MAKE BEAM 06C01 OUTPUT 06C00SAB USING 06C VEL 18.854 AZI 44.236
*
MAKE STX OF 01A00SAB OUTPUT 01A00STX1
MAKE STX OF 01B00SAB OUTPUT 01B00STX1
MAKE STX OF 02B00SAB OUTPUT 02B00STX1
MAKE STX OF 02C00SAB OUTPUT 02C00STX1
MAKE STX OF 03C00SAB OUTPUT 03C00STX1
```

Fig. IV.1 Extracts from the NORSAR detection processor "recipe". All commands except the complete incoherent recipe are listed. An asterisk is used for comments.

```
MAKE STX OF 04C00SAB OUTPUT 04C00STX1
MAKE STX OF 06C00SAB OUTPUT 06C00STX1
*
*
DEFINE NAO-INC1 AS 01A00STX1 01B00STX1 02B00STX1 02C00STX1 03C00STX1
                   04C00STX1 06C00STX1 END
*
*
SET DETECTION STATE TRUE
SET INITIAL LTA      6.000
SET THRESHOLD        2.000
SET STX LENGTH       0.500 Seconds
SET STA LENGTH       1.500 Seconds
SET LTA SIGMA        7.000
SET LTA BETA         6.000
SET LTA DELAY        9.000 Seconds
*
USE NAO-INC1
*
USE BEAM-TABLE NAO-271 TABLE *
*
DETECT INCOHERENT ON BEAM I001
DETECT INCOHERENT ON BEAM I002
DETECT INCOHERENT ON BEAM I005
DETECT INCOHERENT ON BEAM I006
DETECT INCOHERENT ON BEAM I008
DETECT INCOHERENT ON BEAM I010
DETECT INCOHERENT ON BEAM I011
DETECT INCOHERENT ON BEAM I012
DETECT INCOHERENT ON BEAM I013
DETECT INCOHERENT ON BEAM I015
DETECT INCOHERENT ON BEAM I016
DETECT INCOHERENT ON BEAM I018
DETECT INCOHERENT ON BEAM I019
*
```

```

*   NAO-451   Beam Table. NORSAR Coherent beams.
*
* DELAYS FOR BEAM-TABLE NAO-451 FOLLOW
*
STATIONS  01A01   01A02   01A03   01A04   01A05   01A00
           01B01   01B02   01B03   01B04   01B05   01B00
           02B01   02B02   02B03   02B04   02B05   02B00
           02C01   02C02   02C03   02C04   02C05   02C00
           03C01   03C02   03C03   03C04   03C05   03C00
           04C01   04C02   04C03   04C04   04C05   04C00
           06C01   06C02   06C03   06C04   06C05   06C00  END
*
SET REFERENCE 02B00
*
DELAYS FOR BEAM-TABLE NAO-451
*
* NAO #   1 VA 10.890 354.400      GEO 83.0 -7.0
C001     42  -1.665 -1.268  -1.132 -1.382 -1.763 -1.483
          -3.918 -3.757  -3.397 -3.428 -3.929 -3.607
          -3.467 -3.040  -3.128 -3.530 -3.729 -3.402
          -6.124 -5.674  -5.603 -5.963 -6.415 -5.977
          -5.658 -5.223  -5.190 -5.749 -5.917 -5.542
          -3.498 -3.150  -3.280 -3.743 -3.863 -3.518
          -0.683 -0.282   0.000 -0.254 -0.765 -0.441
* NAO #   2 VA  9.243 35.800      GEO 73.0 55.0
C002     42  -0.817 -0.480   0.000 -0.058 -0.646 -0.430
          -2.458 -2.592  -2.171 -1.868 -2.228 -2.138
          -4.004 -3.536  -3.189 -3.533 -3.877 -3.633
          -5.061 -4.621  -4.245 -4.321 -4.985 -4.616
          -7.069 -6.588  -6.154 -6.541 -6.977 -6.670
          -6.305 -5.812  -5.587 -5.935 -6.321 -6.009
          -2.159 -1.779  -1.272 -1.177 -1.719 -1.602
* NAO #   3 VA 12.200 324.900     GEO 72.0 -74.0
C003     42  -2.503 -2.181  -2.259 -2.542 -2.714 -2.475
          -4.408 -4.137  -3.906 -4.101 -4.541 -4.186
          -3.012 -2.721  -3.011 -3.335 -3.405 -3.123
          -5.769 -5.435  -5.541 -5.951 -6.172 -5.816
          -4.207 -3.912  -4.096 -4.595 -4.578 -4.269
          -2.140 -1.961  -2.240 -2.637 -2.588 -2.318
          -0.394 -0.090   0.000 -0.367 -0.724 -0.380

```

Fig. IV.2 Extracts from the NORSAR coherent beam table. The first 3 beams are listed. Beam name C001 - C003 corresponds to 'old' NORSAR partition 1 beam 1 - 3. Delays are here given in seconds relative to the instrument with latest arrival. The program will calculate a correction time for each beam relative to the selected reference station.

```
DATA BUFFER LENGTH 60.0 SECONDS
OLD BUFFER LENGTH 5.0 SECONDS
*
INPUT THE FOLLOWING STATIONS:
A0Z A1Z A2Z A3Z
B1Z B2Z B3Z B4Z B5Z
C1Z C2Z C3Z C4Z C5Z C6Z C7Z
D1Z D2Z D3Z D4Z D5Z D6Z D7Z D8Z D9Z END
*
USE MAX AMPLITUDE FACTOR 3.00 TO MASK DATA
USE NUMBER OF ITERATIONS 2 FOR MAX_AMPLITUDE MASKING
*
SET DETECTION STATE TRUE
SET REDUCTION 3.000 Seconds
SET INITIAL LTA 20.000
SET THRESHOLD 4.000
SET STX LENGTH 0.250 Seconds
SET STA LENGTH 1.000 Seconds
SET LTA SIGMA 6.000
SET LTA BETA 6.000
SET LTA DELAY 5.000 Seconds
*
FILTER FILNAM FILTER FLTTYP BANDLW BANDHG IORD
1 FB2 BU BP 1.0 3.0 3
2 FB3 BU BP 1.5 3.5 3
3 FB4 BU BP 2.0 4.0 3
4 FB5 BU BP 2.5 4.5 3
5 FB6 BU BP 3.0 5.0 3
6 BP41 BU BP 4.0 8.0 3
7 BP42 BU BP 8.0 16.0 3
8 BP60 BU BP 1.0 2.0 3
9 BP61 BU BP 2.0 3.0 3
*
FILTER A0Z WITH FB4 OUTPUT A0FB4
FILTER D1Z WITH FB4 OUTPUT D1FB4
FILTER D2Z WITH FB4 OUTPUT D2FB4
FILTER D3Z WITH FB4 OUTPUT D3FB4
FILTER D4Z WITH FB4 OUTPUT D4FB4
FILTER D5Z WITH FB4 OUTPUT D5FB4
FILTER D6Z WITH FB4 OUTPUT D6FB4
FILTER D7Z WITH FB4 OUTPUT D7FB4
FILTER D8Z WITH FB4 OUTPUT D8FB4
FILTER D9Z WITH FB4 OUTPUT D9FB4
*
FILTER A0Z WITH BP60 OUTPUT A0BP60
FILTER C1Z WITH BP60 OUTPUT C1BP60
FILTER C2Z WITH BP60 OUTPUT C2BP60
FILTER C3Z WITH BP60 OUTPUT C3BP60
FILTER C4Z WITH BP60 OUTPUT C4BP60
FILTER C5Z WITH BP60 OUTPUT C5BP60
FILTER C6Z WITH BP60 OUTPUT C6BP60
FILTER C7Z WITH BP60 OUTPUT C7BP60
*
FILTER A0Z WITH BP61 OUTPUT A0BP61
FILTER C1Z WITH BP61 OUTPUT C1BP61
FILTER C2Z WITH BP61 OUTPUT C2BP61
FILTER C3Z WITH BP61 OUTPUT C3BP61
FILTER C4Z WITH BP61 OUTPUT C4BP61
FILTER C5Z WITH BP61 OUTPUT C5BP61
FILTER C6Z WITH BP61 OUTPUT C6BP61
FILTER C7Z WITH BP61 OUTPUT C7BP61
```

Fig. IV.3 Complete detection "recipe" for emulating RONAPP.  
(page 1 of 3)

```
*
DEFINE TELEV AS A0Z
      C1Z C2Z C3Z C4Z C5Z C6Z C7Z
      D1Z D2Z D3Z D4Z D5Z D6Z D7Z
      E8Z D9Z END
*
*
*
DEFINE INTER AS A0Z
      F1Z B2Z B3Z B4Z B5Z
      C1Z C2Z C3Z C4Z C5Z C6Z C7Z
      D1Z D2Z D3Z D4Z D5Z D6Z D7Z
      E8Z D9Z END
*
*
*
DEFINE CRING AS A0Z
      B1Z B2Z B3Z B4Z B5Z
      C1Z C2Z C3Z C4Z C5Z C6Z C7Z  END
*
*
*
DEFINE BRING AS A0Z A1Z A2Z A3Z
      B1Z B2Z B3Z B4Z B5Z END
*
*
*
MAKE BEAM NRS1  OUTPUT TELEV1  USING TELEV  VEL 99999.9 AZI 0.0
MAKE BEAM NRS2  OUTPUT TELEV2  USING TELEV  VEL 99999.9 AZI 0.0
MAKE BEAM NRS3  OUTPUT INTER3  USING INTER  VEL 99999.9 AZI 0.0
MAKE BEAM NRS4  OUTPUT CRING4  USING CRING  VEL 99999.9 AZI 0.0
MAKE BEAM NRS5  OUTPUT CRING5  USING CRING  VEL 99999.9 AZI 0.0
MAKE BEAM NRS6  OUTPUT BRING6   USING BRING  VEL 99999.9 AZI 0.0
MAKE BEAM NRS7  OUTPUT BRING7   USING BRING  VEL 99999.9 AZI 0.0
MAKE BEAM NRS8  OUTPUT INTER8   USING INTER  VEL 14.3   AZI 0.0
MAKE BEAM NRS9  OUTPUT INTER9   USING INTER  VEL 14.3   AZI 90.0
MAKE BEAM NRS10 OUTPUT INTER10  USING INTER  VEL 14.3   AZI 180.0
MAKE BEAM NRS11 OUTPUT INTER11  USING INTER  VEL 14.3   AZI 15.0
MAKE BEAM NRS12 OUTPUT INTER12  USING INTER  VEL 14.3   AZI 75.0
MAKE BEAM NRS13 OUTPUT INTER13  USING INTER  VEL 14.3   AZI 135.0
MAKE BEAM NRS14 OUTPUT INTER14  USING INTER  VEL 14.3   AZI 25.0
MAKE BEAM NRS15 OUTPUT INTER15  USING INTER  VEL 14.3   AZI 75.0
MAKE BEAM NRS16 OUTPUT INTER16  USING INTER  VEL 14.3   AZI 125.0
MAKE BEAM NRS17 OUTPUT CRING17  USING CRING  VEL 99999.9 AZI 0.0
*
*
*
FILTER TELEV1  WITH FB2   OUTPUT NR01
FILTER TELEV2  WITH FB3   OUTPUT NR02
FILTER INTER3  WITH FB4   OUTPUT NR03
FILTER CRING4  WITH FB5   OUTPUT NR04
FILTER CRING5  WITH FB6   OUTPUT NR05
FILTER BRING6  WITH BP41  OUTPUT NR06
FILTER BRING7  WITH BP42  OUTPUT NR07
FILTER INTER8  WITH FB4   OUTPUT NR08
FILTER INTER9  WITH FB4   OUTPUT NR09
FILTER INTER10 WITH FB4   OUTPUT NR10
FILTER INTER11 WITH FB5   OUTPUT NR11
FILTER INTER12 WITH FB5   OUTPUT NR12
FILTER INTER13 WITH FB5   OUTPUT NR13
FILTER INTER14 WITH FB6   OUTPUT NR14
FILTER INTER15 WITH FB6   OUTPUT NR15
FILTER INTER16 WITH FB6   OUTPUT NR16
FILTER CRING17 WITH FB4   OUTPUT NR17
*
*
*
SET THRESHOLD 4.000
DETECT ON NR01
DETECT ON NR02
DETECT ON NR03
DETECT ON NR08
DETECT ON NR09
```

Fig. IV.3 (page 2 of 3)

```
DETECT ON NR10
DETECT ON NR11
DETECT ON NR12
DETECT ON NR13
DETECT ON NR14
DETECT ON NR15
DETECT ON NR16
DETECT ON NR04
DETECT ON NR05
DETECT ON NR17
SET THRESHOLD 5.000
DETECT ON NR06
DETECT ON NR07
*
MAKE STX OF A0BP60 OUTPUT A0STX60
MAKE STX OF C1BP60 OUTPUT C1STX60
MAKE STX OF C2BP60 OUTPUT C2STX60
MAKE STX OF C3BP60 OUTPUT C3STX60
MAKE STX OF C4BP60 OUTPUT C4STX60
MAKE STX OF C5BP60 OUTPUT C5STX60
MAKE STX OF C6BP60 OUTPUT C6STX60
MAKE STX OF C7BP60 OUTPUT C7STX60
*
DEFINE INCO60 AS A0STX60
C1STX60 C2STX60 C3STX60 C4STX60 C5STX60
C6STX60 C7STX60 END
*
MAKE STX OF A0BP61 OUTPUT A0STX61
MAKE STX OF C1BP61 OUTPUT C1STX61
MAKE STX OF C2BP61 OUTPUT C2STX61
MAKE STX OF C3BP61 OUTPUT C3STX61
MAKE STX OF C4BP61 OUTPUT C4STX61
MAKE STX OF C5BP61 OUTPUT C5STX61
MAKE STX OF C6BP61 OUTPUT C6STX61
MAKE STX OF C7BP61 OUTPUT C7STX61
*
DEFINE INCO61 AS A0STX61
C1STX61 C2STX61 C3STX61 C4STX61 C5STX61
C6STX61 C7STX61 END
*
MAKE STX OF A0FB4 OUTPUT A0STX4
MAKE STX OF D1FB4 OUTPUT D1STX4
MAKE STX OF D2FB4 OUTPUT D2STX4
MAKE STX OF D3FB4 OUTPUT D3STX4
MAKE STX OF D4FB4 OUTPUT D4STX4
MAKE STX OF D5FB4 OUTPUT D5STX4
MAKE STX OF D6FB4 OUTPUT D6STX4
MAKE STX OF D7FB4 OUTPUT D7STX4
MAKE STX OF D8FB4 OUTPUT D8STX4
MAKE STX OF D9FB4 OUTPUT D9STX4
*
DEFINE INCO4 AS A0STX4
D1STX4 D2STX4 D3STX4 D4STX4 D5STX4
D6STX4 D7STX4 D8STX4 D9STX4 END
SET THRESHOLD 2.500
SET INITIAL LTA 100.000
DETECT INCOHERENT ON BEAM IR18 USING INCO60 VEL 99999.9 AZI 0.0
DETECT INCOHERENT ON BEAM IR19 USING INCO61 VEL 99999.9 AZI 0.0
SET THRESHOLD 2.100
DETECT INCOHERENT ON BEAM IR20 USING INCO4 VEL 99999.9 AZI 0.0
*
TERMINAL
*
```

Fig. IV.3 (page 3 of 3)

MORSAR Detector statistics.

MAO = MORSAR Partition 1 Coherent Detector.  
 MAO2 = MORSAR Partition 2 Incoherent Detector.  
 AUT = MORSAR Automatic Event Processor monthly bulletin  
 ARA = MORSAR Analytical Event Processor monthly bulletin  
 DP = MORSAR Beam 001-C180 months 1001-1064 correspond to MORSAR part 1(1-180) and part 2(1-64)  
 DP = JF DP Beams MR01-MR17 and 1R18-1R20 correspond to ROMAPP 1-20  
 MES = MORSAR ROMAPP Detector Results.  
 DAV = MORSAR Event Processor Daily Bulletin.

Detector/DPX	Start time	End tim	Beam#	STA	LTA	SNR	M	Vel	Azi	Comment
Aut	0 118:22-10:39.5	10:39.5		5.10	0.00	0.000	1	33.00	25.3	25.05 178.1W 33C B 4.3 171 SOUTH OF FIJ
MAO	0 118:22-10:39.5	10:39.5		4.40	0.00	0.000	1	17.30	32.0	25.05 178.1W 310G2B 4.2 171 SOUTH OF FIJ
MAO2	64808 118:22-10:39.5	10:43.0	4	1064.00	292.82	1.333	52	31.76	16.6	
DP	0 118:22-10:40.2	10:45.2	C153	1752.78	3.75	14.079	170	31.66	16.6	
DAY	15611 118:22-10:40.2	10:40.2		558.40	0.00	12.800	1	15.80	18.4	59.5W 159.3E 60.7N
MES	15611 118:22-10:41.2	10:44.7	MR04	237.55	18.50	12.773	1	15.81	18.4	
DP	0 118:22-10:42.0	10:43.5	IR19	235.10	15.64	15.035	33	0.00	0.0	
MAO	64810 118:22-10:48.0	10:50.0	154	227.60	68.10	3.342	2	0.00	0.0	
MAO2	64811 118:22-10:48.5	10:50.5	60	1276.00	191.62	6.659	16	38.02	17.1	
DP	0 118:22-10:48.6	10:52.1	1060	1371.00	263.52	5.201	50	38.02	17.1	
DP	0 118:22-10:49.2	10:51.0	IR19	40.87	5.74	7.126	153	38.02	17.0	
AUT	0 118:22-10:49.2	10:51.0		216.29	79.63	2.706	2	40.60	25.3	33.3S 173.5W 33C B 4.1 179 SOUTH OF KER
MAO	15612 118:22-10:49.2	10:49.2		3.20	92.91	4.013	1	8.84	45.0	
MAO2	15612 118:22-10:49.2	10:49.2	1	377.70	46.00	4.400	1	8.80	45.0	
DP	0 118:22-10:49.7	10:49.7	MR01	228.51	54.93	4.160	1	0.00	0.0	
MAO	64812 118:22-10:50.0	10:53.0	154	663.00	177.52	3.733	10	38.02	17.1	
DP	0 118:22-10:51.7	10:52.0	C154	20.63	4.46	4.630	1	0.00	0.0	
MAO	64813 118:22-10:51.7	10:52.0	MR01	242.75	56.18	4.321	1	0.00	0.0	
DP	0 118:22-10:51.7	10:52.0	MR01	587.00	175.12	3.352	2	24.80	13.2	02801 1 02801 1
UP	0 118:22-10:51.7	10:52.0	C177	15.65	4.74	3.300	2	4.70	20.5	
MAO	64814 118:22-10:53.5	10:54.5	251	495.00	148.12	3.342	2	17.37	20.5	
DP	0 118:22-10:53.5	10:56.6	C023	11.92	3.20	3.512	1	8.53	140.1	
DP	0 118:22-10:59.2	20:19.8	C075	11.51	3.85	3.154	1	17.51	273.1	

Fig. IV.4 Extracts from coordinated MORSAR detection log. In this list all information from the different processing systems are coordinated to one list. See comments in the header for explanations.

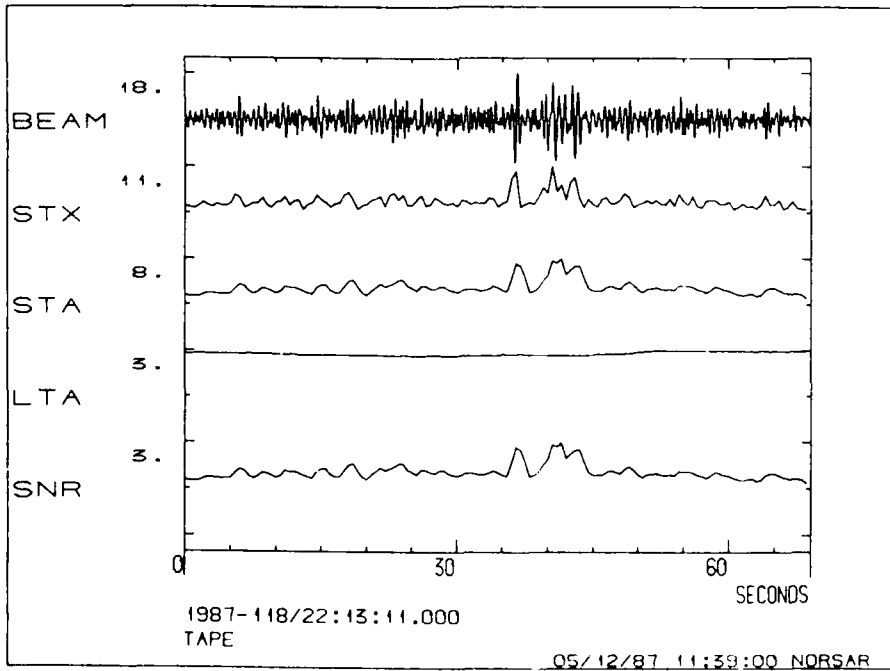
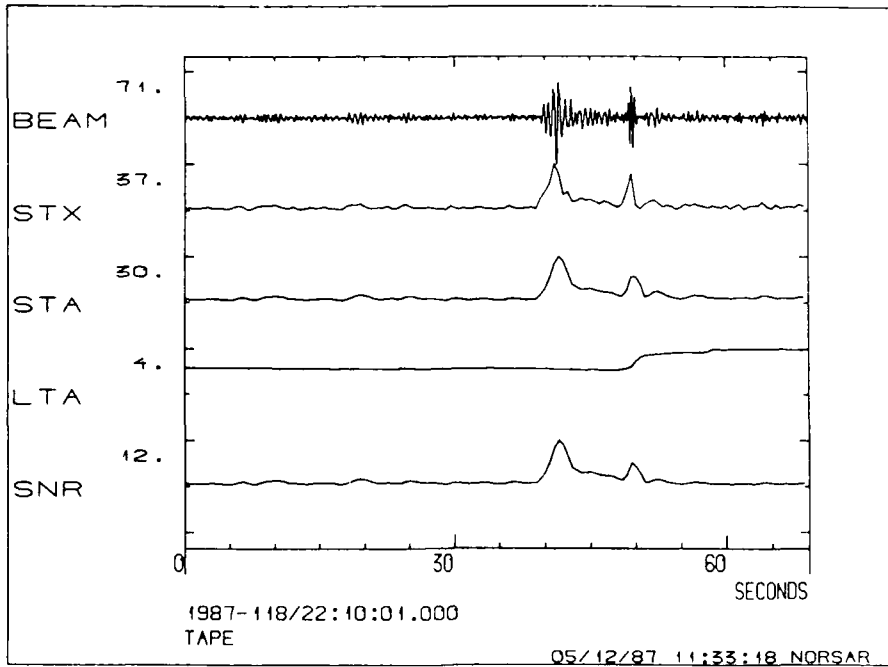


Fig. IV.5 Display of array beam, and STA/LTA detector results for two of the events in Fig. IV.4.

V. MAINTENANCE ACTIVITIES

V.1 Activities in the field and at the Maintenance Center

In the reporting period the NMC staff have been involved in many different tasks related to NORSAR, NORESS, and the second array in Finnmark. The activities have comprised corrective and preventive maintenance for NORSAR and NORESS, including the hub satellite equipment. Meetings and planning related to the second array (NORESS II) and continued HF-experiments in connection with seismometer tests for the HF-installation were also carried out.

At the NMC laboratory, major tasks have been: an amplifier (3-component) for the PDR-2 compuseis Digital Event Recorder built, repair of one CCS-1 communications system equipment, and design of new anti-aliasing filters (8 Hz) for NORSAR.

At the NDPC NORSAR communications circuits (comprising modems and lines) have been regularly monitored.

The NORSAR subarray electronics have been checked and monitored in accordance with established schedules.

A summary of the activities performed during the period is given in Table V.1.

For completeness we list activities carried out for both systems, i.e., NORSAR and NORESS.

Subarray/ area	Task	Date
01A	Gain SP channel 01, 06 adjusted. Mass position all LP seism. adjusted. Test Generator card replaced.	6 Oct
02B	Gain SP channel 01, 03, 04 and 06 adjusted.	7 Oct
02B (tele- metry)	All stations visited in connection with inspection and battery water refilling. Cable channel 05 repaired.	
03C	Visit in connection with communication irregularities, had been unreliable for a while. Several attempts were made to find the source, also NDPC was involved. Data exchange with NDPC OK when the subarray was left, but a concrete malfunction was not located.	1 Oct
04C	Mass position all LP seism. adjusted. Adjusted free period (FP) NS seism. + gain.	15 Oct
04C	Mass position all LP seism., NS FP and gain adjusted.	30 Oct
06C	Adjusted SP gain ch 02, 04, offset ch 03 and mass position NS seism.	2 Oct
NORESS	All vertical GS-13 seismometers glued to the floor. Water leakage in the cable feed trough - tube station 05 stopped.	Oct
Blåsjø	Udenuten station visited and equipment repaired.	27,29 Oct
NDPC	LP/SP-data checked daily. Weekly calibration of SP/LP-instruments. Offline evaluation of 03C SP channels by means of the CHANEV SP-program. Evaluation job 06C rejected by the CHANEV SP program.	Oct
02C	DC-offset all SP/LP-channels adjusted. Channel gain SP 02, 03, 06 + LP vertical and NS adjusted. Mass position and FP all LP seismometers plus FP vertical and NS seism. adjusted.	11,12 Nov

Subarray/ area	Task	Date
SEISNOR	NMC participated in installation of seismometers and amplifiers	18-20 Nov
NDPC	Daily check of SP/LP data. Weekly calibration of SP/LP data. SP-channels all subarrays evaluated by means of the OFF-LINE CHANEV SP program.	Nov
01B	Adjustment of SP channels 01, 04 and 05 gain. Adjustment of mass position (MP) on all LP seismometers.	3,12 Dec
02B	DC-offset SP channel 02, 03, 04 and 05 adjusted. Mass position all LP seismometers corrected. Adjustment of free period vertical seismometers.	12 Dec
02C	Mass position NS seismometer adjusted.	3 Dec
03C	Gain SP channel 01, DC-offset all LP channels and free period vertical/NS seismometers adjusted.	12 Dec
04C	Modem and loop control logic replaced. Adjusted gain SP channel 03-06, Vertical LP channel and mass position (MP) all LP seismometers.	11,12 Dec
06C	Adjusted mass position and free period all LP instruments.	1 Dec
NDPC	Daily routine checks of SP/LP data. Weekly calibration of SP/LP seismometers. A/D converters 01A, 01B evaluated by means of collected data and OFF-LINE MISN program. SP channel 01B evaluated after data collection and the OFF-LINE CHANEV SP program.	Dec

Subarray/ area	Task	Date
		<u>1987</u>
06C	Preventive maintenance in the LP vault	13-15 Jan 19,22 Jan
NMC	Built a 3-component amplifier for the PDR-2 recorder.  Much time spent on planning in connection with the second array in Finnmark.	Jan
NDPC	Daily check of SP/LP data. Weekly calibration of SP/LP seismometers. Besides, OFF-LINE program MISNO run on subarrays U2B, O2C, U3C and O6C in connection with verifying the ability of the A/D conversion.	Jan
O4C	Modem and line tests carried out in cooperation with NDPC.	27 Feb
NMC	Two PDR-2 compuseis Digital Event Recorders and 1 CCS-1 compuseis comm. system have been repaired.  Planning in connection with the second array in Finnmark continued.	Feb
NDPC	Daily routine checks. Weekly calibration of SP/LP instruments.	Feb
O1A	Communication check involving modem lines, etc. Adjustment of gain SP channel O1, U3 and O6; Mass position all LP seismometers, including free period EW seismometer.	25,26 Mar
NORESS	Satellite Tx carrier and output level adjusted.	5 Mar
NMC	Daily routine check of SP/LP data. Weekly calibration of SP/LP instruments.	Mar

Table V.1 Activities in the field and at the NORSAR Maintenance Center, including NDPC activities related to the NORSAR array, 1 October 1986 - 31 March 1987.

V.2      Improvements and modifications (NORSAR array)

No changes since last reporting period.

V.3      Array status

As of 31 March 1987 the following channels deviated from tolerances:

01A	01	8 Hz filter
	02	8 Hz filter
	04	30 dB attenuation
01B	05	
04C	01	
06C	05	Broadband filter installed.

O.A. Hansen

VI. DOCUMENTATION DEVELOPED

Korhonen, H., S. Pirhonen, F. Ringdal, S. Mykkeltveit, T. Kværna,  
P.W. Larsen and R. Paulsen: The Finesa array and preliminary  
results of data analysis, University of Helsinki, Inst. of  
Seismology.

Loughran, L.B. (ed.): Semiannual Technical Summary, 1 April - 30  
September 1986, NORSAR Sci. Rep. No. 1-86/87, Kjeller, Norway.

L.B. Loughran

VII. SUMMARY OF TECHNICAL REPORTS/PAPERS PREPARED

VII.1 Wide-band slowness estimation using a small aperture seismic array

In order to evaluate the location potential of the NORESS array, the slowness of events of known origins have been estimated applying different approaches. The objective of this investigation is to develop methods and rules that can be applied in real-time processing of regional array data and to give an idea of the uncertainty of automatic location estimates.

This study is a continuation of an article presented by Kværna and Ringdal (1986) in the previous semiannual report. In that work, NORESS recordings of ten quarry blasts from a dam construction site in southwestern Norway (Blåsjø) were subjected to detailed analysis applying various types of slowness estimation techniques. Narrow-band and wide-band techniques were compared, and processing in fixed frequency bands were tested against processing in the band with maximum signal-to-noise ratio (SNR). The wide-band, fixed frequency band approach gave by far the most stable results. The maximum spread around the mean for the Pn-phase was only 1 degree. By that approach we were also able to separate the Sn from the Lg phases on the basis of estimated apparent velocity. The mean azimuth of the Lg-phases differed only 1.4 degrees from the theoretical azimuth and the maximum spread around the mean was 2 degrees.

In this study we extend the data base by events from two other sites with known location.

### **Semipalatinsk**

P-wave recordings from sixteen presumed nuclear explosions at Semipalatinsk have been analyzed by the wide band, fixed frequencies approach. A frequency range of 1.5-3.5 Hz was selected. This is for all events close to the optimum filter band for SNR gain on the array beam.

Site coordinates:            50 N 79 E  
True azimuth from NORESS: 75 degrees  
Distance from NORESS:       4200 km

All events, except one, had a very high SNR. As shown in Fig. VII.1.1, the stability of the Semipalatinsk slowness estimates are as good as in the Blåsjø case. The mean azimuth is 78.10 degrees and the maximum spread around the mean is  $\pm 1$  degree.

### **Estonia**

As a third data base for testing of the location algorithms, NORESS recordings of ten mining explosions in the Estonian region of USSR were chosen (see Fig. VII.1.2). These events were located by the network in Finland, and reported by the University of Helsinki.

Site coordinates:            59.5 N 28.5 E  
True azimuth from NORESS: 92 degrees  
Distance from NORESS:       950 km

In the 5.0-7.0 Hz band, the Pn phases of these events had a single channel SNR ranging from 2.7 to 12.6, which is much lower than for the Blåsjø and Semipalatinsk events. The University of Helsinki reported duration magnitudes (Md) in the range 2.5 to 2.9.

Results from wide band slowness estimation of the Pn phases are shown in Fig. VII.1.1. They were all processed in the frequency band 5.0-7.0 Hz. The mean azimuth is 81.38 degrees and the maximum spread around the mean is nine degrees. This is significantly larger than for the two other sites. In addition the mean azimuth has a bias of about ten degrees from the true azimuth of 92 degrees.

#### Automatic estimation of slowness

It is difficult to predetermine fixed frequency bands for slowness estimation, because of the large variation in signal and noise spectra, see Fig. VII.1.3b. A bad choice of frequency may lead to processing in the band with lowest SNR rather than best SNR. A real-time detection processor will use several filter bands and array subgeometries to get the best SNR for different categories of signals. The detection report will therefore contain information about which frequency band and array subgeometry that give the best SNR. By using this information we may stabilize the slowness estimates in various ways. If the SNR is above a given limit, we may if possible, expand the array geometry and thereby make the estimates more stable. We can also stabilize the estimates by increasing the processing bandwidth to higher frequencies, provided the SNR is sufficiently high.

We have tested this idea by processing the ten Estonian events with the same array subgeometry and filter band as for the beam with maximum SNR. The results are shown in Fig. VII.1.3a. The Pn and Sn estimates show a large scatter in both azimuth and velocity. In case of Pn, the scatter is larger than that shown in Fig. VII.1.1, where a fixed frequency band was used. In comparison, the Lg estimates are quite consistent. The mean of the Lg azimuths is 92.98 degrees with a maximum spread around the mean of 6 degrees. We were not able to separate the Sn and Lg phases on the basis of velocity as in the Blasjø case, probably due to lower SNR and a narrower usable bandwidth.

Conclusions and recommendations

This study has shown that employing a wider frequency band clearly tends to increase the stability of the slowness estimates, provided the signal-to-noise ratio is adequate over the band of interest. The stability was found, particularly for Pn, to be remarkably good for the western Norway quarry blasts when using a fixed frequency band for all ten events. The same conclusion applies to the teleseismic P-phases from Semipalatinsk.

If the processing band for slowness estimation is selected from the detection processor information, we should apply the estimated Lg azimuth for location purposes, see Fig. VII.1.3a.

From Fig. VII.1.3b, we can see that the Lg spectra show a more uniform pattern than the Pn spectra. The best frequency band for detection of Lg phases will for this suite of events be 1.0-3.0 Hz, whereas the optimum Pn filter bands will range from 2.5-4.5 Hz to 6.0-8.0 Hz.

The robustness and stability of the Lg azimuth estimates using the detector information are related to the fact that the detection processor for all ten events reports 1.0-3.0 Hz as the filter band with optimum SNR. Thus the detector-based approach is in this case equivalent to the wide-band fixed frequency approach, which we have earlier found to produce the best results.

T. Kværna

References

- Kværna, T and D.J. Doornbos (1986): An integrated approach to slowness analysis with arrays and three-component stations. Semiann. Tech. Summary, 1 Oct - 31 Mar 1986, NOR SAR Sci. Rep. No. 2-85/86 Kjeller, Norway
- Kværna, T. and F. Ringdal (1986): Stability of various f-k estimation methods. Semiann. Tech. Summary, 1 Apr - 30 Sep 1986, NOR SAR Sci. Rep. No. 1-86/87 Kjeller, Norway

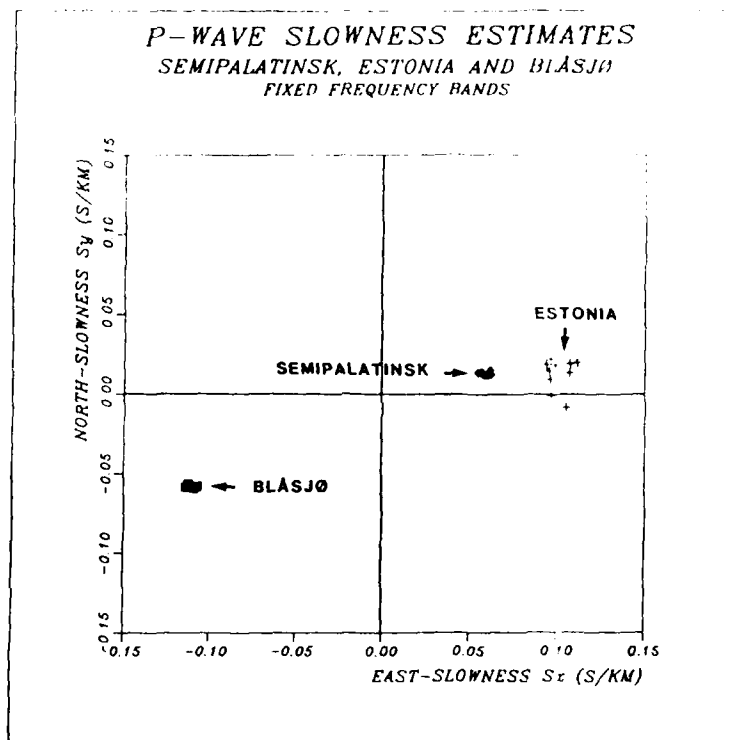


Fig. VII.1.1 Wide band slowness estimates of the P phase for a suite of events from the following sites:

- i) Sixteen presumed nuclear explosions from Semipalatinsk, processed in the 1.5-3-5 Hz band.
- ii) Ten explosions from a mining area in Estonia, USSR, processed in the 5.0-7.0 Hz band.
- iii) Ten quarry blasts at the dam construction site Blåsjø in southwestern Norway, processed in the 5.0-9.0 Hz band.

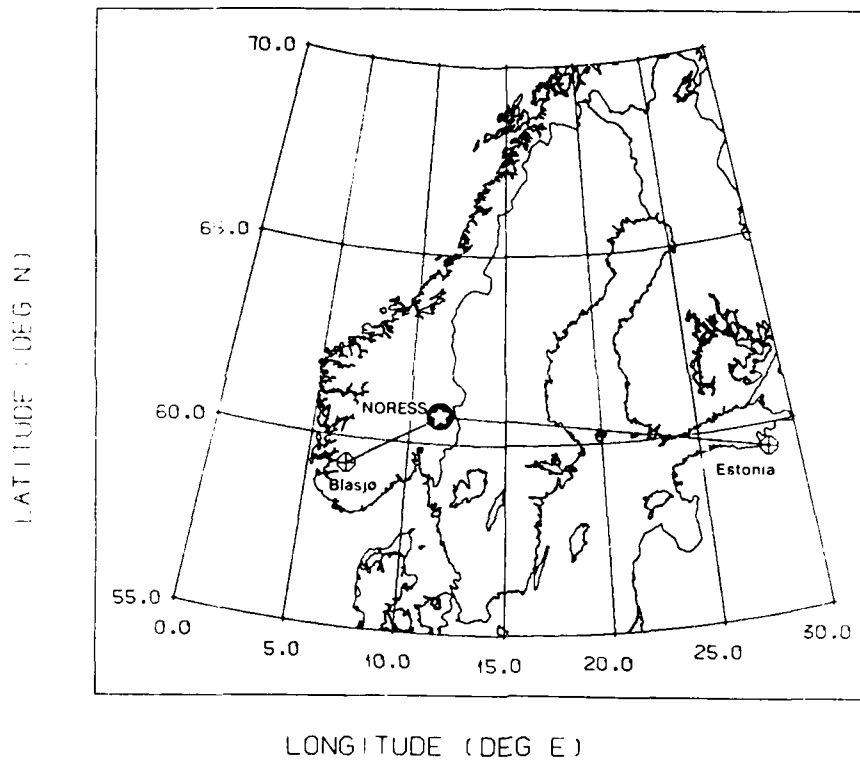
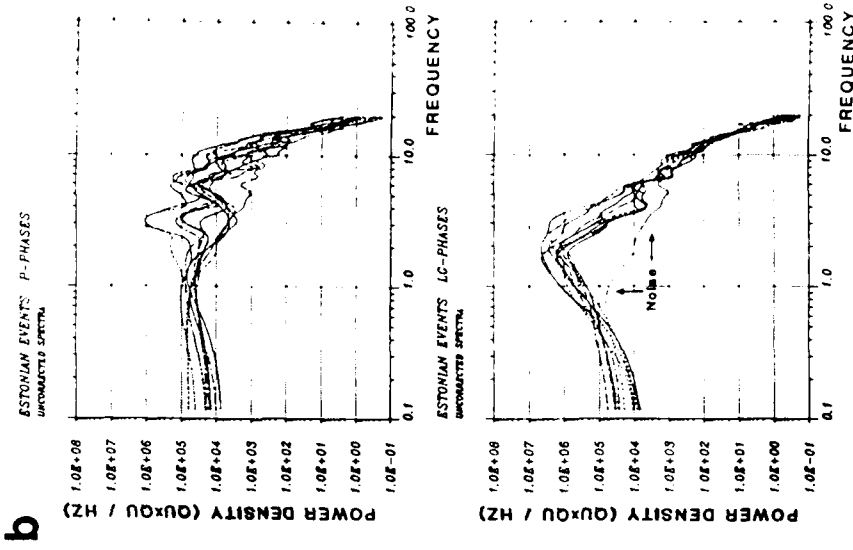
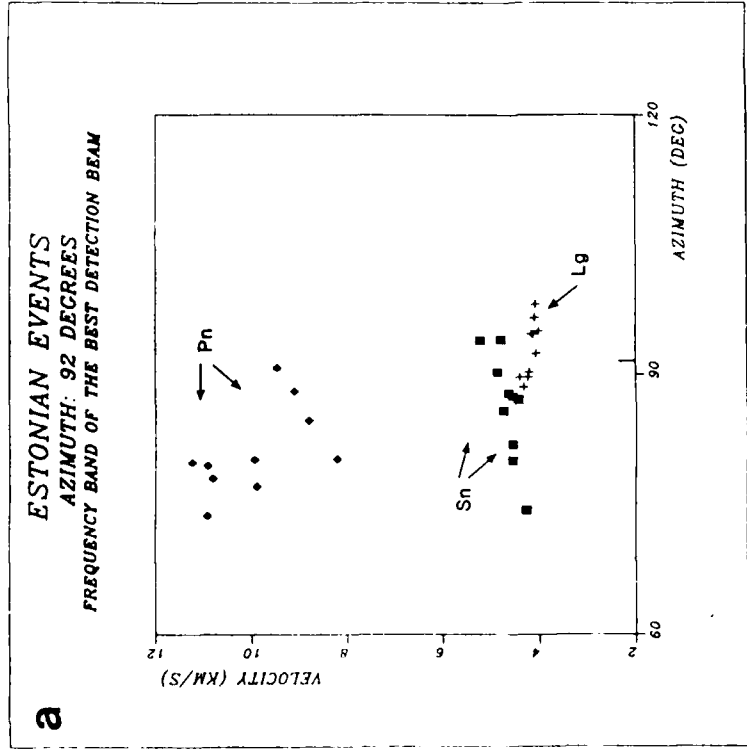


Fig. VII.1.2 Map of Fennoscandia with the NORESS array and the two sites within regional distance from NORESS (Bläsjö and Estonia)



**b**



**a**

Fig. VII.1.1.3 (a) Results using wide band slowness analysis of the Pn, Sn and Lg phases from the ten Estonian explosions. The analysis frequency band has been chosen to be the same as the band of the best detection beam. Note the relatively small spread of the Lg estimates centered around the true azimuth. (b) Pn and Lg spectra for the same events as described in Fig. VII.1.3a. Note the large variation in the Pn spectra of the upper figure with two peaks at about 3 Hz and 6 Hz. The Lg spectra of the lower figure show a more uniform pattern with a peak at about 2 Hz.

VII.2 NORESS noise spectral studies. Noise level characteristics

The NORESS noise recording system has continued to be in operation throughout this reporting period. The system is documented in NORSAR Sci. rep. No 1-86/87, where also results from the first half-year of recording are presented. The system is used to obtain statistics on both noise suppression by beamforming, and the actual variations in the noise level.

The beam suppression results for half a year of data were documented in the referenced report. The continued observation of beam suppression has reconfirmed the conclusions made in that report. The results for the different subarray configurations are consistent and stable over time.

We will therefore not report any further on the beam suppression data, but rather concentrate on the noise level, and in particular extract features important for signal detection.

An initial assessment of diurnal and weekly variations in the NORESS SP noise spectra was given in the mentioned report. Observations from more than one year of data, generally confirm the previous results, but the expanded data base allows us to describe further the effect of cultural noise. To illustrate time-dependent variations we have chosen to use uncorrected data, with variations in power measured in dB. For illustration of the actual noise level, corrected power spectra will also be presented.

Fig. VII.2.1 displays the average NORESS SPZ noise power for a few selected frequencies, plotted versus time for the four-week period Monday, 15 December 1986, through Sunday, 11 January 1987. A vertical dotted grid line is plotted at 00 GMT for every 24 hour period. In

this figure, days which are not normal working days have been identified by hatched rectangles.

As may be seen later from the statistics on seasonal variations, the noise level during the Christmas holidays are among the lowest we have observed throughout one year of data (for frequencies above 2 Hz). We note that although industrial plants are closed, there is a cyclic rise in noise power of 2 -3 dB during the day, with a minimum level at 01 GMT (local time 02).

For days with normal industrial activity the diurnal variation may range from 5 to 15 dB for frequencies above 2 Hz. However, the nighttime minima during the week do not reach the minima we observe during weekends. These observations are consistent throughout one year of data.

These data represent average power from the 25 NORESS SPZ instruments and local effects from wind or other phenomena which may disturb one or a few instruments, will be smoothed out in the average spectra.

To illustrate the seasonal variations we have chosen to use observations made at particular times during each day. For nighttime statistics we have thus chosen local time 02 hours, and for daytime observations we have selected local time 13 on normal working days only. The data time period covered is 31 March 1986 through 04 May 1987. Frequencies selected are the same as used in NORSAR Sci.rep. No. 1-86/87. For each frequency we may compare observations made at 02 and 13 local time to see the effect on noise level from cultural activities. Results are presented in Figs. VII.2 and VII.2.3.

Fig. VII.2.2 shows the noise levels sampled at 02 hours local time. In the figure, each vertical dotted grid line denotes Monday 00 GMT of each week. There are 7 observations within each vertical gridline. We see the cyclic variation of noise level reaching a minimum every

weekend, and a pronounced minimum during Christmas holiday and industry vacation (07 July through 27 July). Thus, the data again show that the variations in the noise level above 2 Hz are to a large extent due to cultural effects. Below 2 Hz we see seasonal variations that are not reflected at the higher frequencies.

Easter holidays (16 - 20 April, 1987), are also characterized by relatively low noise. However, an increase in noise level starts off at the end of the holidays. This is because that time period coincides with the snow melting. This leads to greatly increased water flow in the rivers nearby plus transport of large ice blocks, and the corresponding effects on the seismic noise level are most clearly seen at frequencies above 1.5 Hz.

The snow melting period in Norway normally consists of two phases: first the melting of snow in the low-lands, and later when the snow from the mountains is melting. The first period strongly affects small local rivers, and implies a sharp increase especially in high frequency noise. The second period causes the large more distant rivers to have increased water flow, and the effect on NORESS is mostly confined to a band around 3 Hz.

In 1986 these periods covered the interval late April to early July. The 1987 snow melting started about 20 April. The effect of water flow in the rivers was also documented in former report.

The daytime observations are shown in Fig. VII.2.3. Many of the features are similar to those observed for the nighttime data. Thus, the snow melting period is easily detected. Also, the holidays show pronounced minima, with Christmas being the quietest period.

Otherwise, the noise level at daytime is consistently above that observed at night, even during the common vacation period. (07 July - 27 July 1986).

As displayed in Fig. VII.2.4, data from the NORESS high frequency element (here named HFZ), show the same features with respect to diurnal and weekly variations as do the standard short period instruments. We may infer from the data that above 20.0 Hz, the industrial noise is not as pronounced as for frequencies in the range 2 - 20 Hz. However, as this data is from one single instrument as opposed to the average power from 25 instruments for NORESS SPZ, the data show much more variability. Moreover, the instrument is located at the central site, closer to a road, and high frequency 'signals' from local activity are difficult to eliminate. This is more easily done among the 25 SPZ instruments, where data from each instrument is compared to the average, and excluded from consideration if interpreted as an outlier.

In the lower part of Fig. VII.2.4, we have displayed uncorrected power spectra for the high frequency element observed at 02 local time during the quiet Christmas period. The corrected spectra are shown in Fig. VII.2.5. The peaks in the spectra are due to electronic interference from fans and from the 50 Hz power supply. Fig. VII.2.5 represents a lower bound for NORESS noise level.

As the diurnal and weekly variation is well documented, and seasonal variations are mainly tied to low-frequency noise, we will document the actual noise level at the NORESS site by looking at all observations for selected time points throughout the last two half-year periods. Again we look at local time 02, and local time 13 at work-days. The spectra are corrected for system response, and reported as power density ( $\text{nm}^2/\text{Hz}$ ). Figs. VII.2.6 - VII.2.8 show the results, both for NORESS average SPZ and the High frequency element. NORESS average SPZ data is generally consistent with the high frequency ele-

ment, but small variations may be detected due to the averaging of the SPZ instruments. The data has been divided into the two half-years of recording. During the first half-year, the high frequency data was sampled from the S-3 borehole seismometer at a depth of 60 meter (site F0). During the second half-year, the data is from the GS-13 seismometer, which is located in a shallow avult (site A0). Comparing the MEANZ (average SPZ data) with HFZ for the two periods, we find that the MEANZ and HFZ observations are close to equal during the period when GS-13 was used.

Comparing the upper and lower parts of Fig. VII.2.8, we see some systematic differences. Thus, for frequencies above 6.0 Hz, the surface seismometer shows 5 - 7 dB higher noise level than the borehole instrument.

J. Fyen

86/349:00 - 87/011:23  
MEANZ

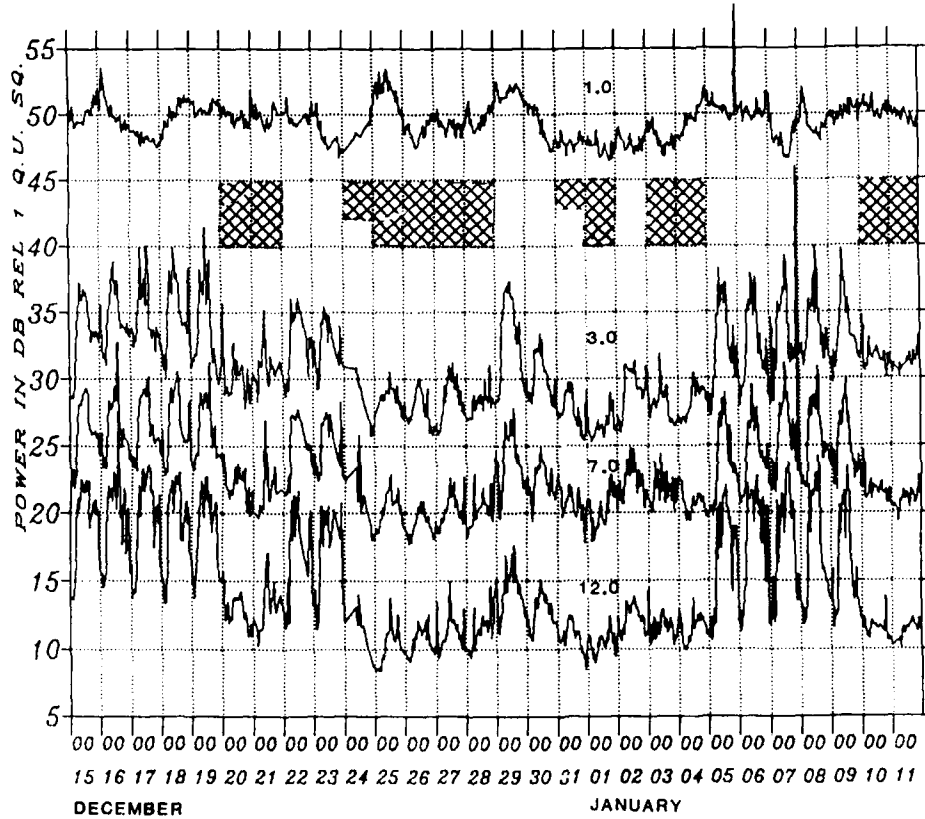
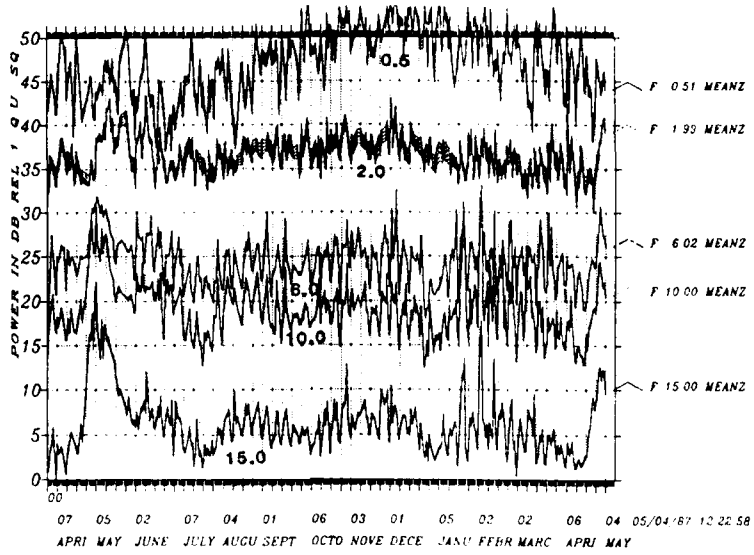


Fig. VII.2.1 Average NORESS SPZ spectral levels plotted on an hourly basis for the four-week period 15 december 1986 through 11 January 1987. Based on the complete noise spectra sampled each hour, the plot shows the power versus time for frequencies within narrow bands ( $\pm 0.1$  Hz). Center frequency for each band is printed on the plot. A vertical dotted grid line is plotted at 00 GMT each day (01 local time). Hatched squares indicate days which are not normal working days.

86/090.00 - 87/130.23 (02 LOCAL ) SINGLE FREQUENCIES  
MEANZ



86/090.00 87/130.23 (02 LOCAL ) SINGLE FREQUENCIES  
MEANZ

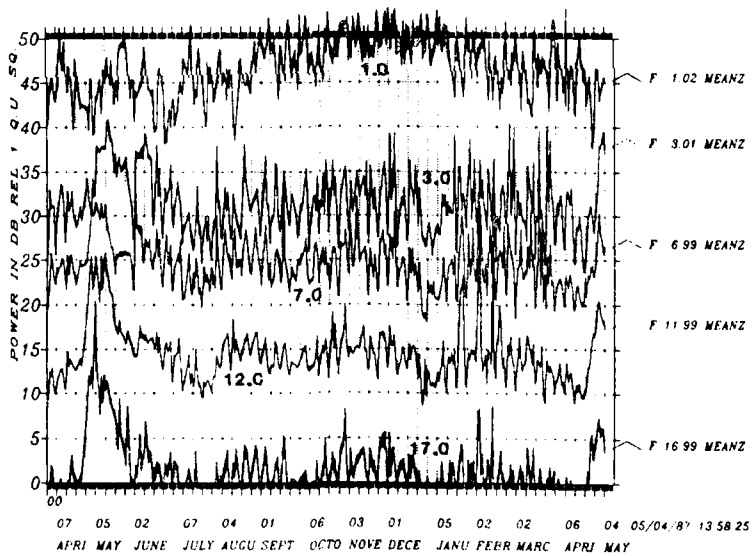
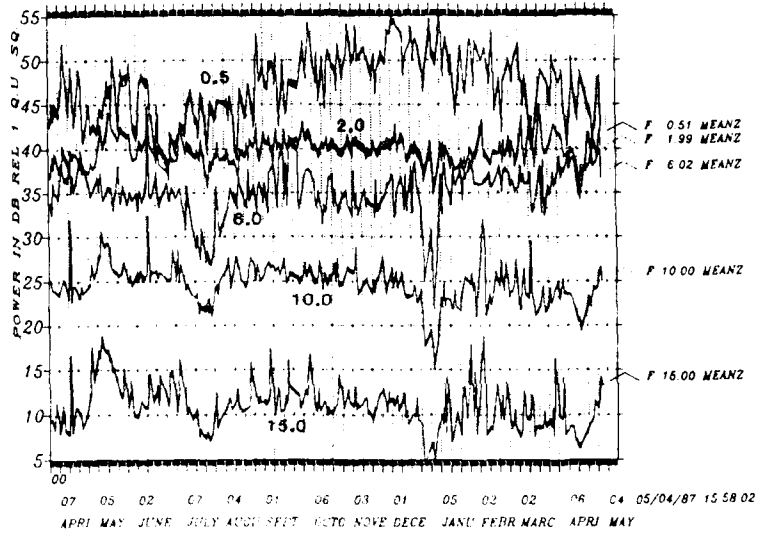


Fig. VII.2.2 Average NORESS SPZ spectral levels observed at 02 local time only, for the period day 090, 1986 through day 130, 1987. There is one point per day per frequency value, and vertical dotted grid lines indicate Monday 00 GMT each week. Frequencies used are identified by the center frequency, and observations that are within  $\pm 0.1$  Hz of center frequency are used. For better legibility, the data are shown in two separate diagrams (top and bottom) with 5 frequency bands in each.

86/090.00 - 87/130.23 (13 LOC WORKDAY) SINGLE FREQUENCIES  
MEANZ



86-090.00 - 87/130.23 (13 LOC WORKDAY) SINGLE FREQUENCIES  
MEANZ

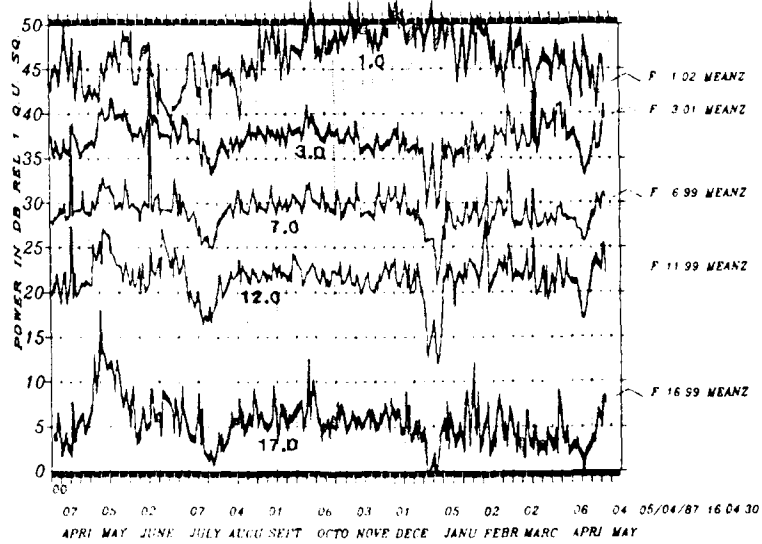
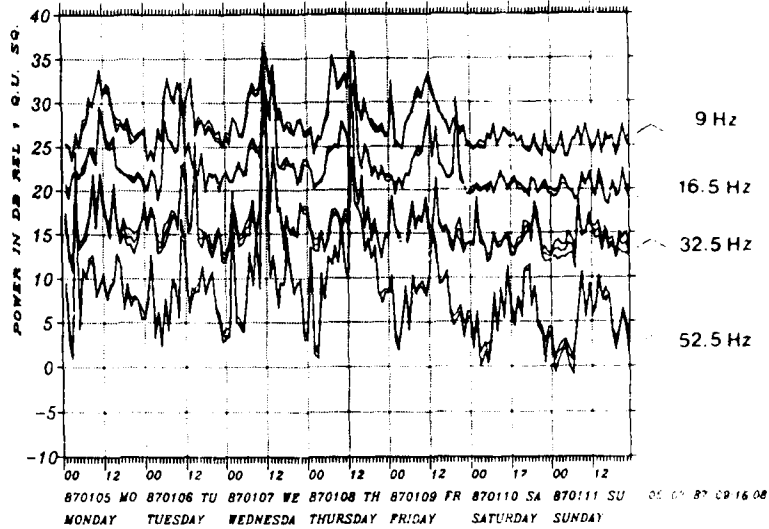


Fig. VII.2.3 Average NORESS SPZ spectral levels as in Fig. VII.2.2, but observed at 13 local time on working days only.

87 WEEK 2 TIME 5: 0 11:23  
HFZ

SINGLE FREQUENCIES



86 TIME 359:00 004:23 (02 LOCAL )  
HFZ

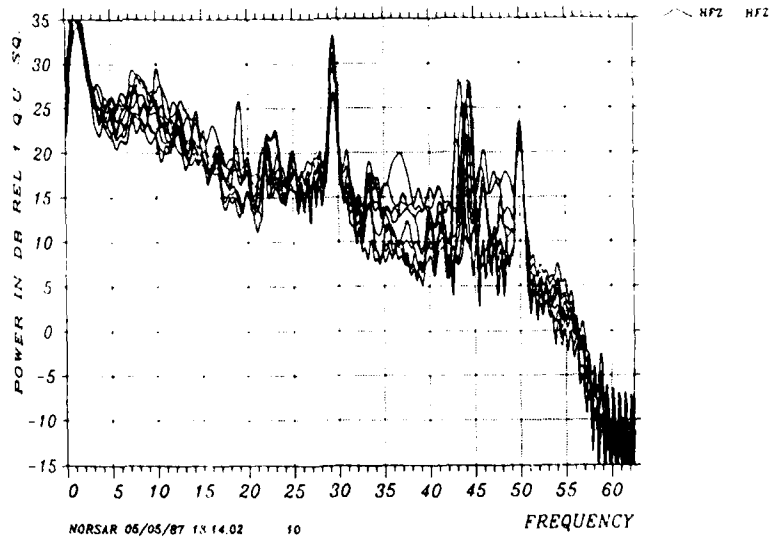


Fig. VII.2.4 NCPSS noise power level as in Fig. VII.2.1, but for the High Frequency Element HFZ. The time period is week 2, 1987 for the upper part of the figure. The lower part show the full spectra for the Christmas holiday period day 359, 1986 through day 004, 1987 at 02 local time only. The spectra have not been corrected for system response.

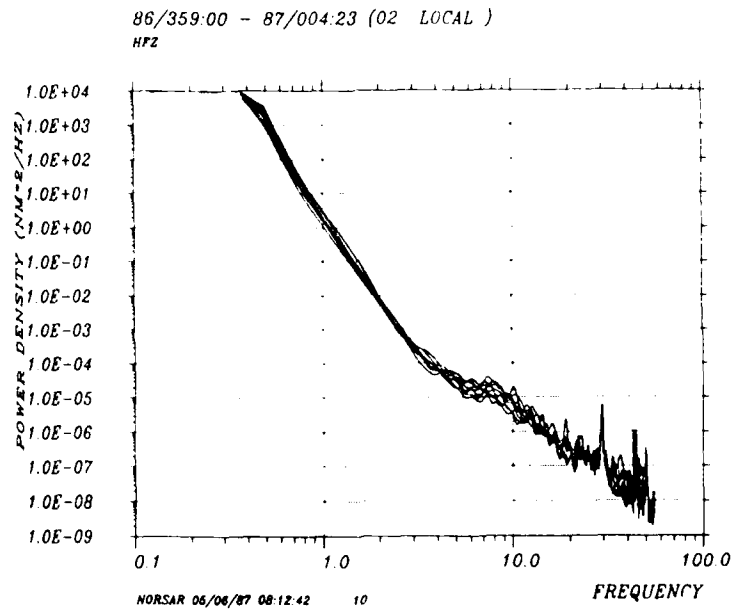
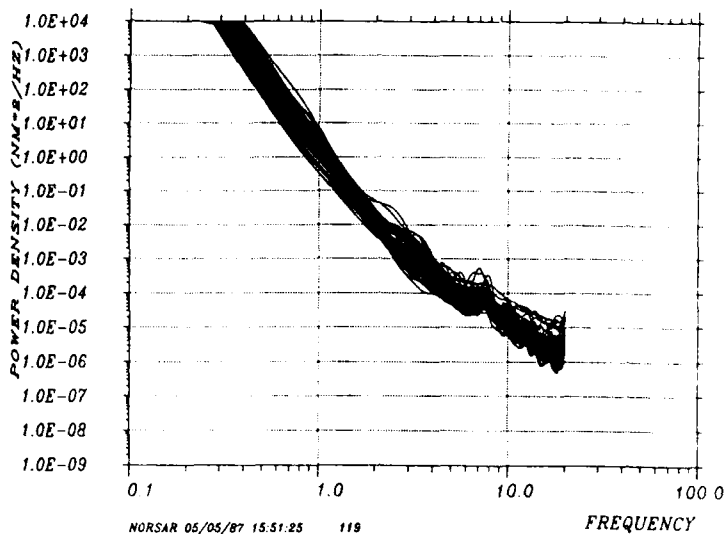


Fig. VII.2.5 NORESS corrected noise power spectra based on data from High Frequency Element. The data are from the period day 359, 1986 through day 004, 1987, observed at 02 local time only.

86/091:00 - 86/273:23 (02 LOCAL )  
MEANZ



86/091:00 - 87/273:23 (02 LOCAL )  
HFZ

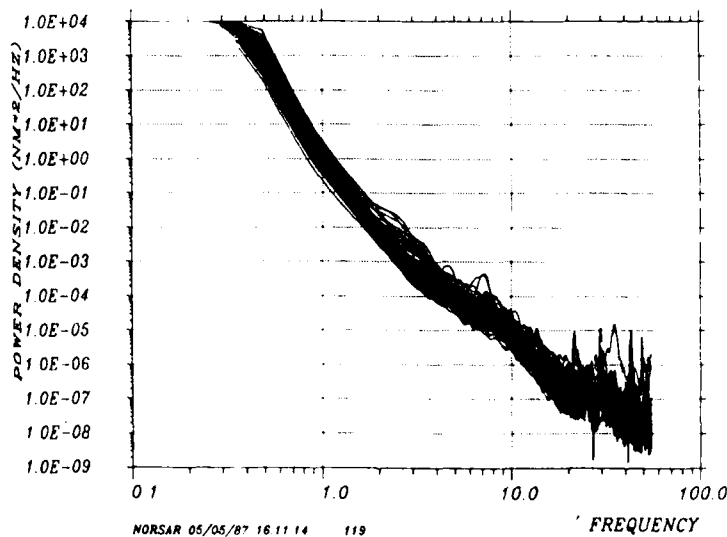
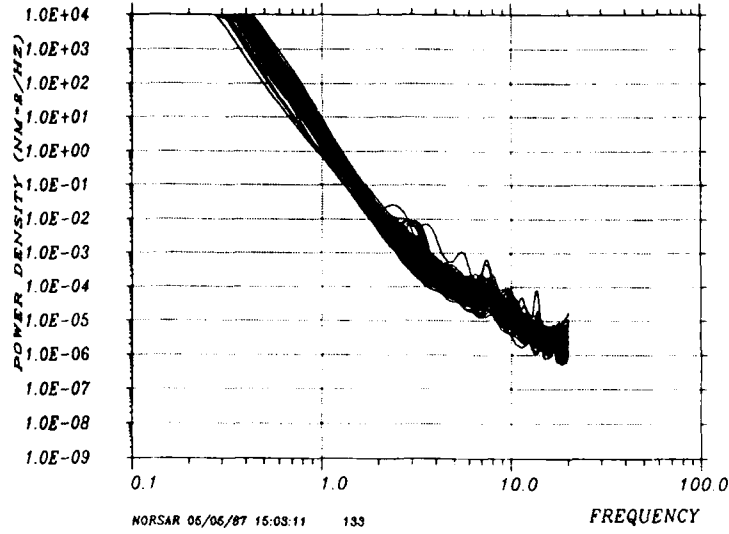


Fig. VII.2.6 NORESS corrected noise power spectra from average of SPZ instruments (upper part) and from NORESS high frequency element (HFZ) on lower part. All spectra observed at 02 local time are displayed. The data are from the period day 091, 1986 through day 273, 1986.

86/274:00 - 87/090:23 (02 LOCAL )  
MEANZ



86/274:00 - 87/090:23 (02 LOCAL )  
HFZ

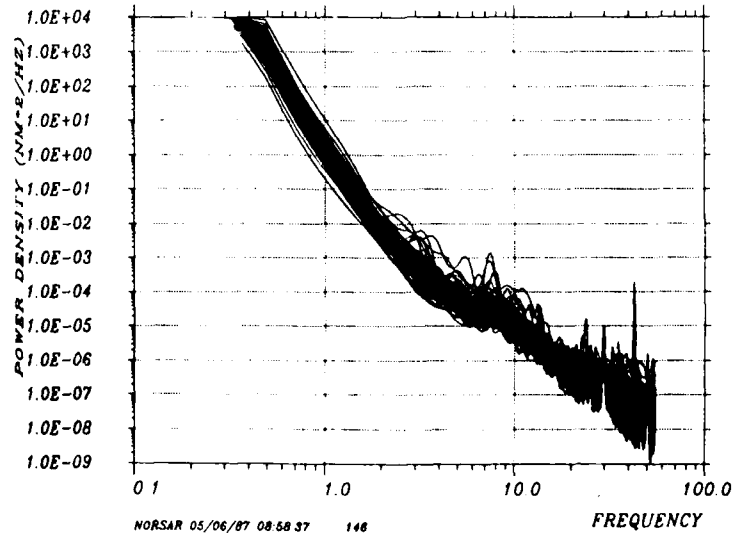
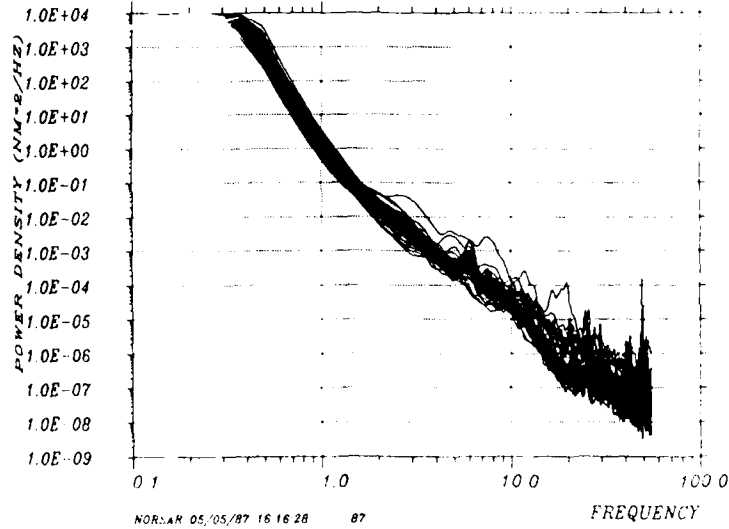


Fig. VII.2.7 NORESS corrected noise power spectra as in Fig. VII.2.4.  
The data are from the period day 274, 1986 through  
day 090, 1987.

86/091:00 - 86/273:23 (13 LOC WORKDAY)  
HFZ



86/274:00 - 87/090:23 (13 LOC WORKDAY)  
HFZ

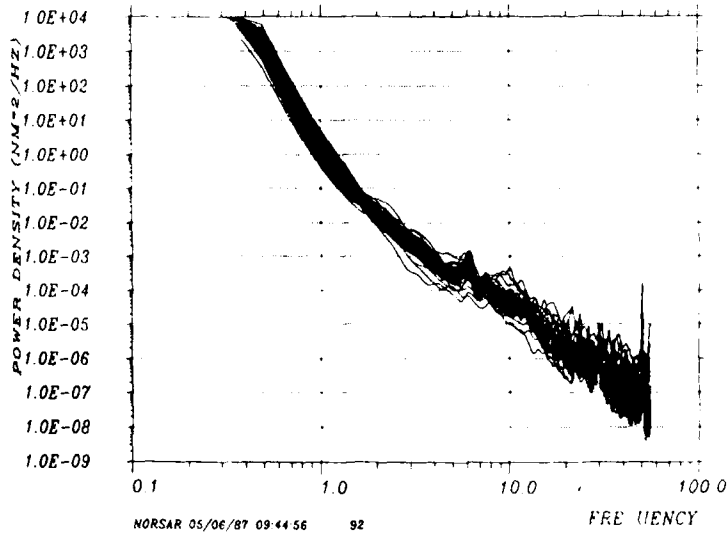


Fig. VII.2.8 NORESS corrected noise power spectra as in Fig. VII.2.4, but for local time 13 and working days only. The data are from the period day 091, 1986 through day 273, 1986 (upper part), and day 274, 1986 through day 090, 1987 (lower part).

VII.3 Initial results from data analysis using the FINESA  
experimental small aperture array

This contribution describes initial research results obtained in conjunction with studies of data recorded by the FINESA experimental array in Finland, and compares these results to those previously obtained at NORESS.

The establishment of FINESA (Finnish Experimental Seismic Array) in late 1985 represents a joint undertaking between the University of Helsinki (Institute of Seismology), Finland, and NTN/NORSAR, Norway. All data and results from the array are openly available to the scientific community.

A comprehensive assessment of the capabilities of FINESA based on the first year of operation has been published by Korhonen et al (1987). The present contribution is essentially a synopsis of that paper, emphasizing features that are particularly relevant to the further development of the small-array concept first introduced with NORESS. The reader is referred to the referenced paper for details on the work described in the following. Copies are available, upon request, from either the University of Helsinki or NTN/NORSAR.

Array deployment

The location of FINESA and the initial array geometry are shown in Fig. VII.3.1. The array is situated near the town of Heinola about 100 km northeast of Helsinki, and the distance to NORESS in Norway is approximately 800 km. FINESA comprises initially a total of 10 SPZ seismometers. The geometry consists of a 3-instrument ring (A1-A3) and a 6-instrument ring (B1-B6). In addition, one element (C1) lies outside these two rings. The maximum intersensor separation is about 1.5 km.

The A1 site also comprises two horizontal SP seismometers, thus providing a 3-component recording system within the array. The coordinates of the individual array sites are given in Table VII.3.1.

The geology of the siting area comprises precambrian gneissic rock, with little or no sedimentary overburden. It was in fact possible to place all seismometers in the initial deployment directly on outcropping rock. Topographically, the area is hilly, with the maximum height difference between sites being about 38 meters.

All 12 seismometers in FINESA are of type Geotech S-13. Data are transmitted in analog form by cables to the central recording site A1. The recorder is a Kinometrics DDS-1105 system, which comprises 12 bits linear A/D converters, a radio receiver for time, a drum recorder (type Kinometrics VRI) and a magnetic tape transport.

The FINESA system has been in operation since November 1985. Most of the time, the recording system has been operated in a trigger mode, using a built-in voting detector. This implies recording typically two minutes of data following each detection. The memory buffer of the Kinometrics system is somewhat limited, but allows 3-4 seconds of noise data preceding each signal onset to be recorded for all channels.

The sampling rate is selectable, with a normal setting of 40 Hz. The anti-alias filter prior to A/D conversion has a high cutoff-frequency of 14.5 Hz. A calibration signal is inserted each time a new tape has been mounted, thus the first file of each tape is a calibration file.

#### Noise studies

For array sites, it is important to establish both the background noise level as a function of frequency and the noise correlation properties, since the gain that can be obtained by beamforming is largely

dependent on the structure of the noise. In the following we summarize our findings regarding ground motion spectra and noise correlation by distance for the FINESA array, and make comparisons with results for the NORESS array.

#### **Ground motion spectra**

In order to obtain an estimate of the ambient noise level at the site of the FINESA array, ground motion spectra were calculated for four time intervals. Two intervals were from November 1985, one during working hours and one during night time. Two intervals from October 1986 were chosen in the same way. For a direct comparison, ground motion spectra for data recorded at the NORESS array were calculated for the same four intervals. All noise spectra were estimated by the indirect covariance method described in Mykkeltveit et al (1985). This method gives the average properties of each noise interval, which in our computations were taken to be 100 seconds long. Each noise interval was visually inspected to ensure the absence of definite signal arrivals.

Fig. VII.3.2 shows ground motion spectra for two of the four intervals, for both FINESA and NORESS. These spectra, and other spectra shown in this report, have been corrected using the system response curves for the arrays.

Our studies so far indicate that for frequencies up to 2 Hz, the noise levels at FINESA and NORESS are comparable. At 1 Hz the noise level ranges between 2 and 20  $\text{nm}^2/\text{Hz}$  for all noise samples. Between 0.5 and 2.0 Hz the falloff of the spectra is generally steep, ranging from 23 to 26 dB/octave for both sites. For both sites, there is a distinct change in the spectral slope at around 2.0 Hz. For frequencies above 2 Hz, however, the shapes of spectra at FINESA differ from those at NORESS, in particular during night time. Between 2.0 and 3.0 Hz the spectral slope has decreased to 7-10 dB/octave for FINESA and 11-13 dB/octave for NORESS. The four FINESA noise samples all show the same

general pattern and reach a minimum level of 42 to 46 dB below the  $1 \text{ nm}^2/\text{Hz}$  level when approaching the Nyquist frequency of 20 Hz.

Comparison of our results with those of Bungum et al (1985) and Tarvainen (1985) confirm that FINESA noise level at high frequencies is relatively high, compared to some other sites in Fennoscandia, but otherwise the results are in good agreement.

#### **Noise correlation by distance**

Both for NORESS and the provisional installations preceding its deployment in 1984, investigations into the correlation properties of the noise field played an important role in design and evaluation efforts. Curves showing intersensor correlation of the noise versus sensor separation can be directly utilized in predicting the signal-to-noise ratio gain that can be obtained by beamforming.

We have computed noise correlation curves for FINESA in the same way as has previously been done for NORESS (see Mykkeltveit et al, 1983; and Bungum et al, 1985). Altogether six noise intervals, each comprising 110 seconds of data, were subjected to correlation analysis in six frequency bands. For each of the frequency bands, the six average correlation curves were plotted on top of each other, and "envelopes" were formed that contained within them all six curves. The results for four of these bands are shown in Fig. VII.3.3, which for comparison also includes envelopes resulting from correlation analysis of noise recorded at NORESS.

All FINESA noise correlation curves show pronounced negative minima for the noise correlation. This feature has been shown to be compatible with a model of isotropic propagating noise near the Rayleigh wave velocity (Mykkeltveit et al, 1983). It has also been demonstrated that a signal-to-noise ratio gain beyond the standard  $\sqrt{N}$  gain ( $N$  being

the number of sensors in the array) can be obtained by taking advantage of the negative correlation properties of the noise, and the "deeper" the negative minima, the larger the array gain.

The FINESA correlation curves appear to attain their minimum values at slightly smaller interstation distances, compared to the NORESS curves and also generally reach lower negative minima. More data analysis, however, is needed to firmly establish this conclusion. The possible implication is that an optimum array at the FINESA site would have a slightly smaller aperture than an optimum array at the NORESS site, and that such an array might have potential for a beamforming gain even exceeding that of NORESS.

#### Signal analysis

In order to demonstrate basic array signal processing techniques and also contribute towards an assessment of the potential of the FINESA miniarray, we have subjected signals from several regional and teleseismic events to detailed analysis. For comparison, NORESS data for two of the regional events were also analyzed, using the same algorithms. Analysis results from two regional events recorded at FINESA are shown in the following; otherwise, reference is made to Korhonen et al (1987).

#### **Detailed analysis of a mining explosion**

Fig. VII.3.4 (top) shows the FINESA data for the three-component station at site A1 for an event at 59.5°N, 28.5°E on December 27, 1985. There are two distinct P phases; the first arriving P phase is followed after about 1.2 s by a much stronger P phase. The dominant phase in the seismograms is the Lg (Sg) phase. We also see clear indications of the 1 Hz Rg phase in the Lg coda. In the bottom part of Fig. VII.3.4 we show the same three seismograms low pass filtered at 1 Hz, and the Rg waves stand out clearly.

Spectra for P, Lg and Rg for this event are shown in Fig. VII.3.5 along with a typical noise spectrum. The signal spectra are computed as described in Mykkeltveit et al (1985) and are based on data window lengths of 5 s for P and Lg and 20 s for Rg. We see that all phases have considerable energy above the noise level throughout the frequency band 1-20 Hz, but we must keep in mind the fact that the Lg signal window used contains high frequency P coda and likewise, the Rg window contains Lg coda arrivals.

Phase velocities and arrival azimuths were estimated using the wide-band frequency wavenumber (f-k) analysis technique described by Kvarna and Doornbos (1986). Fig. VII.3.6 shows frequency-wavenumber spectra for two 1 s long time windows, with each window capturing the onset of a P arrival. Our analysis gives phase velocities that are in good agreement with results from refraction profiling experiments in Finland (e.g., Luosto et al, 1984), for the appropriate epicentral distance. The Lg and Rg phases were also subjected to wide-band f-k analysis and results are shown in Fig. VII.3.7. Again, the phase velocities are indeed as should be expected for these phases. We see that the estimated arrival azimuths are within 2 degrees of the true value (calculated from the network location) for all four phases.

NORESS data for a three component station for this mining explosion (epicentral distance now 954 km) are shown in Fig. VII.3.8 (top). There are three distinct phases: Pn, Sn and Lg. Spectra for these phases and the preceding noise are shown in the bottom part of Fig. VII.3.8. We see that in particular Pn, but also Sn, has energy well above the noise for frequencies up to 15-20 Hz. In comparing FINESA and NORESS P-wave spectra for this event, we see that there are similarities, and both spectra exhibit a pronounced peak at about 6 Hz.

#### **Analysis of FINESA data for a Bothnian Bay earthquake**

FINESA data for an earthquake that occurred in the Bothnian Bay on October 27, 1986 (magnitude  $m_D = 2.6$ , according to the Helsinki bulletin) are shown in Fig. VII.3.9. The epicentral distance from FINESA is 426 km. The phases Pn (very weak, just above the noise amplitude), Pg, Sn and Lg can be seen, and again, Lg is the overall dominant phase. Spectra for Pn, Sn and Lg, as well as the preceding noise are shown in Fig. VII.3.9 (bottom part). We observe that for Pn and Sn, the SNR is essentially constant over the frequency ranges 8-15 Hz and 4-15 Hz, respectively. The SNR may be constant over an even larger frequency range, but in analyzing these data we are limited by the 40 Hz sampling rate and the analog filter cut-off frequency of 14.5 Hz.

Wide-band f-k spectra were computed for the phases Pn, Sn and Lg and results are shown in Fig. VII.3.10. We see that again the resulting phase velocities are in agreement with the expectations, and there is also an indication that Sn has a slightly higher phase velocity than Lg. The derived azimuths are all a little on the high side of the "true" value of 323 degrees.

#### Event detection studies

In the initial mode of operation, the FINESA data acquisition system has been based on event recording using the built-in detector of the Kinometrics DDS-1105. A detection is declared whenever the short-term to long-term signal ratio exceeds a predefined threshold on at least two out of three pre-selected channels.

This mode of operation has provided a considerable amount of event recordings for research purposes, but clearly does not provide a good measure of the inherent detection capability of the array. Therefore, we have also studied in detail continuous recordings over a shorter time period, using off-line processing with more advanced detection

algorithms. The results from this experiment are described in the following.

For the two-week period 21 Oct - 3 Nov 1986, the FINESA array was operated in the continuous recording mode. Because of the frequent tape changing necessary, the standard 40 Hz array data was recorded only during daytime, i.e., from about 0400 GMT to about 1800 GMT. For our purposes, this was quite adequate since the vast majority of reported regional events (quarry blasts) occur during daytime.

Detection analysis of the recorded "continuous" data was done using the RONAPP program (Mykkeltveit and Bungum, 1984) adapted to the FINESA configuration. Thresholds were set equal to those in use at NORESS and this resulted in a relatively large number of false alarms. Nevertheless, actual detections could be confidently identified by checking signal parameters such as SNR, frequency, estimated phase velocity and azimuth, and this was done by the analyst for the time period 21 -31 Oct.

The detections were then associated to the Helsinki regional bulletin. Considering only those bulletin events occurring when the FINESA system was in actual operation, we found that out of 68 reference events, 54 had at least one detected phase at FINESA, i.e., 84 per cent. This could be compared to the typical NORESS performance: For one year (1985) we found that NORESS reported at least one phase for 28 per cent of the events in the Helsinki regional bulletin (996 out of 3521). Thus, the advantage of being close to most epicenters outweighs by far the lower SNR gain in this case.

Both the P and S (or Lg) phases were detected for the majority of events. In addition, several Rg detections were made for events out to about 250 km epicentral distance.

In Fig. VII.3.11 the azimuths estimated for the P and S phases are plotted against true azimuth (derived from the Helsinki bulletin). The median (50%) error is about 5 degrees for both P and S, which is comparable to initial results reported for NORESS (Mykkeltveit and Ringdal, 1981). In that paper, the procedure later adopted for RONAPP was used, although time picks were made by the analyst rather than automatically.

Fig. VII.3.12 shows estimated phase velocities as a function of true azimuth for P and S phases, respectively. The line at 6 km/s is the separation line currently in use at NORESS, and it seems to provide quite good phase discrimination capabilities between primary and secondary phases also at FINESA. However, the separation is not 100 per cent, and there is a fair amount of scatter in the estimated velocities, even for events located close together. We consider that a somewhat larger array geometry will be necessary to obtain more stable phase velocity estimates, although broad-band estimation provides some improvements in this regard.

#### Conclusions

Noise characteristics: The seismic noise level at the FINESA site is slightly higher than that of NORESS at high frequencies (2-15 Hz) and comparable to that of NORESS in the 0-2 Hz band. This is consistent with previous observations for Fennoscandia. No particular noise sources have been identified in the vicinity of the array. The spatial noise correlation between sensors is very similar to that observed at NORESS; in particular the strong negative correlation at selected distance/frequency combinations is present also at FINESA, and appear to be even more pronounced than at NORESS.

Signal characteristics: The signal frequency contents at FINESA are comparable to those observed at NORESS, given similar epicentral distance. Signal correlation across the array is high, as expected,

except at very high frequencies. A noteworthy feature at FINESA is the presence of strong, coherent Rg waves (1 second period) for explosions out to more than 200 km distance. In contrast, NORESS does not observe Rg beyond 50-60 km.

Detection capability: The FINESA detection capability is excellent, both for regional and teleseismic phases. Our initial studies have indicated that with a sensitive KONAPP-type detector the array is capable of detecting more than 80 per cent of all regional events reported in the University of Helsinki Bulletin, in addition to a large number of events not included there. The detection capability is naturally somewhat lower when the built-in voting detector of the present Kinematics system is applied.

Phase characterization: The phase identification capability of the initial FINESA deployment has been evaluated using both single frequency and broadband f-k analysis. The estimated phase velocities are generally reliable indicators of phase type (primary or secondary), although the separation is not 100 per cent. The resolution is not sufficient to separate Sn from Lg on phase velocity alone, a result also found at NORESS. Azimuth estimates are sufficiently accurate for successful phase association; median error was found to be about 5 degrees both for P and S, using automatic, single frequency f-k estimation.

One of the main achievements of the FINESA study has been to demonstrate that many of the processing techniques that have contributed to the outstanding performance of NORESS can be successfully applied also at other sites in Fennoscandia. This opens up for the

possibility of significantly improved capabilities when applying data from several regional arrays in a future multi-array processing scheme.

F. Ringdal  
S. Mykkeltveit  
T. Kværna  
P.W. Larsen  
R. Paulsen  
H. Korhonen, Univ. of Helsinki  
S. Pirhonen, Univ. of Helsinki

#### REFERENCES

- Bungum, H., S. Mykkeltveit & T. Kværna (1985): Seismic noise in Fennoscandia, with emphasis on high frequencies, Bull. Seism. Soc. Am., 75, 1489-1514.
- Korhonen, H., S. Pirhonen, F. Ringdal, S. Mykkeltveit, T. Kværna, P.W. Larsen and R. Paulsen (1987): The Finesa array and preliminary results of data analysis, Univ. of Helsinki, Inst. of Seismology.
- Kværna, T. & D.J. Doornbos (1986): An integrated approach to slowness analysis with arrays and three-component stations. In: NORSAR Semiannual Technical Summary, 1 Oct 85 - 31 Mar 86 (L.B. Loughran, ed.), NORSAR, Kjeller, Norway.
- Luosto, U., E. Lanne, H. Korhonen, A. Guterch, M. Grad, R. Materzok & E. Perchuc (1984): Deep structure of the earth's crust on the SVEKA profile in central Finland. Annales Geophys. 2, 559-570.
- Mykkeltveit, S. & H. Bungum (1984): Processing of regional seismic events using data from small-aperture arrays. Bull. Seism. Soc. Am., 74, 2313-2333.
- Mykkeltveit, S. & F. Ringdal (1981): Phase identification and event location at regional distances using small-aperture array data. In: Identification of Seismic Sources - Earthquakes or Underground Explosion (E.S. Husebye & S. Mykkeltveit, eds.), D. Reidel Publ. Co., Dordrecht, The Netherlands.

Mykkeltveit, S., K. Åstebøl, D.J. Doornbos & E.S. Husebye (1983):  
Seismic array configuration optimization. Bull. Seism. Soc. Am.,  
73, 173-186.

Mykkeltveit, S., D.B. Harris & T. Kvarna (1985): Preliminary  
evaluation of the event detection and location capability of the  
small-aperture NORESS array. In: NORSAR Semiannual Technical  
Summary 1 Oct 84 - 31 Mar 85 (L.B. Loughran, ed.), NORSAR,  
Kjeller, Norway.

Tarvainen, M. (1985): Results of noise studies in Finland 1981-1984,  
Report No. T-30, Inst. of Seismology, Univ. of Helsinki.

Station Code	Latitude (*N)	Longitude (*E)	Altitude (m)
ALNS	61.4444389	26.0793387	137.92
ALZ	61.4444439	26.0793270	137.86
ALEW	61.4444462	26.0793442	137.92
A2	61.4412337	26.0736561	161.60
A3	61.4447211	26.0715517	153.43
B1	61.4422706	26.0844928	164.98
B2	61.4390893	26.0984178	158.69
B3	61.4394023	26.0705952	175.57
B4	61.4435798	26.0650265	157.84
B5	61.4466901	26.0710893	142.68
B6	61.4469378	26.0808177	146.85
C1	61.4384113	26.0595485	157.69

Accuracy internal: 0.1 m  
" global: approx. 10 m

Table VII.3.1 FINESA seismometer coordinates.

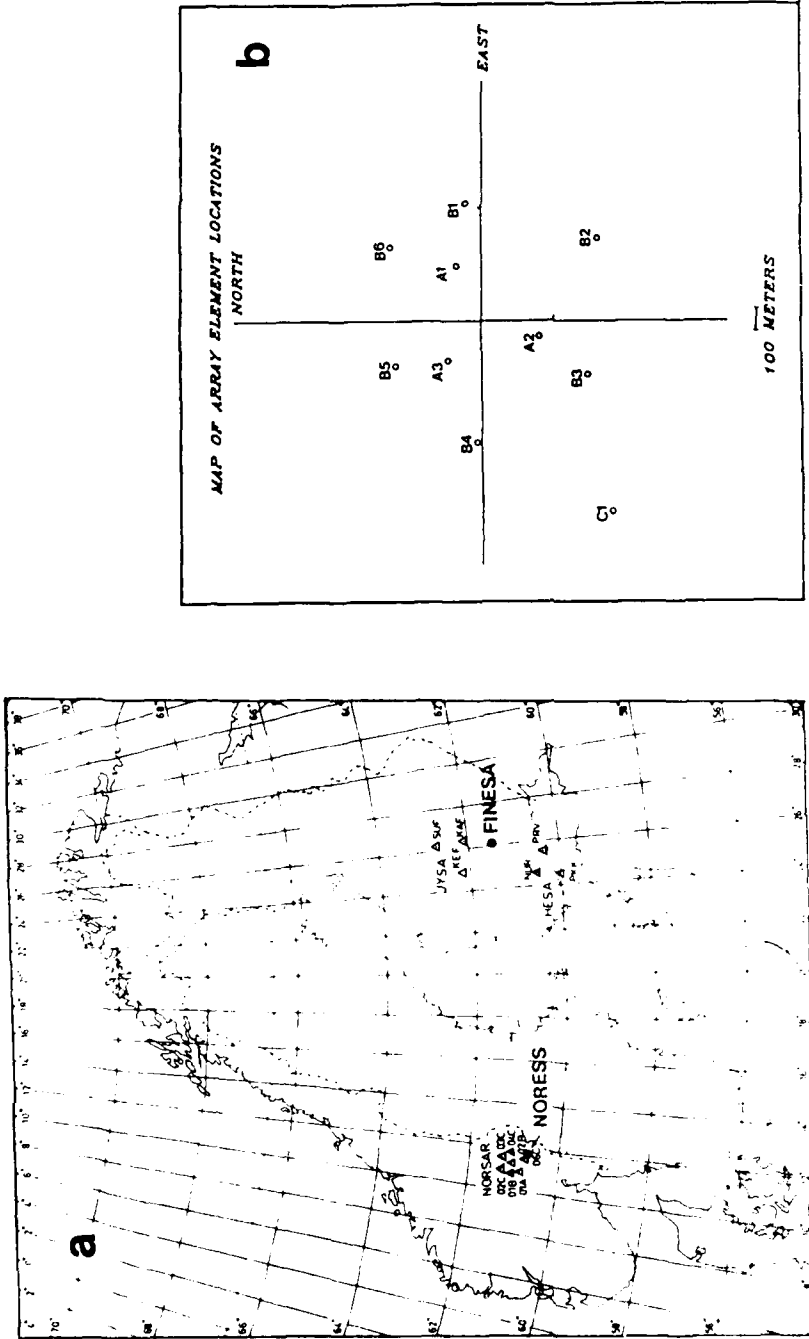


Fig. VII.3.1 (a) A map of Fennoscandia showing the locations of NORESS and FINESA relative to other seismic arrays in Norway and Finland. (b) The initial FINESA geometry is also shown. The central recording equipment is at site A1, which also comprises a three-component short period seismometer system. All other sites contain vertical SP seismometers only.

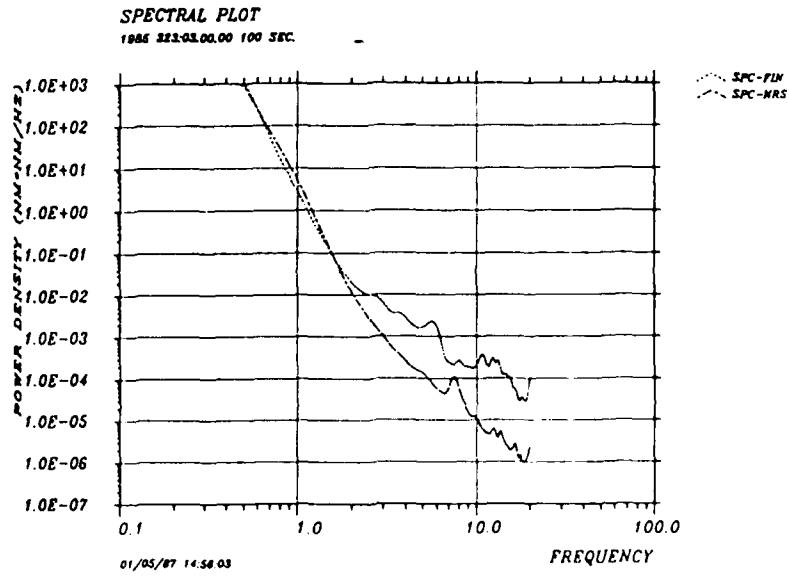
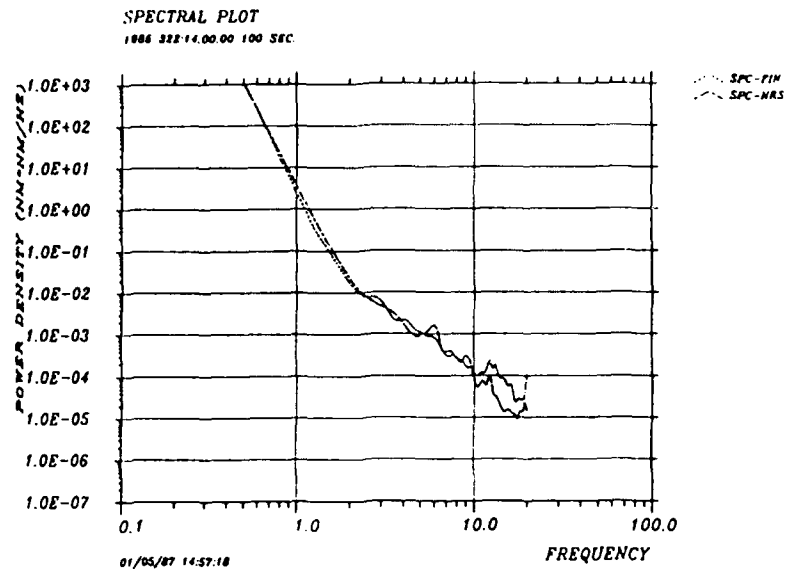


Fig. VII.3.2 FINESA and NORESS ground motion spectra for day 322, 1400 GMT (top) and day 323, 0300 GMT (bottom) of 1985. The FINESA noise spectra are given by dotted lines, whereas the curves for NORESS are dashed-dotted.

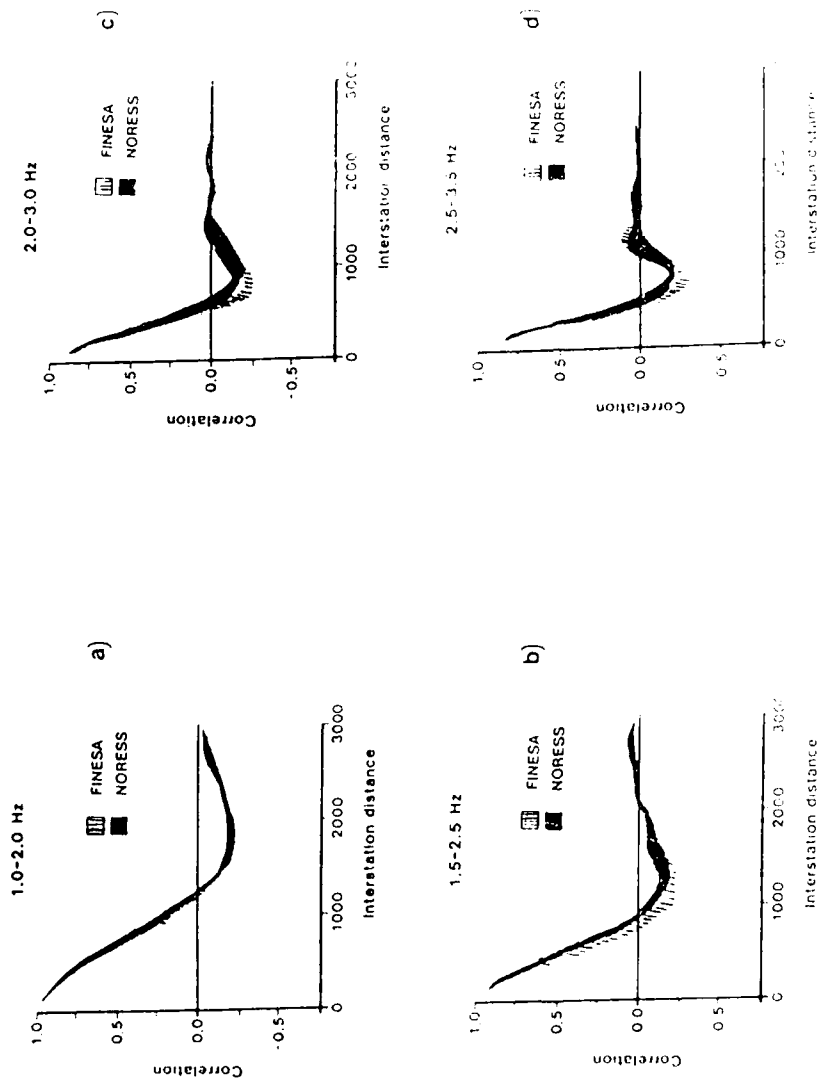


Fig. VII.3.3 Average noise correlations (see text) for four frequency bands for the FINESA and NORESS arrays.

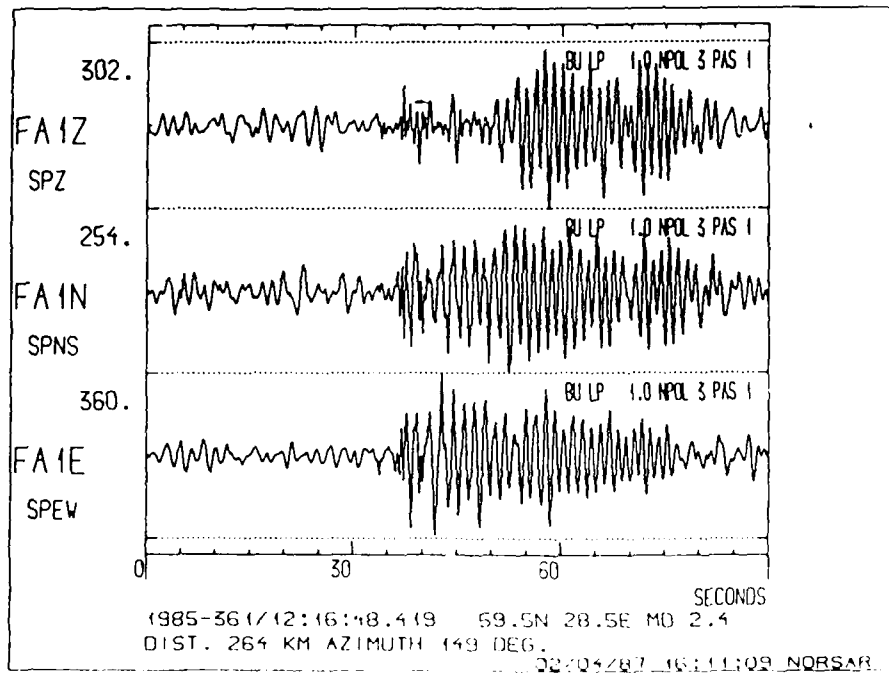
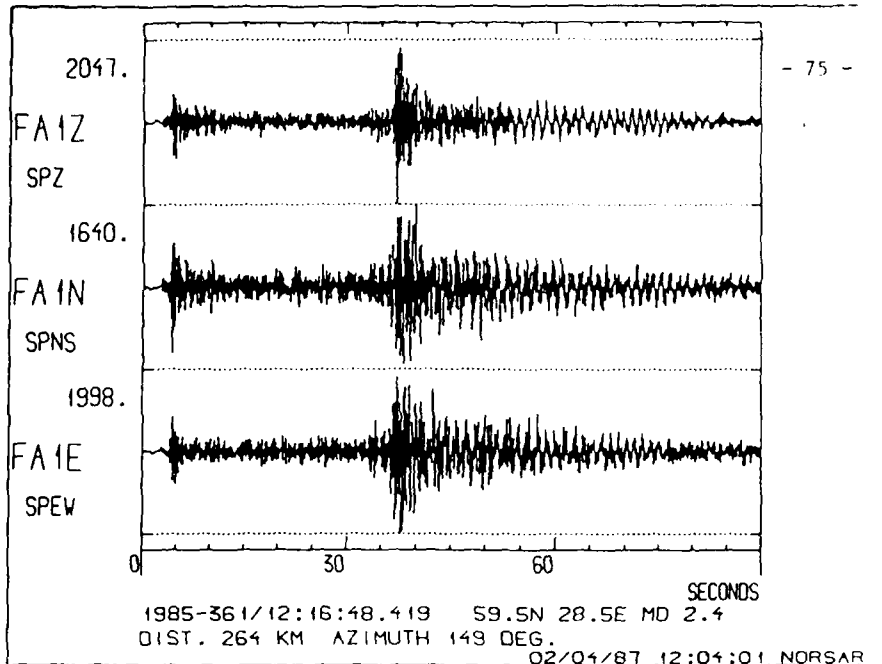


Fig. VII.3.4 FINESA data for a mining explosion (top) and the same data low pass filtered at 1 Hz (bottom). Distance and azimuth given on the plots are according to the epicenter determination by the network of the university of Helsinki.

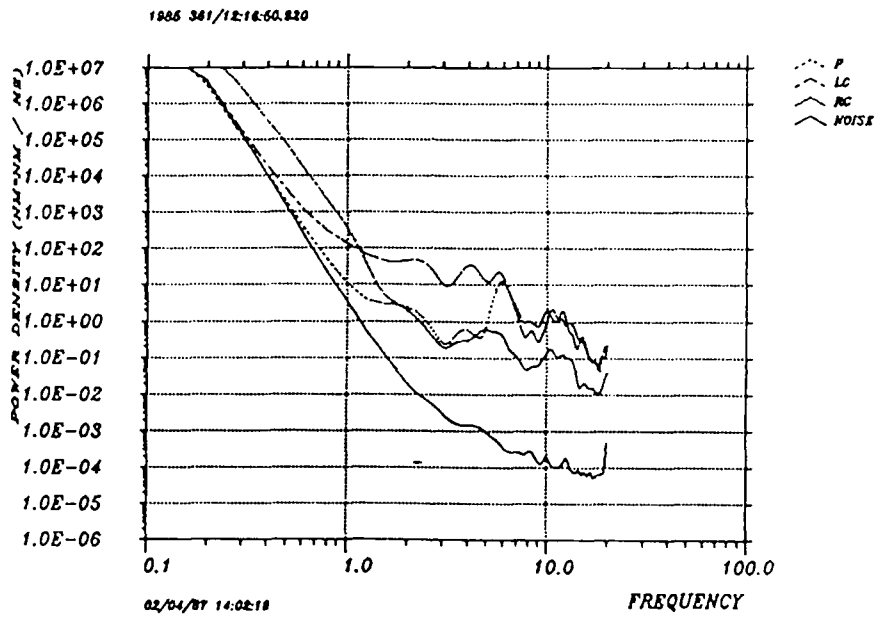
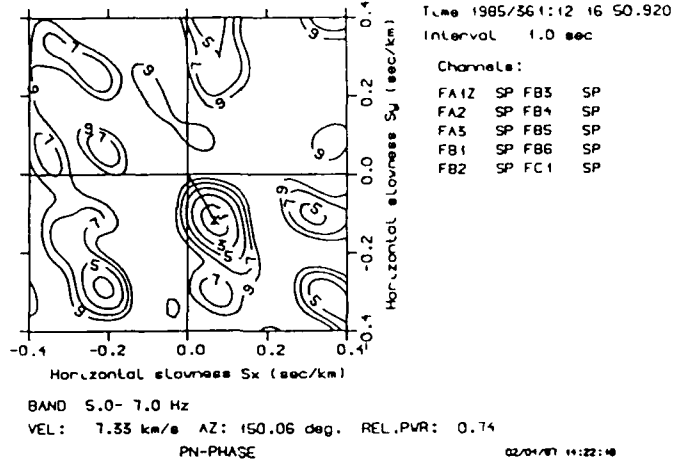


Fig. VII.3.5 Spectra for the phases P, Lg and Rg and noise, for data shown in Fig. VII.3.4.

Wide-band slowness analysis  
Contours in decibels below maximum peak



Wide-band slowness analysis  
Contours in decibels below maximum peak

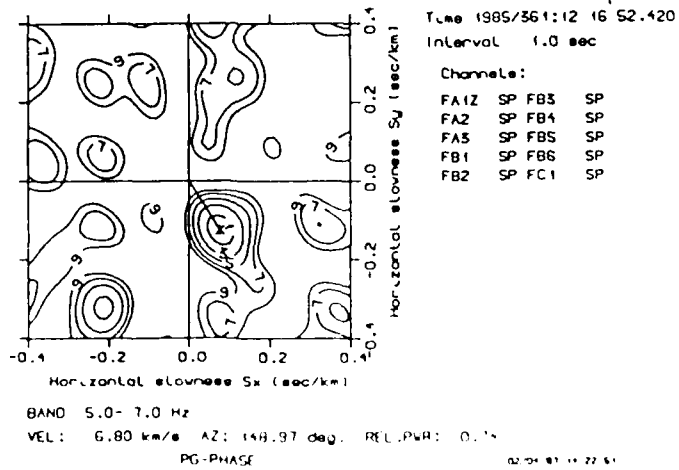
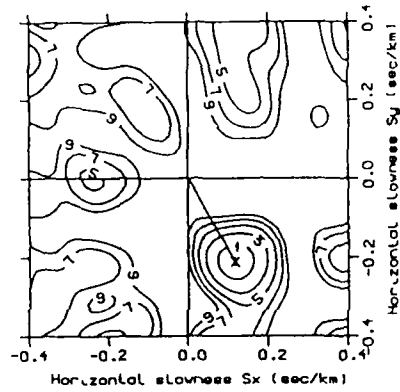


Fig. VII.3.6 Wide-band f-k spectra for the first arriving P phase (top) and the following strong P phase (bottom) of the event in Fig. VII.3.4.

Wide-band slowness analysis  
Contours in decibels below maximum peak



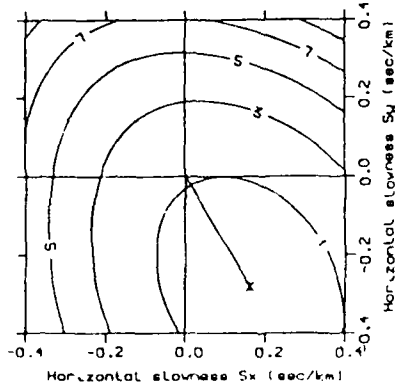
Time 1985/361:12 17'24.420  
Interval 5.0 sec

Channels:  
FA1Z SP FB3 SP  
FA2 SP FB4 SP  
FA3 SP FB5 SP  
FB1 SP FB6 SP  
FB2 SP FC1 SP

BAND 5.0- 7.0 Hz  
VEL: 4.13 km/s AZ: 151.28 deg. REL.PVR: 0.62  
LG-PHASE

02/01/87 11:20:26

Wide-band slowness analysis  
Contours in decibels below maximum peak



Time 1985/361:12 17'41.420  
Interval 24.0 sec

Channels:  
FA1Z SP FB3 SP  
FA2 SP FB4 SP  
FA3 SP FB5 SP  
FB1 SP FB6 SP  
FB2 SP FC1 SP

BAND 0.8- 1.2 Hz  
VEL: 3.08 km/s AZ: 150.13 deg. REL.PVR: 0.96  
RG-PHASE

02/01/87 11:19:12

Fig. VII.3.7 Wide-band t-k spectra for the Lg phase (top) and Rg phase (bottom) of the event in Fig. VII.3.4.

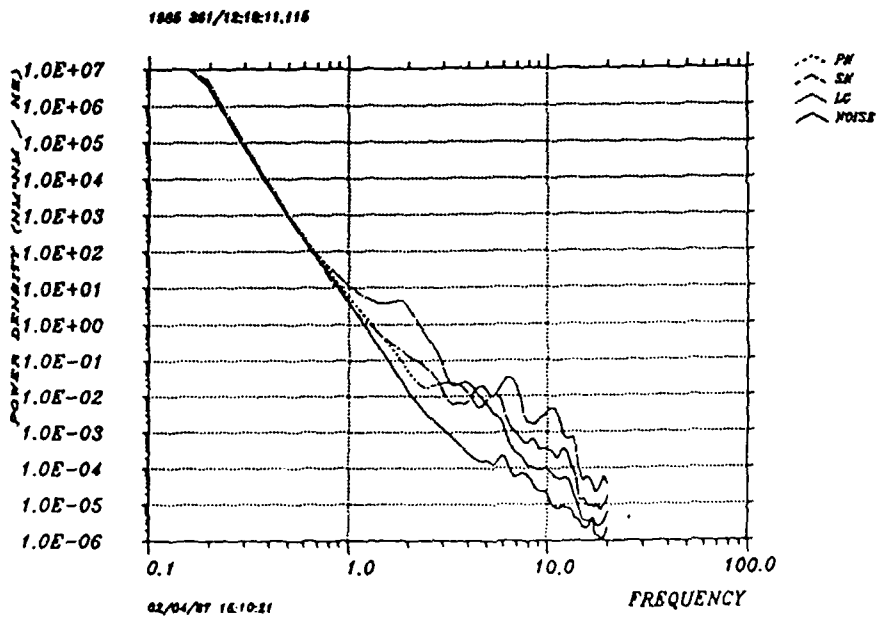
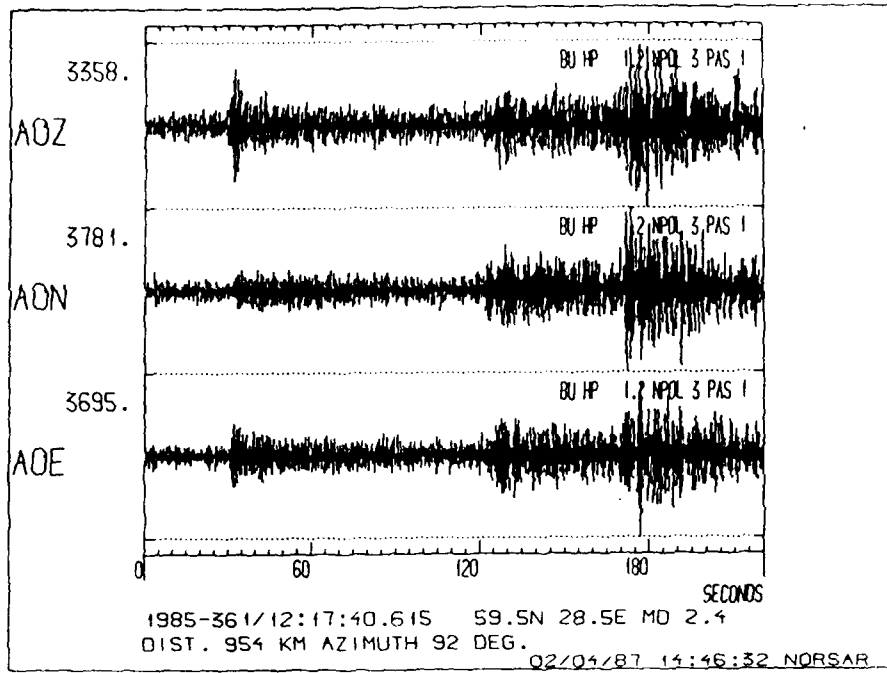


Fig. VII.3.8 NORSEAR data for the mining explosion (top) with spectra (bottom).

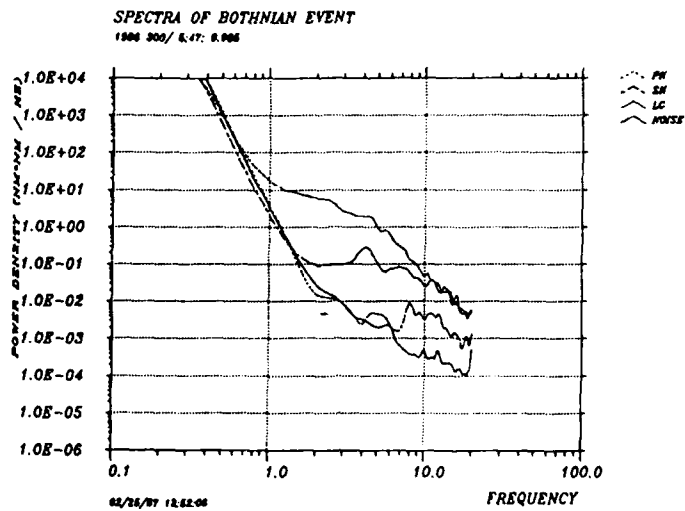
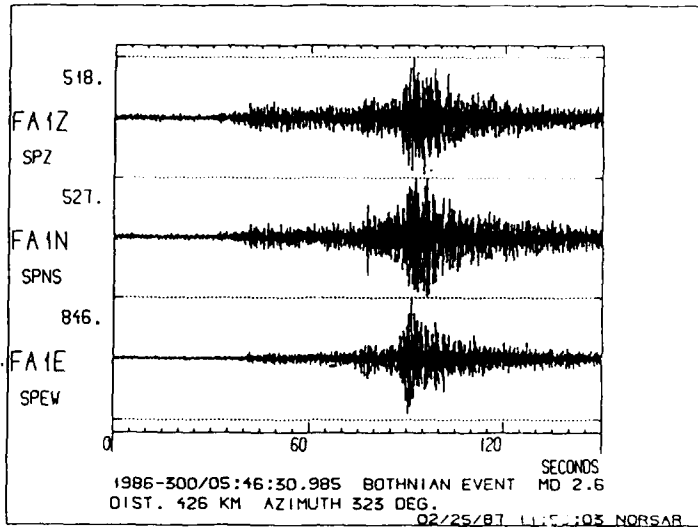


Fig. VII.3.9 FINESA three-component station data for a Bothnian Bay earthquake on October 27, 1986 (top). Spectra for the phases Pn, Sn and Lg for the event together with a spectrum of the preceding noise are shown at the bottom.

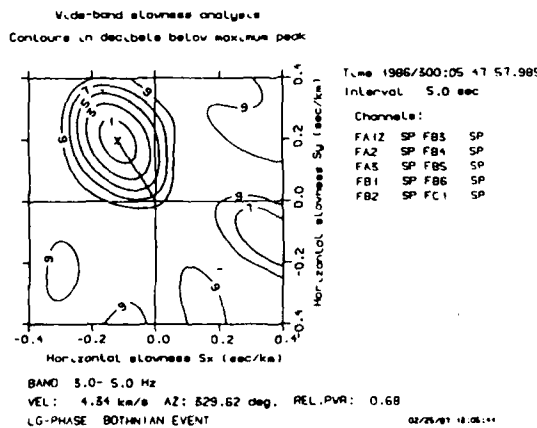
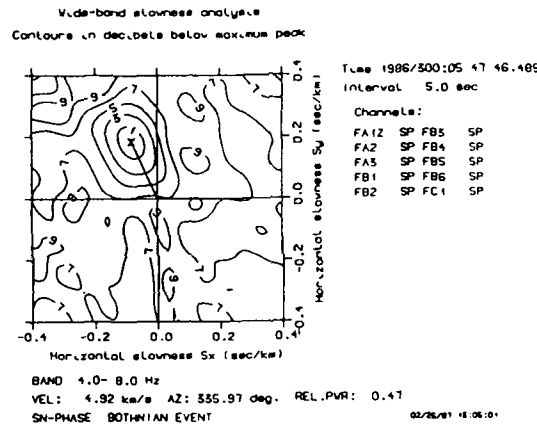
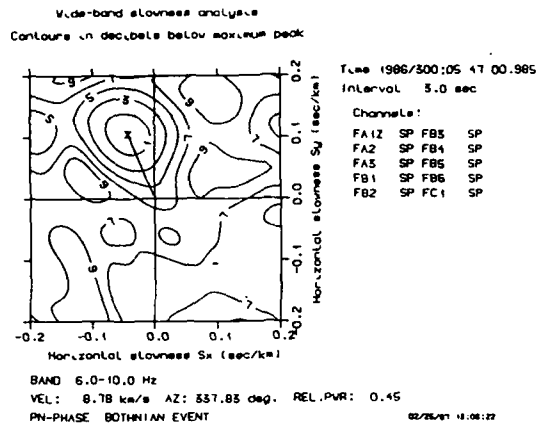


Fig. VII.3.10 Wide-band  $t-k$  spectrum for the Pn, Sn and Lg phases of the event in Fig. VII.3.9.

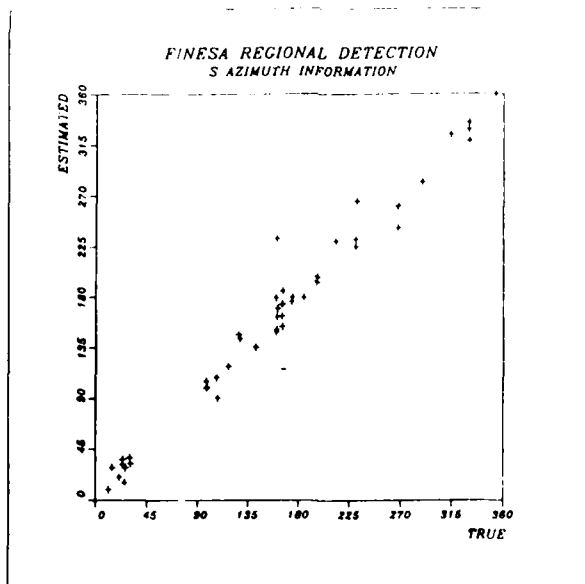
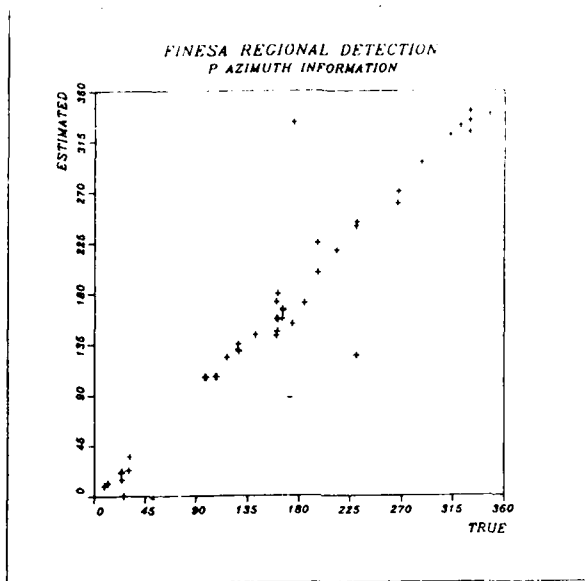


Fig. VII.3.11 Estimated versus true azimuth plotted for detected P and S phases.

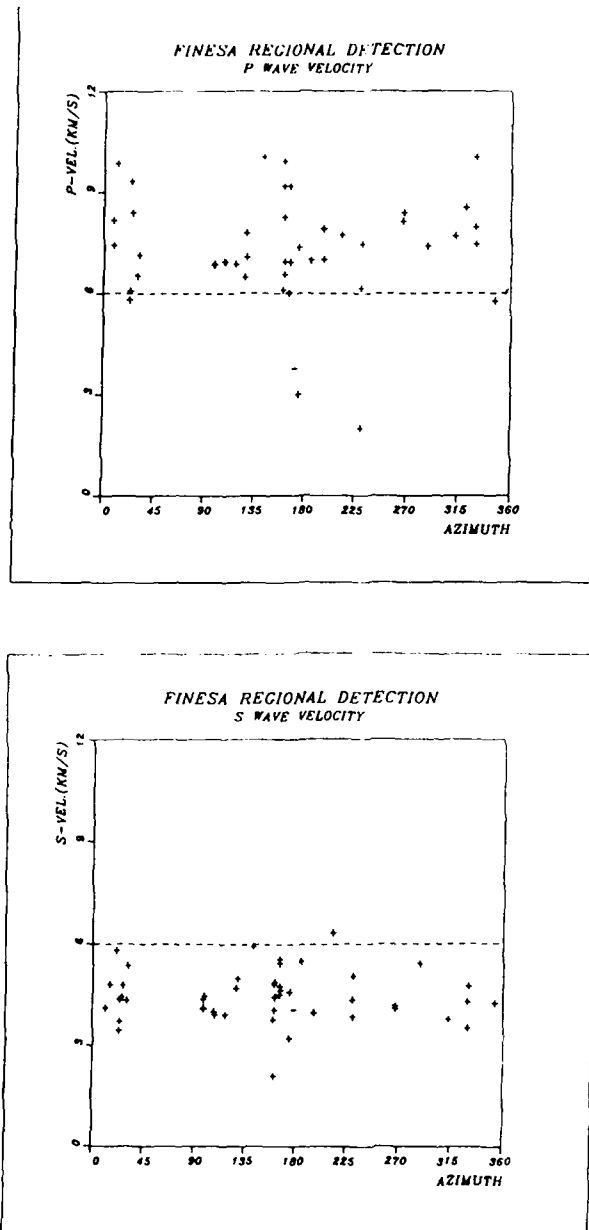


Fig. VII.3.12 Estimated phase velocity plotted versus true azimuth for detected P and S phases.

#### VII.4 Multiple scattering by topographic relief

Wavenumber analysis of NORESS array data has revealed sometimes significant frequency dependent effects. Motivated by these phenomena we have developed a method to account for multiple scattering due to topography of internal boundaries or of the free surface. The method was originally developed for the in comparison simple problem of electromagnetic scattering by a perfectly conducting rough surface, and it is based on the so-called extinction theorem (e.g., Brown, 1985). The result is an approximation since it is given by a perturbation series whose terms are obtained recursively, but the method can be applied to any surface topography, the only restriction being implied by the condition of convergence of the series solution. The Born approximation is simply the first term of the series; it is thus straightforward to make a comparison with previous single scattering results. Here we present results of a comparative study of a rough solid-liquid boundary where explicit single scattering results are available (Doornbos, 1978). Topographic effects of the free surface and of solid-solid interfaces will be considered in later contributions.

The solid-liquid interface forms a relatively complicated problem due to the modified boundary conditions. Let the deviation of the interface from a plane be given by  $z = f(x,y)$ , hence the reference plane is taken to be the  $z = 0$  plane in a cartesian coordinate system. The simplest form of interfacial displacement-traction vector needed to determine the scattered field is

$$\underline{d} = (u_x^+, u_y^+, \underline{v}^T \underline{u}, \underline{v}^T \underline{\tau} \underline{v} / |\underline{v}|^2)^T \quad (1)$$

Here the solid is taken above the interface, i.e.,  $u_x^+$  and  $u_y^+$  are the horizontal displacement components in the solid. The vector  $\underline{v}$  is normal to the interface:

$$(v_x, v_y, v_z) = \left( -\frac{\partial f}{\partial x}, -\frac{\partial f}{\partial y}, 1 \right)$$

hence  $\underline{v}^T \underline{T} \underline{v}$  is the normal traction, and  $\underline{v}^T \underline{u}$  is a constant times the normal displacement component. The solution for  $\underline{d}$  can be obtained recursively in wavenumber space. Let  $\widetilde{\underline{D}}(k_x, k_y)$  be the Fourier transform of  $\underline{d}(x, y)$ , and let

$$\widetilde{\underline{D}}(k_x, k_y) = \sum_{n=0}^{\infty} \widetilde{\underline{D}}^{(n)}(k_x, k_y) \quad (2)$$

then  $\widetilde{\underline{D}}^{(n)}$  is determined from  $\widetilde{\underline{D}}^{(n-m)}$ ,  $m = 1, \dots, n$ . The details of this solution for an incident plane wave are given elsewhere (manuscript in preparation). The scattering coefficients  $\underline{B}^{(n)}$  are similarly determined from  $\widetilde{\underline{D}}^{(n-m)}$ ,  $m = 0, 1, \dots, n$ , and the total scattered field is

$$\underline{B}(k_x, k_y) = \sum_{n=0}^{\infty} \underline{B}^{(n)}(k_x, k_y) \quad (3)$$

The components of  $\underline{B}^{(0)}$  are just the plane wave reflection and transmission coefficients for a plane interface,  $\underline{B}^{(0)}$  is the Born approximation representing single scattering, and  $\underline{B}^{(n)}$ ,  $n > 2$ , include multiple scattering. From the components of  $\underline{B}$  we can a.o. calculate the energy flux for any wave type  $j$ . Per unit of solid angle:

$$E_j(\theta, \phi) \sim \left( \frac{\omega^2}{v_j^2} - k_x^2 - k_y^2 \right)^{\frac{1}{2}} |B_j(k_x, k_y)|^2 \quad (4)$$

where

$$(k_x, k_y) = \frac{\omega}{v_j} (\sin\theta \cos\phi, \sin\theta \sin\phi)$$

and  $v_j$  is the wave velocity.

The following examples are for a velocity-density structure:

$$\begin{aligned} \rho^+ &= 5.56 \text{ g/cm}^3, \quad \rho^- = 9.93 \text{ g/cm}^3, \quad \alpha^+ = 13.64 \text{ km/s}, \quad \alpha^- = 8.08 \text{ km/s}, \\ \beta^+ &= 7.2 \text{ km/s}, \quad \beta^- = 0, \end{aligned}$$

a space-stationary roughness function  $f(x,y)$  characterized by a Gaussian autocorrelation:

$$r(x,y) = h^2 \exp\left(-\frac{x^2+y^2}{\sigma^2}\right)$$

and a lateral scale length  $\sigma = 20$  km for 1 Hz waves:  $\omega = 2\pi$  c/s. Fig. VII.4.1 illustrates the complete series solution for incident and scattered wave directions which are typically observed, and for different topographic height  $h$ . In the same figure we show the phase of the scattered wave due to a single bump with the same autocorrelation as the space-stationary roughness function. The first order phase solution is significantly biased. The bias turns out to be significant for topographic height above a few hundred meters. On the other hand, the first order approximation predicts the scattered energy remarkably

well even for rather high topography ( $h = 3$  km). Two other intuitively obvious features are: (1) The low order solutions are relatively stable for wave types and in wave directions where scattering is relatively strong, and (2) the higher order terms serve to enhance energy relatively far from the specular direction and to reduce energy near the specular direction. This is consistent with the fact that multiple scattering tends to widen the wavenumber spectrum of the scattered field. The difference between the first and higher order solutions becomes particularly pronounced in directions where the scattered field is relatively small, for example, near a zero of the reflection coefficient. Fig. VII.4.2 illustrates this phenomenon in the slowness range above 3 s/deg.

D.J. Doornbos

#### REFERENCES

- Brown, G.S. (1985): A comparison of approximate theories for scattering from rough surfaces. *Wave Motion*, 8, 155-205.
- Doornbos, D.J. (1978): On seismic wave scattering by a rough core-mantle boundary. *Geophys. J.K. astr. Soc.*, 53, 643-662.

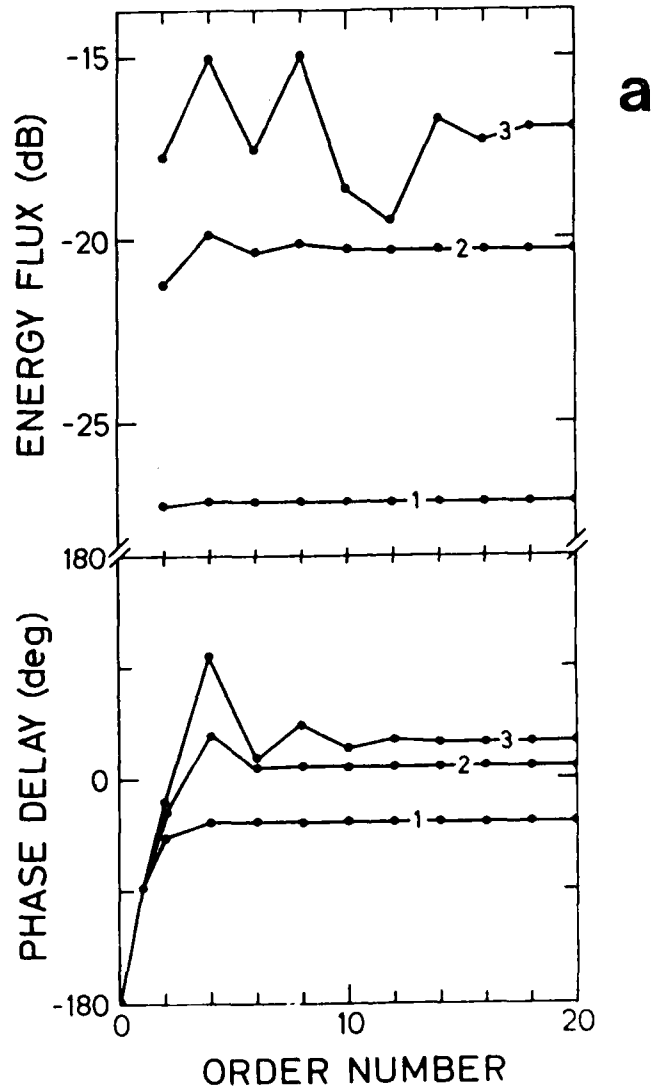


Fig. VII.4.1 (a) Energy flux and phase delay of scattered wave at 1 Hz, for subsequent orders of the series solution. Solid-liquid interface with velocity-density structure given in the text. The boundary roughness parameters are  $\sigma = 20$  km and  $l = 1$  km (1), 2 km (2), 3 km (3). Scattered P in the liquid from incident P in the liquid. The incident and scattered ray parameters are both 2.43 s/deg. The vertical planes through the incident and scattered rays differ by 44 degrees.

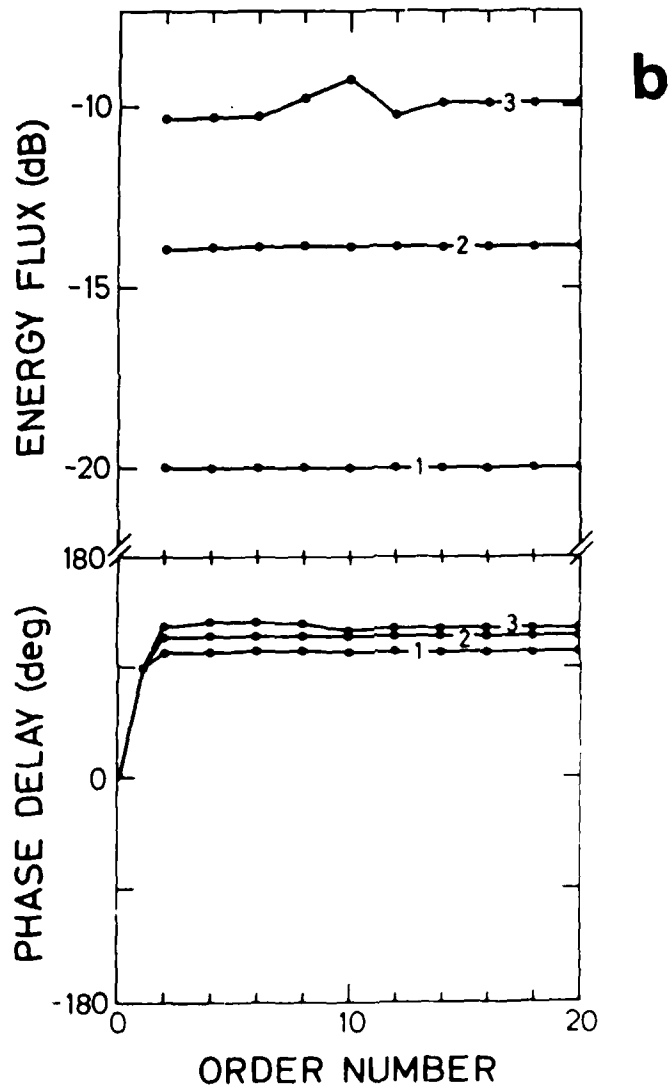


Fig. VII.4.1 (b) Scattered P in the solid from incident P in the liquid. Other details as in Fig. VII.4.1a.

4D-A185 968

NORSAR DETECTION PROCESSING SYSTEM(U) ROYAL NORWEGIAN  
COUNCIL FOR SCIENTIFIC AND INDUSTRIAL RESEARCH KJELLER  
L B LOUGHMAN 31 MAY 87 NORSAR-SCIENTIFIC-2-86 87

2/2

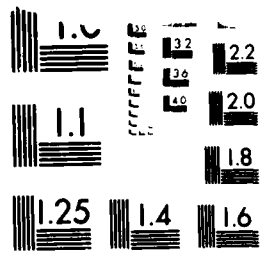
UNCLASSIFIED

F08606-86-C-0004

P/G 17/10

NL

END  
17  
17



MICROCOPY RESOLUTION TEST CHART  
NATIONAL BUREAU OF STANDARDS-1963-A

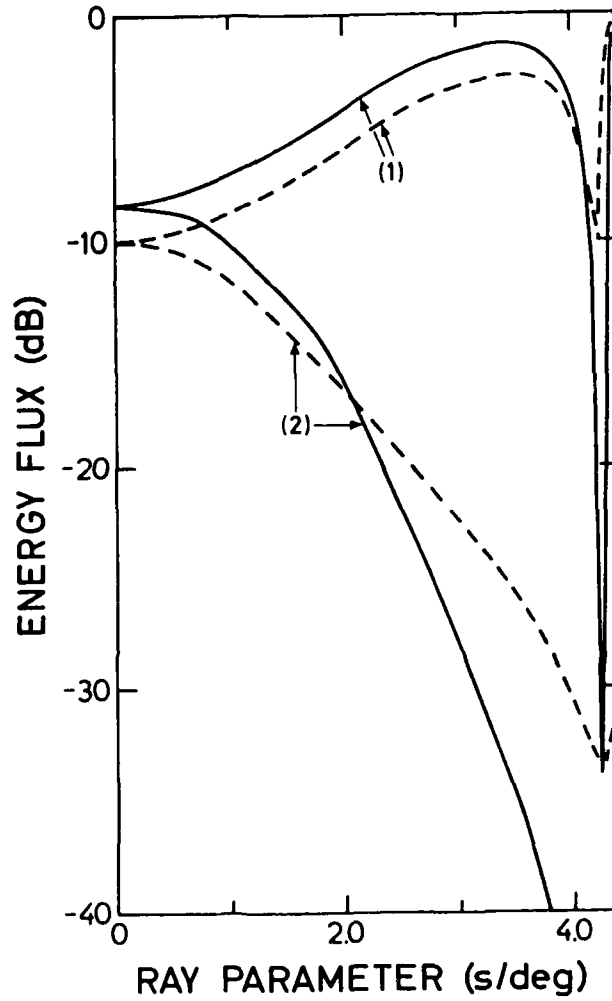


Fig. VII.4.2 Energy flux at 1 Hz through solid-liquid interface with the same specifications as in Fig. VII.x.1, and  $h = 2$  km. Scattered P in the liquid from incident P in the liquid. The incident and scattered ray parameters are equal. (1): Specular direction. (2): The vertical planes through the incident and scattered rays differ by 44 degrees. Solid lines: first order approximation. Dashed lines: complete solution.

VII.5 NORESS capability for detection and location of mining tremors in the Lubin area in Poland

The small-aperture NORESS array in Norway has been in operation since October 1984. The geometry of the array is shown in Fig. VII.5.1. The array is composed of 25 short period vertical seismometers distributed in four concentric rings A, B, C and D around the central site. Since January 1985 data from NORESS have been processed in real time at the NORSAR data center at Kjeller. The data used in the detection processing comprise 25 short period channels, sampled at a rate of 40 samples per second. The detection and location algorithm RONAPP, described by Mykkeltveit and Bungum (1984) consists of digital narrow-band filtering, beamforming, linear STA/LTA detector, frequency-wavenumber analysis and association of regional phases.

Preliminary evaluation of the NORESS detection and location capability of regional and local events was made by Mykkeltveit et al (1985), Ringdal (1986a, b) and Mykkeltveit (1986). Ringdal (1986b) concluded that the NORESS detection capability appears to be at a level of magnitude  $M_L = 2.5$  or better up to a distance of at least 1500 km. Mykkeltveit (1986) studied the NORESS automatic performance for seismic events in Western Norway and the North Sea, situated at distances from 250 to 700 km from NORESS and within a magnitude range from 1.4 to 3.1. He found that the RONAPP performance for events at a distance of 400 km from NORESS is highly satisfactory for events with magnitude 2 and greater.

This report is yet another attempt to evaluate the NORESS real time performance related to small events induced by mining in the Lubin copper basin in Poland. The Lubin basin is situated at a distance of about 1060 km from NORESS, in a tectonically disturbed area, behind the Tornquist-Teisseyre tectonic zone.

#### Data

In the Lubin basin several thousand mining tremors are recorded and located each year, with local magnitude up to 3.5 and occasionally even up to 4. All seismic events are recorded by three-dimensional underground seismic networks operated by the mining industry. They are located with high accuracy, unobtainable in earthquake seismology. The most accurate parameters are the epicenter coordinates with an error usually not larger than about 50-100 m. The depth corresponds in general to the depth of mining excavations. The least accurate parameter is the origin time which is not determined by the mine networks, since this parameter is not needed for mining operations. The origin time is determined for larger events only, in most cases from the records of KSP station, situated at a distance of about 60 km from the mining area. Its accuracy is not better than about 0.2-0.4 sec, occasionally worse. Seismic energy rather than magnitude of each located tremor is routinely calculated from the duration of the seismograms recorded by mining networks. The energy can be readily converted into magnitude. Additionally, the magnitudes of larger events are computed and verified from the records of KSP station.

Between January 1985 and March 1986 three hundred and eighteen mining tremors with local magnitude from 2.0 to 3.4 have occurred in the Lubin basin. A complete list of these events is stored in the NORSAR filing system. The NORESS array was in operation during the occurrence of 265 events (83 % of the total number, Table VII.5.1), and it was assumed that these tremors have been recorded, regardless of their SNK values.

The records of (a) all tremors with magnitude  $M_L > 2.5$ , (b) all events detected on-line with smaller magnitude and additionally (c) 25 smaller and undetected events were collected on separate tapes and processed using the interactive computer program DISPAT (Harri; and Kværna, 1985). Altogether the records of 112 seismic events (Table VII.5.1)

were processed by beamforming, bandpass filtering and spectral analysis of P- and S-wave groups. As a result of the previous experience with NORESS records of regional events (e.g., Mykkeltveit et al, 1985) and preliminary experiments with the records of Lubin tremors, a fixed array configuration was selected, composed of the center instrument, C-ring and D-ring. The processed records and spectra were plotted and then compared with the results of the RONAPP processing on-line.

#### Detection

Three data sources related to seismic events detected by NORESS are available at NORSAR: the event detection list and standard plots of seismic records and frequency - wavenumber analysis, produced automatically in almost real time, and the NORESS event bulletin (available from April 26, 1985) which is based on the detection list, verified and processed by an analyst. These sources were checked against our data base of mining tremors from the Lubin area. It was found that 68 events were detected automatically by RONAPP (26 % of the recorded number, Table VII.5.1). The number of recorded and automatically detected events as a function of magnitude is shown in Fig. VII.5.2.

In 57 cases P waves were detected and specified as such, in 5 cases secondary phases (specified by RONAPP as Lg) were detected as first arrivals and in 4 cases the first arrivals were unspecified. In 2 cases the detection included two events separated in time by one minute (events L 102 and L 103) and by half a minute (events L 337 and L 338). Out of 5 cases, in which the first arrivals were specified as secondary phases, in 3 cases they are P waves (events L 151, L 161, L 251 with magnitude 2.9, 2.7 and 2.5, respectively). Similarly, the four unspecified first arrivals were found to be P waves (events L 267, L 300, L 314 with magnitude from 2.2 to 2.6). These 7 events are not listed in the NORESS event bulletin. The arrival azimuth of recognized P waves ranges from 127° to 187° against the true value of

about 163°. The azimuth of P waves not identified by RONAPP as such ranges from about 80° to 300°.

The accuracy of automatic determinations of P arrival times was tested by comparison with the arrival times, in terms of travel time residuals, read directly from seismic records after beam forming and bandpass filtering. First of all, the average apparent velocity of P waves between NORESS and the Lubin area was calculated from 46 selected records with clear onsets of first arrivals. The velocity of 7.9 km/sec was found, and this value was accepted for the calculation of travel time residuals (observed - calculated travel times). The results are shown in Fig. VII.5.3, where a few additional observations from the RONAPP processing in the off-line mode of undetected events are also included. The residuals calculated from direct readings range from about -1 to 1 sec, while those corresponding to automatic determination of arrival times range from about -1 to 3 sec. The largest difference in epicentral distances between NORESS and the Lubin sources is about 15 km. Thus the arrival times picked up automatically are on the average 1 sec later than the true arrivals and often they are late by several seconds. This delay depends strongly on the shape and corner frequency of recorded phases. A number of records and spectra are used below to illustrate the on-line detection and location problems. The seismic events used as examples are listed in Table VII.5.2. An example of P-wave records from event L 311 with the arrival time determined automatically about 1 sec later than the onset read from the records is shown in Fig. VII.5.4. The upper trace is the NORESS steered beam and the consecutive traces show the beam filtered by various bandpass filters listed in Table VII.5.3. The power density spectra for the beam signal of 6.5 sec duration and beam noise of 30 sec duration preceding P arrivals are also shown in Fig. VII.5.4. The spectra were obtained by a prewhitening of the data, windowing and transforming the auto-correlation function and then compensating for the prewhitening (Harris and Kværna, 1986). The onset picked up by RONAPP corresponds to the wave packet with maximum amplitudes and

corner frequency of about 3.5 Hz, arriving about 1 sec after the first arrival which can be seen at lower frequencies. Another example of P-wave records from event L 119 with the onset determined automatically about 2 sec later than that read from the records is shown in Fig. VII.5.5. Here again, the automatic determination of first arrivals corresponds to high-frequency wave packets with maximum amplitudes, although the real first arrivals are clearly recorded.

From Fig. VII.5.2 it follows that no clear magnitude threshold, above which all events are automatically detected, can be established. Possibly magnitude 2.7 approaches such a threshold. There are 9 events with  $M_L = 2.6$  and 10 events with  $M_L > 2.6$  which were not detected. Out of the 9 events with  $M_L = 2.6$ , five tremors could not be identified by visual inspection of the traces and thus are not expected to be automatically detected. This only confirms that the magnitude value of small seismic events alone is not a sufficient criterion of detection. The noise level, dependent on the season of a year, day of a week and time of a day (e.g., Fyen, 1986), is a major factor controlling the SNR values. Four events, however, with  $M_L = 2.6$  are clearly recorded and should have been detected (events L 146, L 169, L 281, L 286). Similarly, out of 10 undetected events with  $M_L > 2.6$ , four tremors with magnitude 2.7 and 2.8 were not visually identified, but 5 events are well recorded (events L 112, L 139, L 175, L 306, L 353) and not detected. The sixth event L 104 with  $M_L = 3.0$  occurred 3.5 minutes after the occurrence of major tremor L 103 with  $M_L = 3.4$ , and this possibly prevented its separate detection. This somewhat erratic behavior of RONAPP was tested by standard automatic processing in the off-line mode of 23 selected events, well recorded by NORESS. The assumption was that possibly RONAPP is not always in operation even when NORESS provides undisturbed recording (RONAPP operation time was not available). The test was inconclusive. Out of 23 tremors 6 were detected in the off-line mode: event L 169 with  $M_L = 2.6$ , event L 306 with  $M_L = 2.9$  and 4 events with smaller magnitudes (L 57, L 60, L 298 and L 302 which was also located). The number of tremors detected by

RONAPP in the off-line mode is shown in brackets in Table VII.5.1. Two larger events L 175 with  $M_L = 2.9$  and L 353 with  $M_L = 3.0$  were detected neither in the on-line nor in the off-line mode. An example of such a case is given in Fig. VII.5.6 where the P-wave records and spectra from event L 112 with  $M_L = 2.7$  are shown.

Occasionally, however, when the noise level is exceptionally low, the RONAPP package performs extremely well and seismic events with magnitude as low as 2.0 are detected (Fig. VII.5.2). Such a case is presented in Fig. VII.5.7 where the P-wave records and spectra from event L 129 with  $M_L = 2.2$  are shown. The tremor was recorded on Saturday in April when the man-made noise with a maximum peak at 6 Hz (e.g., Fyen 1986) was absent. This is, however, another example of the automatic detection of first arrivals being late by 1.3 sec from the true onset time.

#### Location

Out of 68 events detected on-line by RONAPP, 11 tremors were automatically located (16 per cent of the detected number, Table VII.5.1). The number of detected and located events as a function of magnitude is shown in Fig. VII.5.8, and the list of located events is given in Table VII.5.4, where the distance between the NORESS location and the true epicenter is also included. The essential part of the location procedure is the association of P- and S-wave arrivals from the same event, leading directly to the determination of an epicenter, since the arrival azimuth is already known from f-k analysis (Mykkeltveit and Bungum, 1984). The azimuth determination for the 11 located tremors is rather consistent; the azimuth ranges from 149° to 180° for P waves and from 158° to 169° for S waves against the true value of 163°. P- and S-wave arrival times from 12 located tremors (one additional event L 302 located by RONAPP in the off-line mode) were read directly from the records and compared with the automatic readings. S-P intervals from automatic detections against those read from the

records are shown in Fig. VII.5.9. The differences between those two values are on the average about 2 sec and occasionally as large as 4 sec, which corresponds to the difference in epicentral distance of about 40-45 km.

The automatic location seems to be the most unreliable part of the RONAPP processing package, and the problem does not lie in the accuracy of the location. In most cases the secondary phases are not recognized by the system, even when they are clearly recorded, and the phase association part of the processing package is not activated. A number of such cases were found on the records processed with DISPAT and one example is shown in Fig. VII.5.10 where well-recorded S waves from event L 82 and their spectrum are presented. Naturally, the secondary phases are characterized by lower corner frequencies than those of P waves and only the records filtered with lower bandpass frequencies display distinct S-wave groups. The regional event location algorithm of RONAPP is based on the assumption that the largest secondary detected phase is Lg propagating with a group velocity of 3.5 km/sec. This assumption is valid for propagation paths confined to continental shield type structures, like Fennoscandia, but is not observed for propagation paths crossing significant tectonic disturbances. Even the Tornquist-Teisseyre tectonic zone in Poland is an effective barrier to the propagation of Lg waves (Kvarna and Mykkeltveit, 1986), and the dominant secondary phases recorded by NORESS from the Lubin area are Sn waves propagating with a velocity of 4.5 km/sec. This is a well known fact and further studies on regional characteristics of secondary phases will lead to a vast improvement in the event location of regional array processing.

The epicenters of 11 tremors located by the current version of the NORESS processing package are shown in Fig. VII.5.11 (filled circles). They are situated at a distance of about 400 km from the Lubin area (Table VII.5.4), except the epicenter of event L 258 whose location is based on a misidentified secondary arrival by 35 sec. These epicenters

were relocated by replacing the velocities corresponding to  $L_g-P_n$  time intervals by those corresponding to  $S_n-P_n$  intervals, taken from the Jeffreys-Bullen travel time tables. The results are also shown in Fig. VII.5.11 (open circles) and the corrected distances between the new and true epicenters are listed in Table VII.5.4. The distances are still short by about 50-60 km of the true locations as a result of the real regional wave velocities being slightly higher than those from the J-B tables, but the result is rather impressive considering that it is obtained from a single small-aperture array.

The NORESS event bulletin gives an additional indication of possible location of seismic events for which only P waves are detected. The f-k analysis, performed automatically for all detected P waves, provides the arrival azimuth and apparent velocity, which in turn is converted into the epicentral distance. It is well known that this approach is of highly limited value and could provide only very rough indication of event location, and should not be discussed here. It was found, however, that the records of P-wave groups display characteristic patterns from events repeatedly located at the same sites. This fact could be of interest for an expert system approach to regional array processing.

From the NORESS bulletin 30 Lubin events were found to be located from P waves alone. Their location is shown in Fig. VII.5.11 by crosses; 9 tremors are located in Roumania, 4 events in Bulgaria and Yugoslavia, 4 events in Italy, 3 events in Czechoslovakia and 4 tremors are located elsewhere. Disregarding the last four events which are randomly distributed, the specific locations of the Lubin tremors seem to be related to characteristic patterns of P-wave records, which reflect the source properties. This problem will be considered elsewhere. Here only selected examples of P-wave patterns are given. An example of characteristic P-wave records and spectrum from event L 160 located in Roumania are shown in Fig. VII.5.12. The largest amplitudes are observed at higher frequencies between 4.0 and 8.0 Hz, about 2 sec

after the onset (marked by the first arrow) of P waves, and they were recognized by RONAPP as P first arrivals (marked by the second arrow). The corner frequency is 5 Hz (Fig. VII.5.12c). Another example of P-wave records and spectrum from event L 337 located in Italy is shown in Fig. VII.5.13. Here the largest amplitudes are observed at lower frequencies between 1.5 and 3.5 Hz at the very beginning of P-wave group and the onset of P waves determined automatically is very close to the real one. The corner frequency is about 2.5 Hz (Fig. VII.5.13c). An intermediate case is presented in Fig. VII.5.14 where P-wave records and spectrum from event L 330 located in Bulgaria are shown. Here the maximum amplitudes are observed at two frequency bands, between 1.5 and 3.5 Hz and between 4.0 and 8.0 Hz. Two corner frequencies of about 3 and 5 Hz are also observed. The arrival time is about 1.7 s later than the onset read directly from the records, though the first arrivals at lower frequencies are rather distinct (Fig. 14b).

#### Conclusions

1. A data base of 318 mining tremors, with magnitude from 2.0 to 3.4, from the Lubin area in Poland, was used to evaluate the NORESS real time performance in detection and location of small regional seismic events. The tremors have occurred between January 1985 and March 1986 at a distance of about 1060 km from NORESS.
2. The array was in operation during the occurrence of 265 Lubin tremors and 26 % of them were detected on-line. There is no distinct magnitude threshold above which all events are detected, but magnitude  $M_L = 2.7$  approaches such a limit. The accuracy of detected arrival times and azimuths depends strongly on the shape and corner frequency of recorded phases. The detection system works somewhat erratically: several well-recorded P waves were not detected. NORESS is obviously a unique seismic system capable of recording so small events at a distance of one thousand kilometers, but the detection system certainly needs refinement.

Possibly a detector operating in the frequency rather than in the time domain would be more suitable for the identification of emergent phases and those recorded with low SNR (Gledhill, 1985).

3. The location algorithm is the most unreliable part of the processing system and only 16 % of detected events were located on-line. Although the accuracy of location is rather good (within 50-60 km from the source area after replacing  $L_g$  by  $S_n$  velocities), it can be further improved by using the broad-band  $f$ - $k$  estimation of azimuths and velocities instead of the narrow-band  $f$ - $k$  analysis presently employed by the RONAPP package (Kværna and Ringdal, 1986). In most cases, however, the secondary phases are not recognized, even when they are clearly recorded, and the phase association part of RONAPP is not activated. The application of horizontal components for the secondary phase detection seems to be promising (Kværna, 1986), but it is not clear how this approach would work with smaller events. A rough estimate of event location from P waves alone could be improved by the recognition of characteristic patterns of P-wave records, reflecting the source properties, from events repeatedly located at the specific sites. Such information could be implemented into an expert system approach to regional array processing.
4. Obviously, a set-up of another regional array of the NORESS type would vastly improve the overall capability for seismic detection and location on-line. At the present stage, however, a more vigorous human interaction with the NORESS automatic system is badly needed.

#### **Acknowledgements**

I am grateful to Tormod Kværna, Bernt Hokland and Frode Ringdal for their introduction to the NORSAR data processing system. I acknowledge financial support from NORSAR during my 3-month stay at Kjeller at the end of 1986.

S.J. Gibowicz, inst. of Geophysics  
Polish Academy of Sciences, Warsaw

#### References

- Fyen, J. (1986): NORESS noise spectral studies, preliminary report, NORSAR Sci. Rep. No. 2-85/86, 48-59.
- Gledhill, K.R. (1985): An earthquake detector employing frequency domain techniques, Bull. Seism. Soc. Am., 75, 1827-1835.
- Harris, D.B. and T. Kværna (1985): Interactive analysis program for use with NORESS data, NORSAR Sci. Rep. No. 2-84/85, 53-61.
- Kværna, T. (1986): Applicability of horizontal components for detection and phase discrimination, NORSAR Sci. Rep. No. 1-86/87, 51-60.
- Kværna, T. and S. Mykkeltveit (1986): Propagation characteristics of regional phases recorded at NORSAR, NORSAR Sci. Rep. No. 1-85/86, 21-29.
- Kværna, T. and F. Ringdal (1986): Stability of various  $f$ - $k$  estimation techniques, NORSAR Sci. Rep. No. 1-86/87, 29-40.
- Mykkeltveit, S. (1986): NORESS real time processing performance for events in Western Norway and the North Sea, NORSAR Sci. Rep. No. 2-85/86, 40-47.
- Mykkeltveit, S. and H. Bungum (1984): Processing of regional seismic events using data from small-aperture arrays, Bull. Seism. Soc. Am., 74, 2313-2333.

- Mykkeltveit, S., D.B. Harris and T. Kværna (1985): Preliminary evaluation of the event detection and location capability of the small-aperture NORESS array, NORSAR Sci. Rep. No. 2-84/85, 30-42.
- Ringdal, F. (1986a): Initial results from NORESS detection processing, NORSAR Sci. Rep. No. 1-85/86, 40-51.
- Ringdal, F. (1986b): Regional event detection using the NORESS array, NORSAR Sci. Rep. No. 2-85/86, 21-30.

Magnitude M <sub>L</sub>	Number of Events				
	Reported	Recorded	Detected on-line	Located on-line	Processed with DISPAT
2.0	54	44	3		4
2.1	33	28	1		2
2.2	41	32	2		2
2.3	51	42	6		14
2.4	38	32	5 (3)	(1)	13
2.5	29	25	8 (1)		15
2.6	22	20	11 (1)	2	20
2.7	20	17	13	1	17
2.8	11	10	8	3	10
2.9	10	7	5 (1)	1	7
3.0	7	7	5	4	7
3.1	1	0	0	0	0
3.4	1	1	1	0	1
<b>Total</b>	<b>318</b>	<b>265</b>	<b>68 (74)</b>	<b>11 (12)</b>	<b>112</b>
<b>Per cent</b>		<b>83</b>	<b>26 (28)</b>	<b>16 (16)</b>	
		<b>of</b>	<b>of</b>	<b>of</b>	
		<b>reported</b>	<b>recorded</b>	<b>detected</b>	

Table VII.5.1 Number of mining tremors from the Lubin area recorded and detected by NORESS from January 1985 to March 1986. The number of events detected by RONAPP in the off-line mode is shown in brackets.

Event No.	Date	Origin time UT	Epicenter		M <sub>L</sub>	Distance km	Azimuth deg.	Arrival time UT
			Lat. N	Lon. E				
L 82	8 Feb. 1985	08:54:14.7	51.486	16.018	2.8	1063.3	163.0	08:58:10.9
L 112	12 March 1985	05:17:45.1	51.516	16.100	2.7	1061.4	162.7	05:19:59.5
L 119	23 March 1985	01:20:52.8	51.488	16.019	2.5	1063.1	163.0	01:23:08.1
L 129	6 Apr. 1985	13:31:25.3	51.437	16.136	2.2	1070.5	162.6	13:33:41.2
L 160	25 May 1985	16:12:09.4	51.483	16.022	2.6	1063.7	163.0	16:14:24.9
L 311	1 Jan. 1986	12:15:58.3	51.425	16.155	2.4	1072.1	162.6	12:18:14.8
L 330	12 Feb. 1986	14:37:00.1	51.486	16.016	2.6	1063.3	163.0	14:39:14.8
L 337	26 Feb. 1986	20:34:04.0	51.510	16.030	2.5	1060.9	162.9	20:36:19.1

Table VII.5.2 List of seismic events recorded by NORESS and used as examples to illustrate the on-line detection and location problems.

Center Frequency Hz	Filter Band Hz
2.0	1.0 - 3.0
2.5	1.5 - 3.5
3.0	2.0 - 4.0
3.5	2.5 - 4.5
4.0	3.0 - 5.0
4.5	3.5 - 5.5
6.0	4.0 - 8.0
8.0	4.0 - 11.0
9.0	6.0 - 12.0
12.0	8.0 - 16.0

Table VII.5.3 Bandpass filters used for numerical filtration of beamed records.

Event No.	Date	Origin time UT	M <sub>L</sub>	Epicenter		Origin time UT		NORESS location		Distance km	Corrected distance km
				Lat.°N	Lon.°E	Lat.°N	Lon.°E				
1985											
L128	Apr 06	07:55:53.9	2.8	51.520	16.046	07:56:36.8	54.83	14.59	380	54	
L134	Apr 13	09:09:40.0	2.8	51.487	16.021	09:10:27.7	55.0	14.5	403	90	
L181	Jun 20	02:33:42.9	2.6	51.488	16.951	02:31:26.4	54.81	14.60	382	55	
L227	Aug 18	04:28:14.0	3.0	51.510	16.030	04:28:54.4	54.88	15.55	370	36	
L247	Sep 21	03:39:56.9	3.0	51.487	16.049	03:40:38.4	54.63	13.64	375	44	
L258	Oct 08	03:57:39.5	2.6	51.483	16.027	03:57:56.8	52.91	14.75	174	48	
L282	Nov 08	00:08:03.5	3.0	51.512	16.033	00:08:46.0	54.79	14.60	377	48	
L299	Dec 11	20:20:16.8	2.9	51.510	16.030	20:20:59.6	54.68	13.85	375	45	
1986											
L318	Jan 09	20:34:38.1	3.0	51.510	16.030	20:35:21.6	54.84	14.58	383	59	
L351	Mar 06	04:02:24.5	2.8	51.487	16.045	04:03:08.8	54.87	14.57	389	67	
L352	Mar 07	00:49:14.0	2.7	51.500	16.060	00:50:01.3	54.86	14.30	390	71	

Table VII.5.4 List of mining tremors located automatically by NORESS from January 1985 to March 1986.

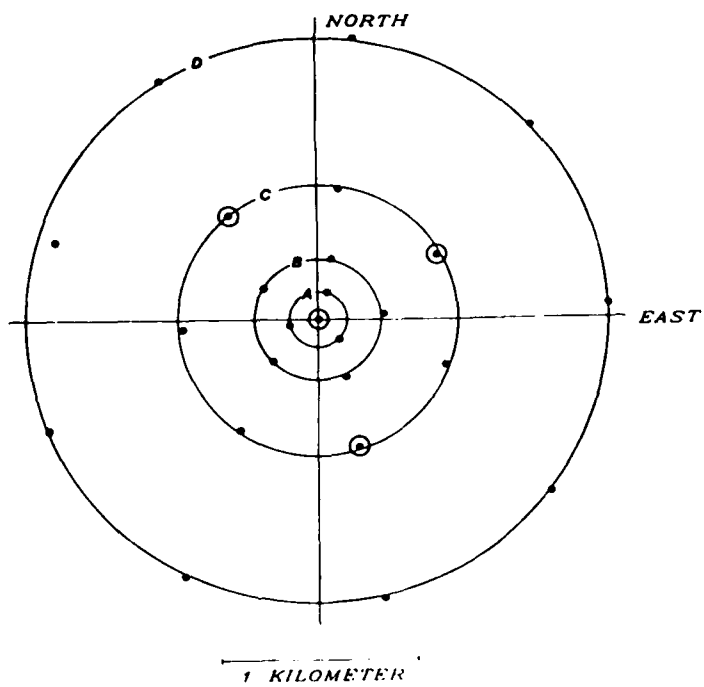


Fig. VII.5.1 Geometry of the NORESS array. The four rings are marked by letters A, B, C and D and the four three-component stations are marked by small circles.

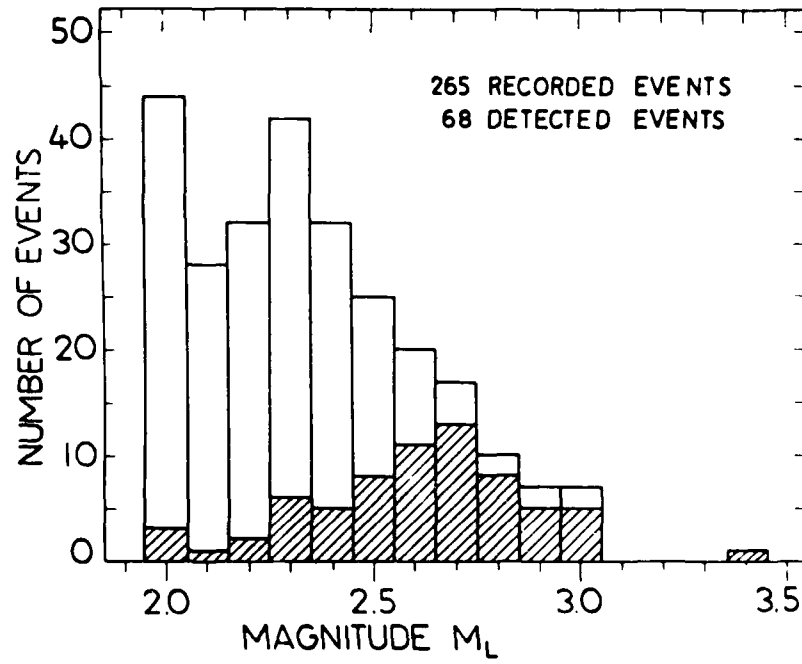


Fig. VII.5.2 Number of recorded and automatically detected events as a function of local magnitude  $M_L$ .

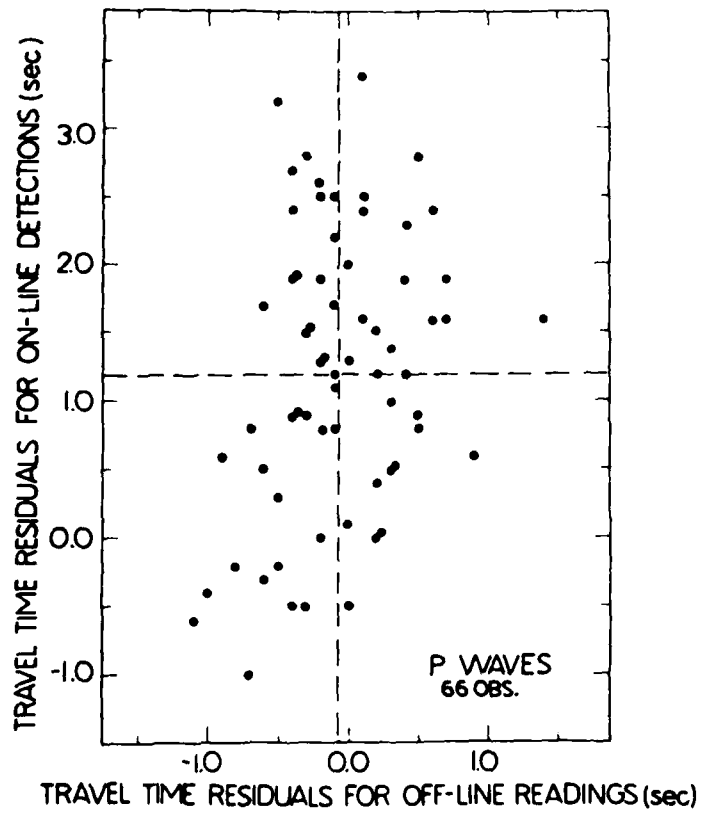


Fig. VII.5.3 Travel time residuals of P waves calculated for automatic determination of arrival times against those read from the records. The mean values are shown by dashed lines.

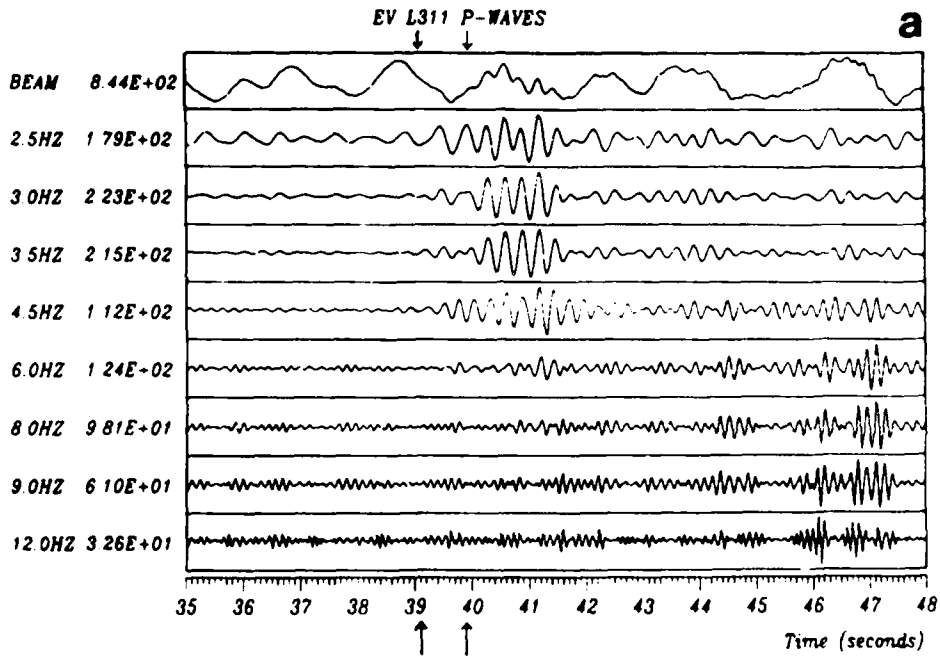


Fig. VII.5.4 (a) Example of P-wave records from event 1311 (Table VII.5.2) with the arrival time determined automatically about 1 sec later than the onset read from the records (marked by arrows). The upper trace is the NORESS steered beam formed from the center, C-ring and D-ring vertical instruments. The consecutive traces show the beam filtered by various bandpass filters with center frequencies marked at the records; filter bands are listed in Table VII.5.3. The time scale is relative: the absolute P arrival time corresponding to the first arrow is given in Table VII.5.2.

EV L311 P-WAVE

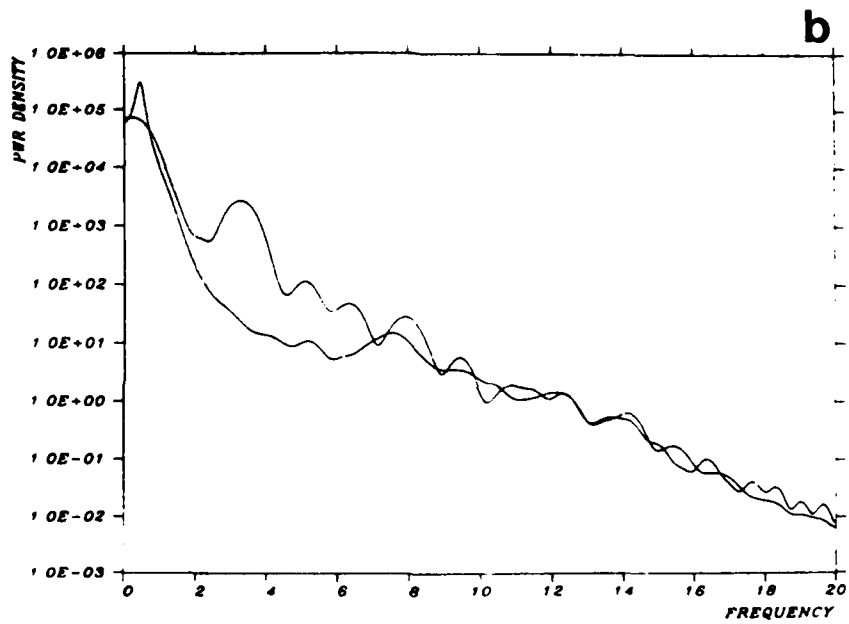


Fig. VII.5.4 (b) Power density spectra, uncorrected for instrumental response, for the beam signal of 6.5 sec duration (upper curve) and beam noise of 30 sec duration preceding P arrival (lower curve).

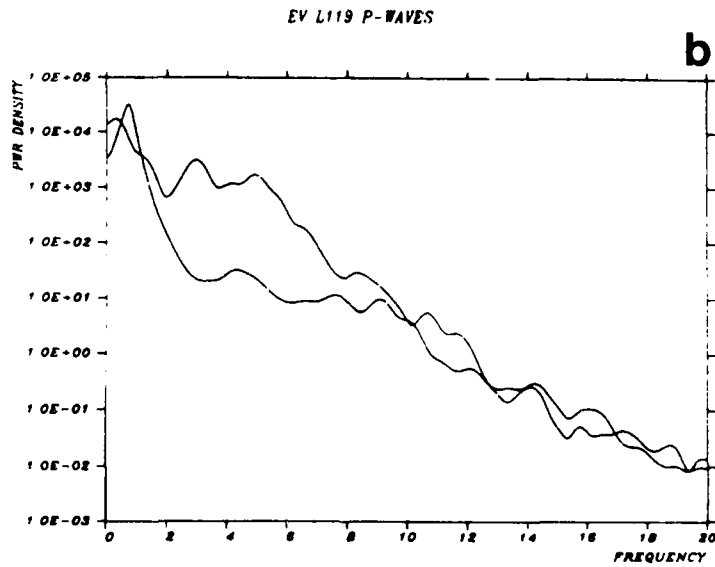
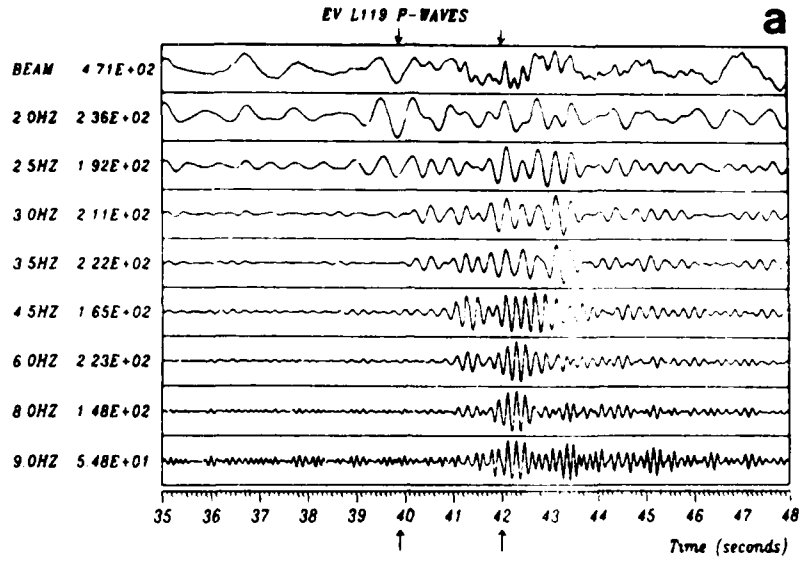


Fig. VII.5.5 (a) Example of P-wave records from event L119 with the onset determined automatically about 2 sec later than that read from the records (marked by arrows).  
(b) Power spectra for the beam signal of 7 sec duration and beam noise.

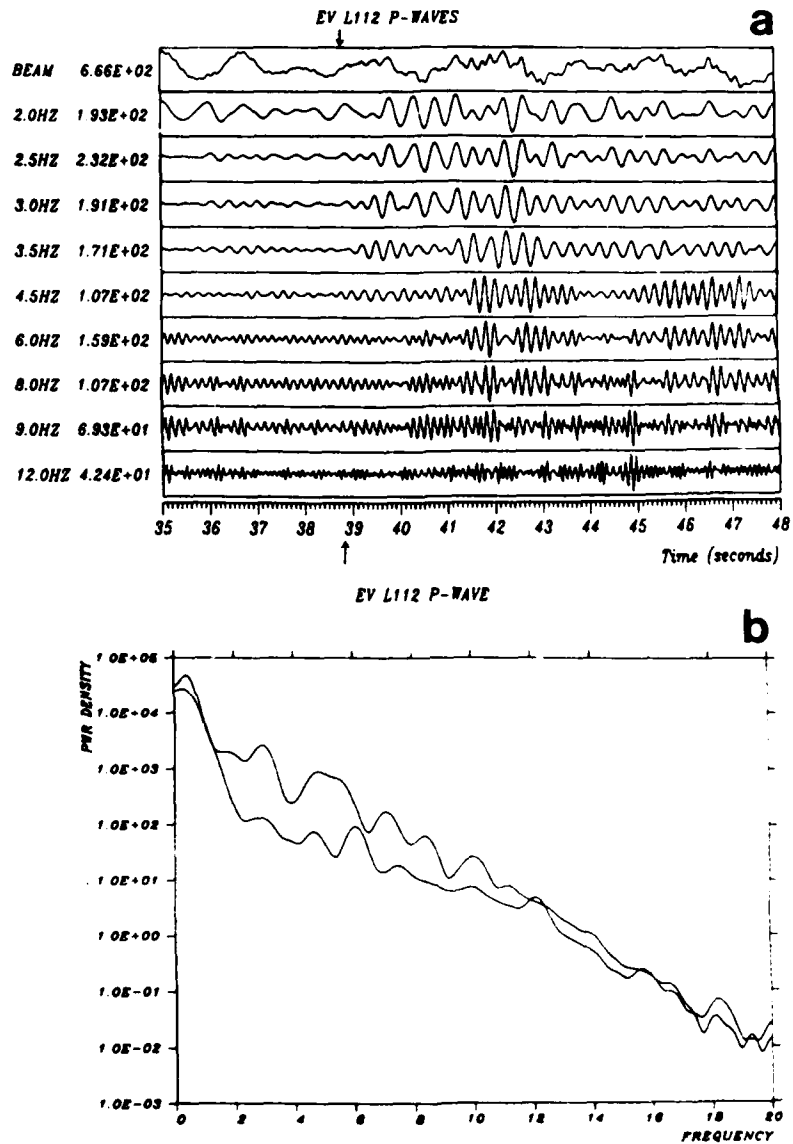


Fig. VII.5.6 (a) Example of P-wave records from event L112 not detected by RONAPP. (b) Power spectra for the beam signal of 8 sec duration and beam noise.

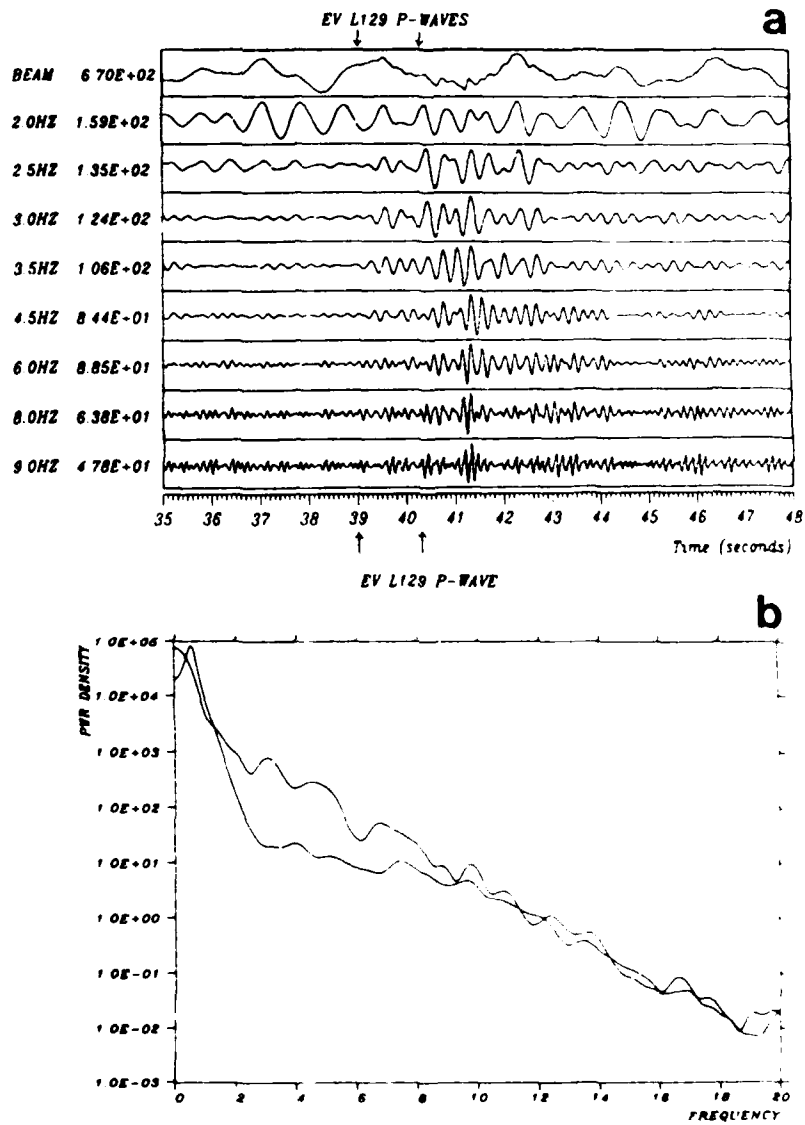


Fig. VII.5.7 (a) Example of P-wave records from the small event L129 detected automatically as a result of unusually low noise level. (b) Power spectra for the beam signal of 6 sec duration and beam noise.

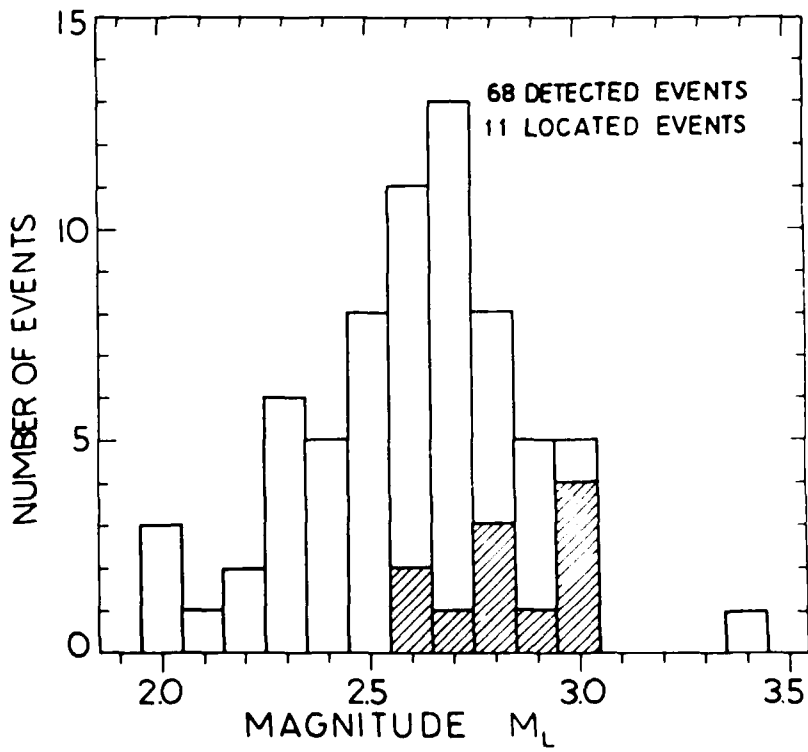


Fig. VII.5.8 Number of automatically detected and located events as a function of magnitude  $M_L$ .

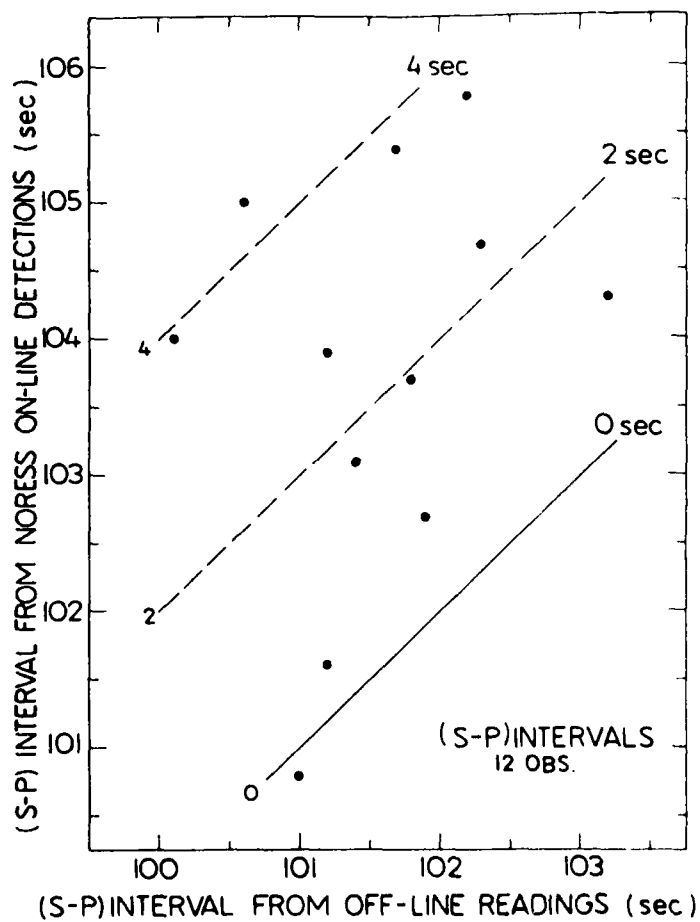


Fig. VII.5.9 (S-P) intervals from automatic detections against those read from the records. The differences in their values are shown by straight lines.

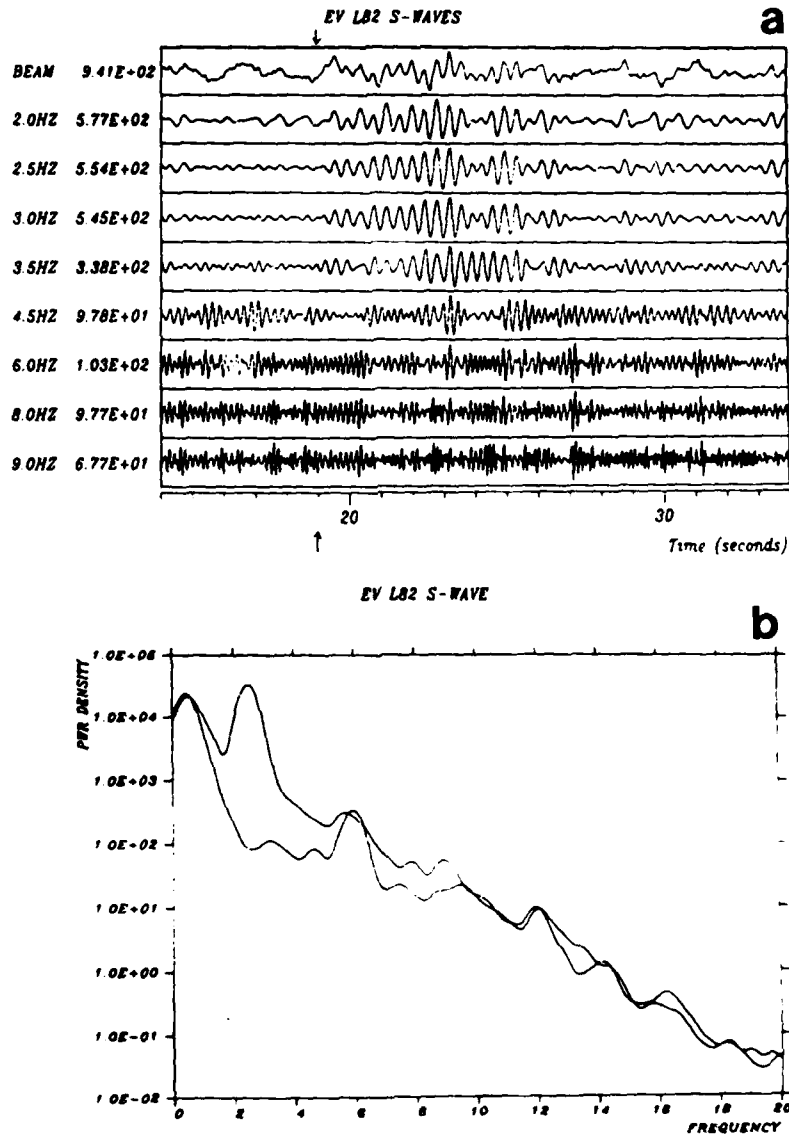


Fig. VII.5.10 (a) Example of well recorded S waves, event L82, not detected by RONAPP. (b) Power spectra for the beam signal of 9.5 sec duration and beam noise.

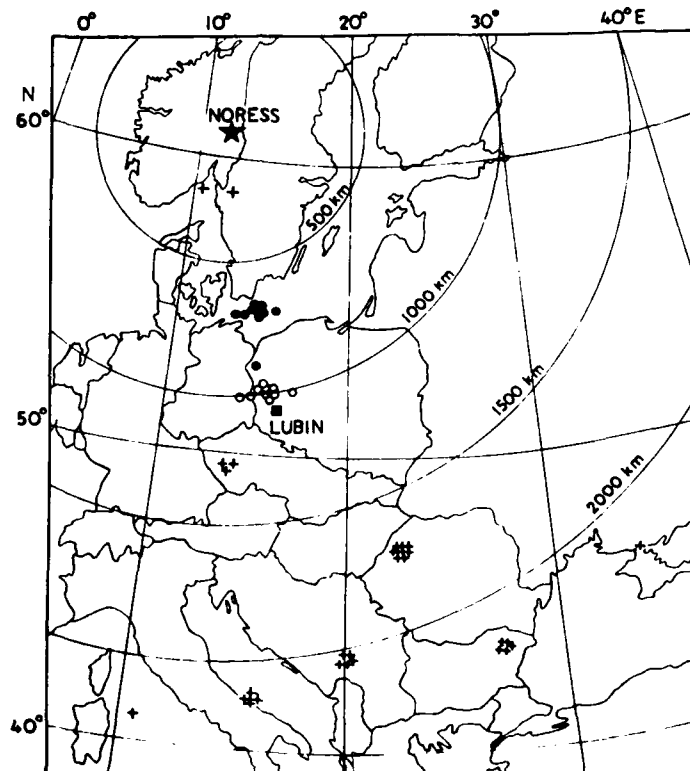


Fig. VII.5.11 Geographical distribution of seismic events from the Lubin area (marked by a square) located automatically by NORESS (marked by a star). The epicenters located from P and secondary phases are indicated by filled circles and their positions recalculated by replacing  $L_g$  by  $S_n$  velocities are denoted by open circles. The indications of location from P waves alone are marked by crosses.

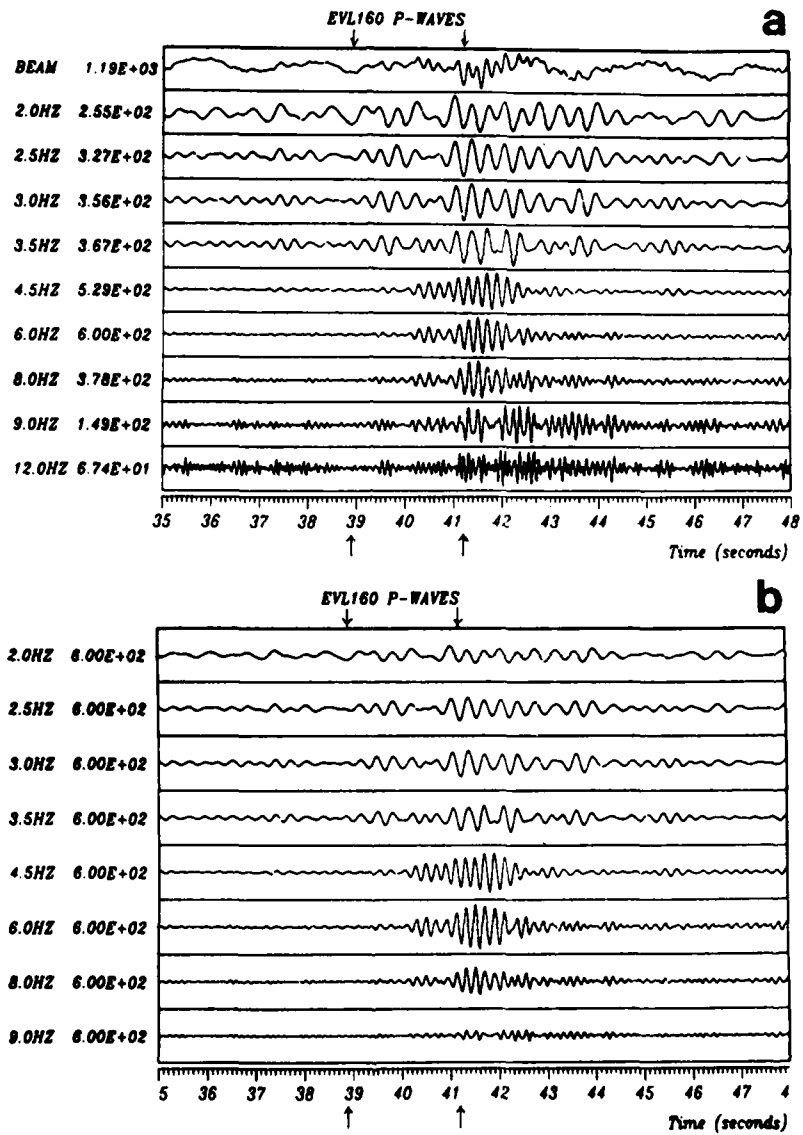


Fig. VII.5.12 (a) Example of characteristic P-wave records, event L160, located from P waves only in Romania, with the largest amplitudes at higher frequencies between 4.0 and 8.0 Hz (center frequency 6.0 Hz). (b) P-wave records scaled to the maximum amplitude at the center frequency of 6.0 Hz.

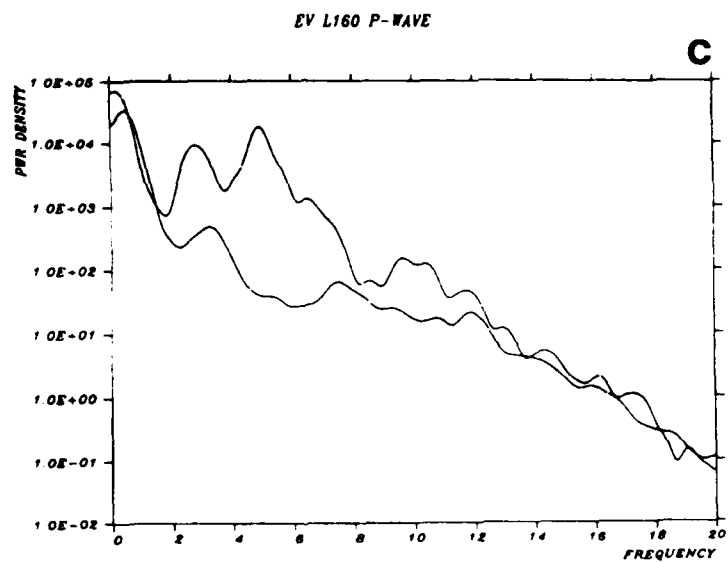


Fig. VII.5.12 (cont.)

(c) power spectra for the beam signal of 7 sec duration and beam noise.

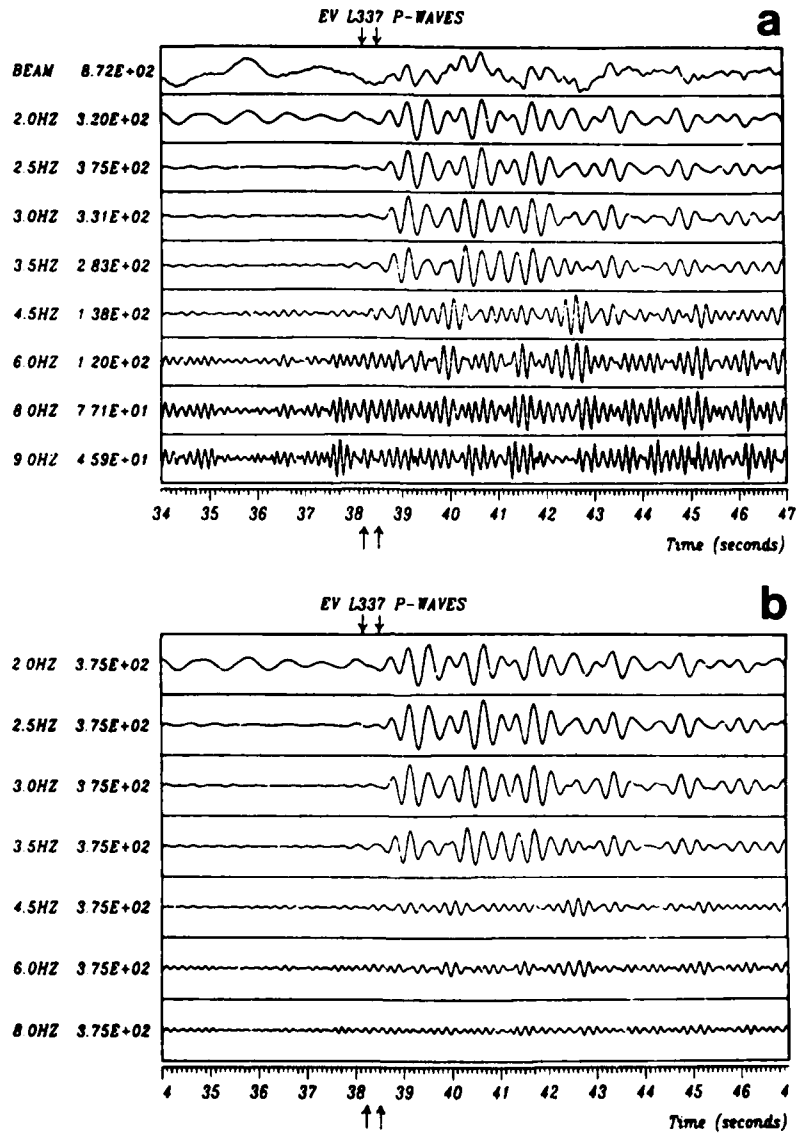


Fig. VII.5.13 (a) Example of characteristic P-wave records, event L337, located from P waves in Italy, with the largest amplitudes at lower frequencies between 1.5 and 3.5 Hz (center frequency of 2.5 Hz). (b) P-wave records scaled to the maximum amplitude at the center frequency of 2.5 Hz.

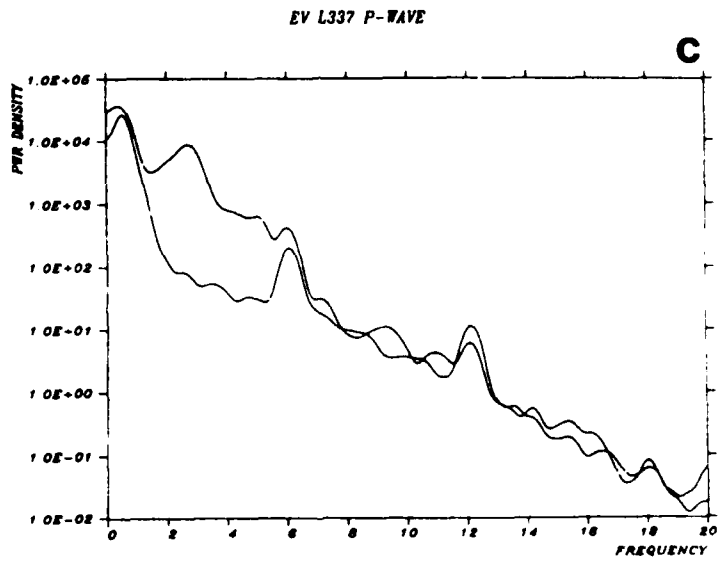


Fig. VII.5.13 (cont.)

(c) Power spectra for the beam signal of 8 sec duration and beam noise.

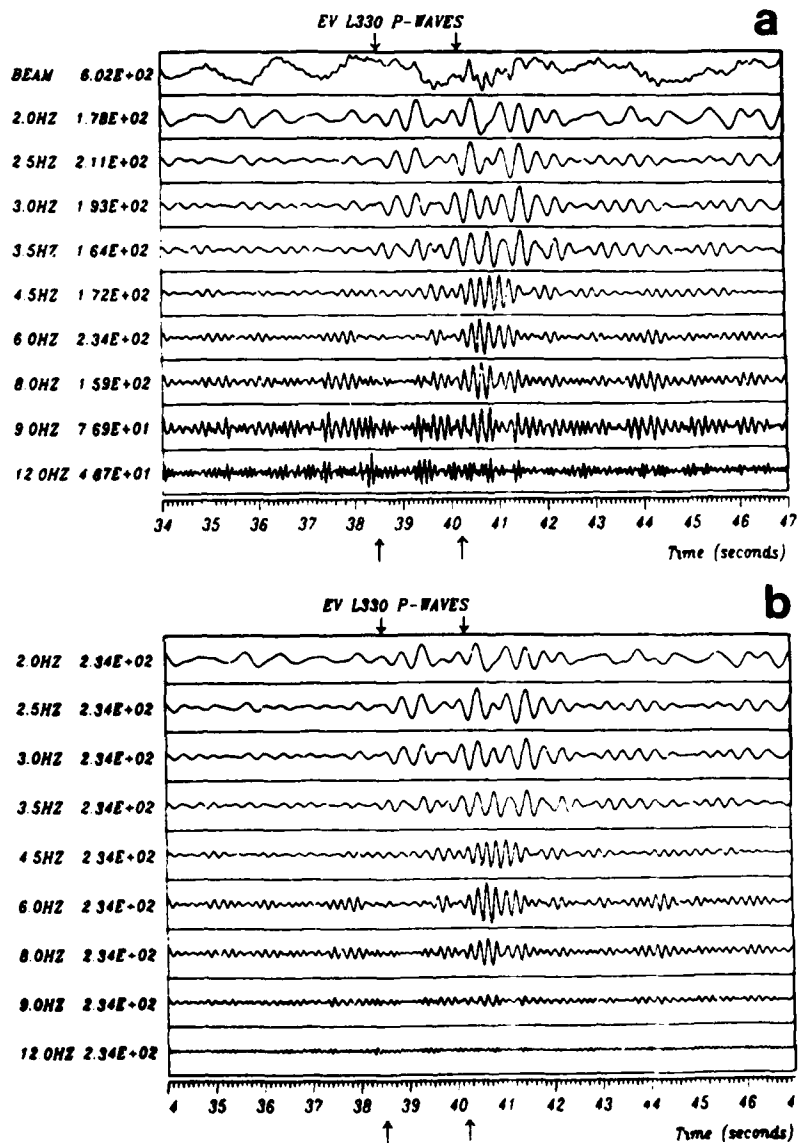


Fig. VII.5.14 (a) Example of characteristic P-wave records, event L330, located from P waves in Bulgaria, with the largest amplitudes at two frequencies, between 1.5 and 3.5 Hz (center frequency 2.5 Hz) and between 4.0 and 8.0 Hz (center frequency 6.0 Hz). (b) P-wave records scaled to the maximum amplitude at the center frequency of 6.0 Hz.

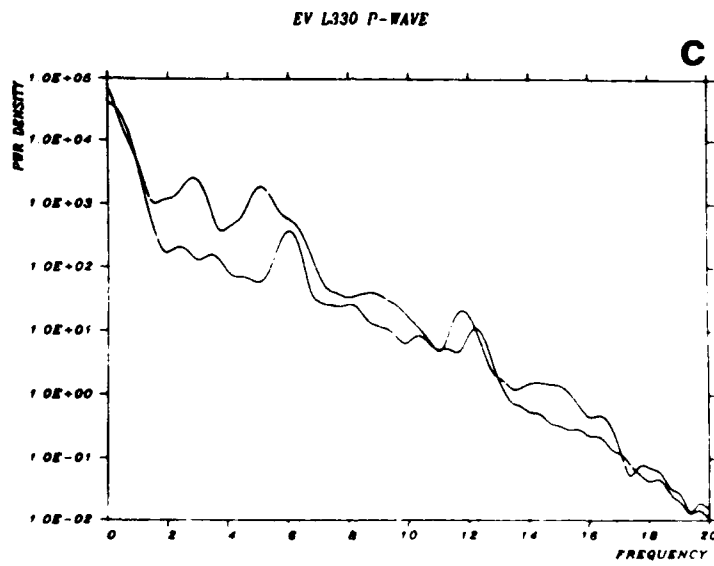


Fig. VII.5.14 (cont.)

(c) Power spectra for the beam signal of 6.5 sec duration and beam noise.

END

DATE  
FILMED

12 87